

NANOSCALE MECHANICS

By
Adam E. Cohen

THIS DISSERTATION IS SUBMITTED
FOR THE DEGREE OF
DOCTOR OF PHILOSOPHY
AT
CAMBRIDGE UNIVERSITY
CAMBRIDGE, UK
SEPTEMBER 2003

© Copyright by Adam E. Cohen, 2003

CAMBRIDGE UNIVERSITY
DEPARTMENT OF
SEMICONDUCTOR PHYSICS

The undersigned hereby certify that they have read and recommend to the Faculty of Cavendish Laboratory for acceptance a thesis entitled “**Nanoscale Mechanics**” by **Adam E. Cohen** in partial fulfillment of the requirements for the degree of **Doctor of Philosophy**.

Dated: September 2003

External Examiner:

Research Supervisor:

Michael Pepper

Examining Committee:

To my parents

Table of Contents

Table of Contents	v
Abstract	viii
Acknowledgements	ix
Introduction	1
1 Generalized Response Functions (GRFs)	5
1.1 Introduction	6
1.2 Nonlinear response functions	7
1.3 Superoperators in Liouville space	10
1.4 Multitime observables	15
2 Two-Body Interactions	20
2.1 Introduction	20
2.2 Factorization of two-body response function	23
2.3 Factorization in the L, R representation	29
3 Nonequilibrium van der Waals Forces	33
3.1 Introduction	33
3.2 Interaction Hamiltonian	37
3.3 McLachlan formalism	39
3.4 Response function formalism	42
3.4.1 Forces and dissipation	44
3.5 Examples	47
3.5.1 First order interaction	48
3.5.2 Second order interaction, different temperatures	49
3.6 Higher order forces	62

3.7	Discussion	63
4	Excited state forces	64
4.1	Eigenstate picture	65
4.1.1	Two-level system	66
4.2	FRET force	70
4.2.1	Electrodynamic derivation	73
4.2.2	Application to FRET	75
4.2.3	Kramers-Kronig relations	75
4.2.4	Eigenstate derivation	76
4.2.5	Superoperator derivation	80
4.2.6	Examples	82
4.2.7	Sample calculation	83
4.3	Discussion	85
5	Optical Control of Intermolecular Forces	90
5.1	Introduction	90
5.2	Local field approximation	92
5.2.1	Linear regime	94
5.2.2	Nonlinear regime	99
5.2.3	van der Waals forces within the LFA	101
5.3	Superoperator approach	104
5.4	Application to the van der Waals gas	108
5.5	Discussion	110
6	Biological Solitons	112
6.1	Introduction	112
6.2	Kinks in filamentous aggregates	113
6.2.1	Finite temperature	121
6.3	Kinks on polymers	122
6.3.1	Freely jointed chain	125
6.3.2	Kinks	129
6.3.3	The kink gas	130
6.3.4	Free energy of a kink	135
6.3.5	WLC under large tension	143
6.3.6	Discussion	144
6.4	Kinks in confined polymers	146

A Symmetries of the GRFs	152
A.1 Causality and time-translation invariance	152
A.2 Initial thermal equilibrium	155
Bibliography	159

Abstract

The mechanical properties of very small systems are often strikingly different from the properties of everyday objects. As one considers ever smaller objects, thermal fluctuations, and then quantum fluctuations, start to be important. In this thesis I explain some unusual nanoscale mechanical effects, and predict some new effects.

The bulk of the thesis is devoted to calculating the forces between bodies that are closely spaced, but not touching. These van der Waals forces have been studied in detail for bodies in thermal equilibrium. Most of the world is not in thermal equilibrium, and van der Waals forces in this regime are very different from their equilibrium cousins. In contrast to equilibrium forces, nonequilibrium forces are much stronger and may show chemical specificity. There is a *friction* associated with the van der Waals force between bodies in relative motion. When the bodies are at different temperatures, this friction may be negative. Intermolecular forces with one molecule excited are far stronger than ground-state forces and may be attractive or repulsive. Any optical effect in matter modifies the forces between the constituent molecules.

The second part of this thesis is on solitonic kinks in fibrillar materials (e.g. polymers, actin bundles, microtubules, carbon nanotubes). All of these materials may support stable kinks, and these kinks play an important role in determining the mechanical properties; often more important than the detailed chemical makeup of the materials.

Acknowledgements

I have been extremely fortunate to have many energetic, helpful, and kind collaborators over the course of this project. Professors L. Mahadevan and Shaul Mukamel each took me in when I appeared at their doorsteps. They devoted countless hours to explaining the basics of their respective fields, pointing out references, and brainstorming new ideas.

I thank Dr. Anton Middelberg in Chemical Engineering and Dr. Giles Davies in Semiconductor Physics (now at Leeds) for supporting my experimental efforts; Christoph Wälti, André Germishuizen, Rene Wirtz, Alessandro Rospigliosi in the bioproducts and nanotechnology group for many discussions about DNA; Prof. Mark Warner and James Adams for talking to me about solitons; my friends in Trinity for making it fun to stay in Cambridge and hard to leave.

Finally I thank Prof. Michael Pepper for encouraging me to explore new ideas and supporting my academic wanderings.

Thanks to the Marshall Foundation, Hertz Foundation, and Trinity College for financial support.

Cambridge, England

Adam Cohen

Introduction

This thesis is a theoretical examination of some unusual mechanical effects that occur in very small objects (ranging in size from single atoms to cellular organelles). The problems studied range from atomic collisions to the shape of an organelle in the sperm of horseshoe crabs. The solutions are united by a common approach: I strive to use as few material parameters as possible while preserving the essential physics. This often means identifying quasiparticle modes whose motion encompasses that of a great many degrees of freedom. This analytical approach runs counter to current trends in massive atomistic simulations. What is lost in detail is gained in understanding.

The first two chapters are devoted to formalism. The question is: given two quantum systems with unknown properties, is it possible to perform a set of measurements on the individual systems from which one can predict the outcome of a measurement when the two systems interact with each other? The answer to this question is yes, provided one allows a sufficiently broad class of measurements on the individual systems. I present a simple procedure for calculating the properties of a coupled quantum system in terms of properties of its constituent parts.

Chapters 3, 4, and 5 apply the formalism to the problem of intermolecular forces in systems far from thermodynamic equilibrium. In Chapter 3 I consider two molecules at different temperatures and subject to a time-dependent coupling. The van der

Waals force may be dramatically enhanced when molecules are at different temperatures, and the force is dissipative for molecules in relative motion. Perhaps the most surprising result of this thesis is that under certain conditions of temperature and molecular structure, the van der Waals friction may become *negative*. Negative friction does not violate the laws of thermodynamics, because it always occurs in systems simultaneously in contact with hot and cold reservoirs.

Chapter 4 is on the force between two molecules, one of which is excited. The force may be attractive or repulsive, and is far stronger than the ground-state van der Waals force. I suggest a simple interpretation of excited-state forces, which provides a framework for interpreting well-known phenomena such as concentration-quenching, and suggests ways of using optical or chemical excitation to direct the assembly of nanoscale objects.

Any optical effect in matter at finite density modifies the forces between the constituent molecules. This is because the same electrons mediate the optical response and provide for the long-range intermolecular forces. In Chapter 5 I develop a method to calculate the intermolecular force accompanying an arbitrary optical process. In the dark, the theory reproduces the ground-state van der Waals force. Previous attempts to develop such a theory are shown to be incorrect.

The last chapter is largely independent of the rest of the thesis. I study four examples of fibrillar nanomaterials (the *Limulus* acrosome, multiwalled carbon nanotubes, DNA in an AC electric field, and a polymer in a confined geometry), and show how sine-Gordon solitons arise in each. These sine-Gordon solitons play an important role in determining the mechanical properties of the materials. This last chapter and the rest of the thesis share a common ancestor, but divergent evolution has rendered the

link obscure. Rather than trying to forge an artificial link, I present this chapter as an interesting diversion.

All of the topics addressed in this thesis are my own ideas, but I benefited greatly from interactions with Prof. L. Mahadevan in DAMTP and Prof. Shaul Mukamel at the University of Rochester, NY. Professor Mahadevan early on encouraged me to work on fibrillar materials. Section 6.2 on kinks in the *Limulus* acrosome and multiwalled carbon nanotubes is the result of our collaboration. Professor Mukamel introduced me to Liouville space superoperators and provided many helpful comments on the material in Chapters 1-5.

The work on kinks in polymers was inspired by experiments on AC dielectrophoresis of DNA conducted by André Germishuizen and Dr. Christoph Wälti working in the Chemical Engineering department under Dr. Anton Middelberg. The theoretical development of the kink-gas and loop-gas models of polymers (Sections 6.3 and 6.4) was done essentially in isolation, although after I had completed it Prof. Mark Warner and James Adams provided many useful comments.

The papers describing the work in this thesis are:

- A. Cohen and S. Mukamel, “A Mechanical Force Accompanies Fluorescence Resonance Energy Transfer (FRET),” *J. Phys. Chem. A*, **107** (19), 3633-3638, 15 May 2003.
- A. Cohen and L. Mahadevan, “Kinks, Rings, and Rackets in Filamentous Structures,” *Proc. Natl. Acad. Sci. USA*, **100**, 12141-12146, 14 Oct. 2003.
- A. Cohen and S. Mukamel, “Resonant Enhancement and Dissipation in Nonequilibrium van der Waals Forces,” *Phys. Rev. Lett.*, **91**, 233202, 5 Dec. 2003.

- A. Cohen, “Force-Extension Curve of a Polymer in a High-Frequency Electric Field,” *Phys. Rev. Lett.*, **91**, 235506, 5 Dec. 2003.
- A. Cohen, “Statistical Mechanics of a Polymer in a High Frequency Electric Field”, *to be submitted*.

Over the past two years I also wrote two items that are not discussed in this thesis:

- A. Cohen, “Carbon Nanotubes Provide a Charge,” *Science* (Letter to the Editor), **300** (5623): 1235, May 23 2003.
- A. Cohen, C. T. Black, R. Sandstrom, C. B. Murray, “Scanning Probe Microscopy Tips Composed of Nanoparticles and Methods to form Same” U.S. Patent Pending.

Chapter 1

Generalized Response Functions (GRFs)

We consider an arbitrary quantum system subject to a perturbation. The change in the expectation value of an internal coordinate may be calculated using linear and nonlinear response functions. In a classical system at zero temperature, each coordinate has a well-defined value, so the response functions provide a complete description of the system. In a quantum system or a classical ensemble at finite temperature, correlations between coordinates have a life independent of the expectation values of the individual coordinates. Generalized response functions (GRFs) give the change in the *correlations* induced by a perturbation. The GRFs characterize all measurable aspects of a quantum system at finite temperature, and have simple expressions in terms of time-ordered products of Liouville space superoperators. In the following chapter we express the GRFs of a composite quantum system in terms of the GRFs of its constituent parts.

1.1 Introduction

When dealing with a complex quantum system, it is often impractical to solve the time-dependent Schrödinger equation analytically, or even on a computer. This is not such a tragedy, because the wavefunction, $|\Psi(t)\rangle$, is rarely of interest. The quantities of interest are observables, given by the expectation value of a Hermitian operator, B . The process of computing the expectation value, $\langle\Psi|B|\Psi\rangle$, discards most of the information in the wavefunction.

To avoid unnecessary computation, it is often advisable to work directly with the equation of motion for the observable. The closed time path Green function (CTPGF) formalism of Schwinger [166] and Keldysh [95] does just this. The fundamental objects of this formalism are multitime correlation functions of Hermitian operators in Hilbert space. Judiciously chosen linear combinations of these correlation functions give the response of an observable. Hao and coworkers applied the CTPGF formalism to calculate nonlinear response functions [80, 116, 117]. For an extensive review of the CTPGF, see [35].

In most real systems, the observable of interest depends on only a small number of modes, but these modes are coupled to an infinite ensemble of modes in the environment. In condensed matter, the environmental modes correspond to phononic, conformational, and orientational degrees of freedom, but even for molecules in vacuum it is impossible to escape the continuum of vacuum radiation modes, which are responsible for spontaneous emission and the Lamb shift. It is generally undesirable (and also impossible) to calculate the evolution of the full density matrix of the system and bath. The bath may be incorporated by switching from Hilbert space to Liouville space. In Liouville space one may write reduced equations of motion that

include the effect of the bath in a *self-energy*. Sophisticated techniques have been developed to calculate self-energies [137].

In this chapter we start with a purely mathematical review of nonlinear response theory. The *physics* is introduced when we calculate the nonlinear response functions in terms of multitime correlation functions of Liouville space superoperators. By reformulating the closed time path Green function formalism with superoperators in Liouville space, we calculate response functions that include the role of the bath via a self energy. Then we generalize the concept of response functions to include changes in the fluctuations of a quantity brought on by a perturbation. Many of the familiar properties of linear and nonlinear response functions also apply to generalized response functions.

1.2 Nonlinear response functions

Consider a causal system with a set of internal coordinates $\{q_i\}$ and subject to a set of perturbing forces, $\{f_j(t)\}$. The most general expression relating the expectation value of a particular coordinate, $\langle q_i(t) \rangle$, to the forces at past times is the Volterra series

$$\langle q_i(t) \rangle = \langle q_i \rangle_0 + \int_{-\infty}^t R_{ij}^{(1)}(t, t_1) f_j(t_1) + \int_{-\infty}^t dt_2 \int_{-\infty}^{t_2} dt_1 R_{ijk}^{(2)}(t, t_2, t_1) f_j(t_2) f_k(t_1) + \dots, \quad (1.1)$$

where $\langle q_i \rangle_0$ is the expectation value in the unperturbed state, $R^{(n)}$ are as-yet-unknown response functions, and summation over repeated indices j, k, \dots is implied. We now define

$$R^{(n)}(t, t_n, \dots, t_1) = 0 \text{ if } \max(t_n, \dots, t_1) > t, \quad (1.2)$$

so that the upper limits of integration in Eq. 1.1 may be set to $+\infty$.

When a system is initially in a steady state, then the response depends only on the *intervals*, $\tau_1 \equiv t - t_1$, $\tau_2 \equiv t - t_2, \dots$. The n^{th} order term in Eq. 1.1 may then be rewritten as

$$\langle q_i^{(n)}(t) \rangle = \int_0^\infty d\tau_n \cdots \int_0^\infty d\tau_1 G_{ij\dots l}^{(n)}(\tau_n, \dots, \tau_1) f_j(t - \tau_n) \cdots f_l(t - \tau_1), \quad (1.3)$$

where the Green function is defined

$$G^{(n)}(\tau_n, \dots, \tau_1) \equiv R^{(n)}(0, -\tau_n, \dots, -\tau_1), \quad (1.4)$$

and the causality condition is

$$G^{(n)}(\tau_n, \dots, \tau_1) = 0 \text{ if } \min(\tau_n, \dots, \tau_1) < 0, \quad (1.5)$$

Taking the Fourier transform of Eq. 1.3 yields ¹

$$\langle \tilde{q}_i(\omega) \rangle = \langle q_i \rangle_0 \delta(\omega) + \chi_{ij}^{(1)}(\omega) \tilde{f}_j(\omega) + \int d\omega_2 \int d\omega_1 \chi_{ijk}^{(2)}(-\omega; \omega_2, \omega_1) \tilde{f}_j(\omega_2) \tilde{f}_k(\omega_1) + \dots, \quad (1.6)$$

where frequency-domain quantities are indicated with a ($\tilde{}$) and the n^{th} order susceptibility is defined

$$\chi^{(n)}(-\omega_s; \omega_n, \dots, \omega_1) \equiv \int_{-\infty}^\infty d\tau_n \cdots \int_{-\infty}^\infty d\tau_1 G^{(n)}(\tau_n, \dots, \tau_1) e^{i(\omega_n \tau_n + \dots + \omega_1 \tau_1)} \delta(\omega_s - \omega_n - \dots - \omega_1). \quad (1.7)$$

In the field of nonlinear optics, the first three susceptibilities are often denoted $\alpha(\omega)$, $\beta(-\omega; \omega_2, \omega_1)$, and $\gamma(-\omega; \omega_3, \omega_2, \omega_1)$, respectively.

For $n \geq 2$, there exist many different n^{th} order response functions that when plugged into the r.h.s. of Eq. 1.1 yield the same l.h.s. The $R^{(n)}$ defined in Eq. 1.1

¹Throughout this thesis we use the Fourier convention $\tilde{A}(\omega) = \frac{1}{2\pi} \int_{-\infty}^\infty dt A(t) e^{i\omega t}$ and $A(t) = \int_{-\infty}^\infty d\omega \tilde{A}(\omega) e^{-i\omega t}$.

is known as the *symmetric kernel* [158]. Another commonly used convention is the *triangular kernel*, defined by

$$\langle q_i^{(n)}(t) \rangle = \int_{-\infty}^t dt_n \cdots \int_{-\infty}^{t_2} dt_1 \mathcal{R}_{ij\dots l}^{(n)}(t, t_n, \dots, t_1) f_j(t_n) \cdots f_l(t_1). \quad (1.8)$$

The difference between Eq. 1.1 and 1.8 is in the limits of integration. The symmetric kernel is invariant under a permutation of any of its last n time arguments accompanied by the same permutation of its indices. Each term in Eq. 1.1 goes through all $n!$ sequences of the time-ordering, and thus has $n!$ identical contributions. In Eq. 1.8 we selected the single time-ordering in which $t \geq t_n \geq \dots \geq t_1$. We now define $\mathcal{R}^{(n)}$ to be zero if its time-arguments are not in this sequence, so that the upper limits of integration in Eq. 1.8 may also be set to $+\infty$. The symmetric and triangular kernels are related by

$$R^{(n)}(t, t_n, \dots, t_1) = \frac{1}{n!} \sum_p \mathcal{R}^{(n)}(t, t_n, \dots, t_1), \quad (1.9)$$

where the sum is over all $n!$ permutations of the last n time arguments of $\mathcal{R}^{(n)}$. In a time-translation invariant system, the triangular kernel is associated with a Green function which gives the response via

$$\langle q_i^{(n)}(t) \rangle = \int_0^\infty d\tau_n \cdots \int_0^\infty d\tau_1 \mathcal{G}_{ij\dots l}^{(n)}(\tau_n, \dots, \tau_1) f_j(t-\tau_n) \cdots f_l(t-\tau_n-\dots-\tau_1). \quad (1.10)$$

The existence of multiple ways to define the nonlinear response has occasionally caused confusion. In this thesis $R^{(n)}$ always refers to the symmetric kernel, $\mathcal{R}^{(n)}$ to the triangular kernel, $G^{(n)}$ to the symmetric Green function and $\mathcal{G}^{(n)}$ to the triangular Green function.

1.3 Superoperators in Liouville space

To imbue the response functions with physical meaning, we need to calculate the time-evolution of a quantum system subject to a time-dependent perturbation. Consider the Hamiltonian

$$H = H_0 + V(t), \quad (1.11)$$

where the reference Hamiltonian, H_0 is time-independent and the time-dependence of $V(t)$ arises from an externally driven classical source with $V(-\infty) = 0$. We will be interested in calculating the expectation value of some observable, B , given by $\langle B(t) \rangle$.

The following notation will be used. The expectation value of an operator, $\langle A \rangle$, is defined $\langle A \rangle \equiv \text{Tr}\{A\rho\}$, where ρ is the density matrix. When the expectation value is written $\langle \dots \rangle_0$ we are to use the unperturbed density matrix, ρ_0 , of the equilibrium system at time $-\infty$.

We introduce Liouville space superoperators and review some of their useful properties. A fuller review is given in [138]. The elements of an $n \times n$ density matrix in Hilbert space are arranged as a vector of length n^2 in Liouville space. The ordering of elements is inconsequential provided a consistent convention is adopted. A superoperator in Liouville space can be represented by a matrix of dimensions $n^2 \times n^2$. The profusion of elements is no handicap because we will never write the matrix expression for a superoperator.

Multiplication by a superoperator can implement a much wider class of transformations on the density matrix than can multiplication by a regular operator. In particular, the commutator and anticommutator can each be implemented with a single multiplication by a Liouville space superoperator. For any Hilbert space operator

we define Liouville space superoperators A_+ , A_- , A_L and A_R by their action on another operator X :

$$\begin{array}{ll} \text{Liouville Space} & \text{Hilbert Space} \\ A_- X & \Leftrightarrow [A, X] \end{array} \quad (1.12a)$$

$$A_+ X \Leftrightarrow \frac{1}{2}(AX + XA), \quad (1.12b)$$

and

$$A_L X \Leftrightarrow AX \quad (1.13a)$$

$$A_R X \Leftrightarrow -XA. \quad (1.13b)$$

Relations 1.12 and 1.13 are not written as equalities because X is a vector in Liouville space and a matrix in Hilbert space. A series of \pm superoperators multiplied together implements a series of nested commutators and anticommutators in Hilbert space.

The L and R superoperators are related to the $+$ and $-$ superoperators by a simple linear transformation

$$A_- = A_L + A_R \quad (1.14a)$$

$$A_+ = \frac{1}{2}(A_L - A_R), \quad (1.14b)$$

and its inverse

$$A_L = A_+ + \frac{1}{2}A_- \quad (1.15a)$$

$$A_R = -A_+ + \frac{1}{2}A_-. \quad (1.15b)$$

The expectation value of a superoperator is obtained by evaluating the trace of the corresponding operator expression. For any operators A and X , the following useful

identities may be verified by applying the definitions of the superoperators and the invariance of the trace to a cyclic permutation of its arguments:

$$\langle AX \rangle = \langle A_+ X \rangle = \langle A_L X \rangle = - \langle A_R X \rangle \quad (1.16a)$$

$$\langle A_- X \rangle = 0. \quad (1.16b)$$

Whenever the leftmost superoperator in an expression is a $(-)$, the expectation value is zero because the trace of a commutator vanishes. The introduction of the $+$, $-$, L , R superoperators may seem like a notational complication, but they greatly simplify the expressions below.

We introduce two useful operators, \mathcal{T} and Θ , related to time-ordering in Liouville space. The time-ordering operator, \mathcal{T} , takes all the superoperators to its right and arranges them from left to right in order of decreasing time argument. Multiplying by \mathcal{T} on the left allows us to manipulate superoperators as numbers, e.g. replacing time-ordered exponentials by regular exponentials without worrying about commutations. The unit-step operator in Liouville space, Θ , is 1 if all the superoperators to its right are in a time-ordered sequence, and 0 otherwise.

The density matrix evolves under the Liouville equation:

$$\dot{\rho} = -\frac{i}{\hbar} H_- \rho. \quad (1.17)$$

In reduced descriptions (e.g. a molecule coupled to a bath) we relax the constraint that the *Liouvillian*, H_- , implements a commutator. Every Hamiltonian has a corresponding Liouvillian, but in reduced descriptions the Liouvillian has no corresponding Hamiltonian. Phenomena involving relaxation and dissipation can *only* be calculated in Liouville space.

The Liouville equation has the formal solution

$$\rho(t) = \mathcal{U}(t, -\infty)\rho_0, \quad (1.18)$$

where the Liouville space time evolution operator is

$$\mathcal{U}(t, -\infty) = \mathcal{T} \exp \left(-\frac{i}{\hbar} \int_{-\infty}^t H_-(t') dt' \right). \quad (1.19)$$

The expectation value of our observable, B is thus

$$\langle B(t) \rangle = \langle B_+ \mathcal{U}(t, -\infty) \rangle_0. \quad (1.20)$$

Assuming we can solve for, or measure, the dynamics subject to H_0 alone, it makes sense to treat the term H_0 explicitly and $V(t)$ as a perturbation. This is accomplished by switching to the *interaction picture*. Superoperators in the interaction picture (denoted with a $\hat{\ }(\)$) are related to their counterparts in the Schrödinger picture by:

$$\hat{B}_+(t) \equiv \exp \left(\frac{i}{\hbar} H_0 t \right) B_+ \exp \left(-\frac{i}{\hbar} H_0 t \right) \quad (1.21a)$$

$$\hat{V}_-(t') \equiv \exp \left(\frac{i}{\hbar} H_0 t' \right) V_-(t') \exp \left(-\frac{i}{\hbar} H_0 t' \right), \quad (1.21b)$$

so that the time-evolution superoperator in the interaction picture becomes

$$\hat{\mathcal{U}}(t, -\infty) = \mathcal{T} \exp \left(-\frac{i}{\hbar} \int_{-\infty}^t \hat{V}_-(t') dt' \right). \quad (1.22)$$

The expectation value $\langle B(t) \rangle$ is given by

$$\langle B(t) \rangle = \left\langle \hat{B}_+(t) \hat{\mathcal{U}}(t, -\infty) \right\rangle_0. \quad (1.23)$$

Eq. 1.23 is typically evaluated by expanding $\hat{\mathcal{U}}(t, -\infty)$ in a power series in \hat{V}_- , so $\langle B(t) \rangle = \langle B^{(0)}(t) \rangle + \langle B^{(1)}(t) \rangle + \dots$. The n^{th} term in this series is

$$\langle B^{(n)}(t) \rangle = \frac{1}{n!} \left(\frac{-i}{\hbar} \right)^n \int_{-\infty}^t dt_n \cdots \int_{-\infty}^t dt_1 \left\langle \mathcal{T} \hat{B}_+(t) \hat{V}_-(t_n) \cdots \hat{V}_-(t_1) \right\rangle_0 \quad (1.24)$$

Outside the indicated domain of integration in Eq. 1.24, the \mathcal{T} guarantees that the leftmost superoperator in the brackets is a $(-)$. The integrand then goes to zero because the trace of a commutator vanishes (Eq. 1.16b). Thus the limits of integration may be set to $\pm\infty$, with the burden on the integrand to be zero wherever appropriate.

To relate Eq. 1.24 to the definition of the response function (Eq. 1.1), consider a system with a set of internal coordinates, $\{q_i\}$. The observable of interest is the displacement of one coordinate, $\langle q_i(t) \rangle$. Any perturbation that acts linearly on the coordinates can be decomposed as $V(t) = -\sum_j f_j(t)q_j$, where $f_j(t)$ are scalars corresponding to classical external forces and the initial $(-)$ is a convention. We may take the $f_j(t)$ outside of the expectation value, so that

$$\begin{aligned} \langle q_i^{(n)}(t) \rangle &= \frac{1}{n!} \left(\frac{i}{\hbar} \right)^n \int_{-\infty}^t dt_n \cdots \int_{-\infty}^t dt_1 \langle \mathcal{T} \hat{q}_{i+}(t) \hat{q}_{j-}(t_n) \cdots \hat{q}_{l-}(t_1) \rangle_0 \\ &\quad \times f_j(t_n) \cdots f_l(t_1), \end{aligned} \quad (1.25)$$

where, as before, summation over repeated indices is implied. Comparison of Eq. 1.25 with Eq. 1.1 yields the response function:

$$\boxed{R_{i,j,\dots,l}^{(n)}(t, t_n, \dots, t_1) = \frac{1}{n!} \left(\frac{i}{\hbar} \right)^n \langle \mathcal{T} \hat{q}_{i+}(t) \hat{q}_{j-}(t_n) \cdots \hat{q}_{l-}(t_1) \rangle_0.} \quad (1.26)$$

Eq. 1.26 is the most compact and useful expression of the response function, so we comment on its structure. A $(+)$ superoperator can be thought of as implementing a measurement and a $(-)$ superoperator can be thought of as implementing a perturbation by an external source. The general structure of a response function is a $(+)$ at the measurement time, followed by a series of $(-)$'s at the interaction times.

Eq. 1.26 can also be written in the L, R representation by making the substitutions

$\hat{q}_+ \rightarrow \hat{q}_L$ (Eq. 1.16a) and $\hat{q}_- \rightarrow \hat{q}_L + \hat{q}_R$ (Eq. 1.14a), so that

$$R_{i,j,\dots,l}^{(n)}(t, t_n, \dots, t_1) = \frac{1}{n!} \left(\frac{i}{\hbar} \right)^n \sum_{\{\eta_\alpha\}} \langle \mathcal{T} \hat{q}_{iL}(t) \hat{q}_{j\eta_n}(t_n) \dots \hat{q}_{l\eta_1}(t_1) \rangle_0 \quad \eta_\alpha = L, R, \quad (1.27)$$

where the sum is over all 2^n sequences $\{\eta_n, \dots, \eta_1\}$. Each such sequence is called a *Liouville space pathway*. Double-sided Feynman diagrams provide a convenient way to calculate and keep track of Liouville space pathways [137].

The triangular kernel may also be extracted from Eq. 1.24. Evaluating the time-ordering operator cancels the initial factor of $\frac{1}{n!}$ and yields

$$\langle B^{(n)}(t) \rangle = \left(\frac{-i}{\hbar} \right)^n \int_{-\infty}^t dt_n \dots \int_{-\infty}^{t_2} dt_1 \langle \Theta \hat{B}_+(t) \hat{V}_-(t_n) \dots \hat{V}_-(t_1) \rangle_0, \quad (1.28)$$

whence the triangular kernel is

$$\mathcal{R}_{i,j,\dots,l}^{(n)}(t, t_n, \dots, t_1) = \left(\frac{i}{\hbar} \right)^n \langle \Theta \hat{q}_{i+}(t) \hat{q}_{j-}(t_n) \dots \hat{q}_{l-}(t_1) \rangle_0. \quad (1.29)$$

Eq. 1.29 is equivalent to the possibly more familiar Hilbert space expression:

$$\mathcal{R}_{i,j,\dots,l}^{(n)}(t, t_n, \dots, t_1) = \theta(t, t_n, \dots, t_1) \left(\frac{i}{\hbar} \right)^n \text{Tr} \{ \hat{q}_i(t) [\hat{q}_j(t_n), \dots, [\hat{q}_l(t_1), \rho_0]] \}, \quad (1.30)$$

where the multivariate Heaviside step function $\theta(t, t_n, \dots, t_1) = 1$ if $t > t_n > \dots > t_1$ and 0 otherwise. Hilbert space operators in the interaction picture are defined in analogy to Eq. 1.21, $\hat{q}(t) \equiv e^{iH_0 t/\hbar} q e^{-iH_0 t/\hbar}$.

1.4 Multitime observables

We now introduce a generalization of the response function formalism. First some comments about measurements. We somewhat cavalierly associated the *physical*

operation of taking a measurement with the *mathematical* operation of calculating $\langle q_i(t) \rangle \equiv \text{Tr}\{q_i\rho(t)\}$. What does this mean?

A quantum system may exist in a superposition of states, so measuring an expectation value, $\langle \Psi(t)|q_i|\Psi(t) \rangle$, does not completely specify the state. A classical ensemble at finite temperature may exist in any of a great many microstates, so measuring an ensemble average, $\overline{q_i(t)}$, does not completely specify the state—even if q_i is a classical variable. When we construct a Liouville operator that includes a self-energy, the resulting density matrix, $\rho(t)$, already includes the ensemble average. Calculating $\text{Tr}\{q_i\rho(t)\}$ takes an expectation value in a double sense: it is the ensemble average of the quantum expectation value of q_i . Both types of averaging discard information.

We can regain some of the lost information from measurements of correlations between coordinates, $\langle q_i(t_2)q_j(t_1) \rangle$, $\langle q_i(t_3)q_j(t_2)q_k(t_1) \rangle$, etc. Measurements of fluctuations constitute a special class of correlation measurements, where $i = j = \dots$ and $t_1 = t_2 = \dots$. As an example of the usefulness of correlation measurements, let the coordinate q describe the displacement of a particle in a 1-dimensional harmonic well. A measurement of $\langle q \rangle$ yields zero, which is not very informative. However, a measurement of $\langle q^2 \rangle$ tells us the steepness of the potential. This is true for a quantum system at zero temperature, a classical ensemble at finite temperature, and a quantum ensemble at finite temperature. Because these multitime correlation functions provide additional information about our system, we would like to know how they change in response to a perturbation.

It is necessary to exercise caution in defining multitime observables. A product of Hilbert space Hermitian operators, such as $\hat{q}_i(t_n) \dots \hat{q}_j(t_1)$, is not necessarily Hermitian and thus may not correspond to an observable. However, the Liouville space

quantity $\mathcal{T}\hat{q}_{i+}(t_n)\dots\hat{q}_{j+}(t_1)$ is Hermitian and also symmetric under interchange of its time arguments. Thus we take time-ordered products of (+) superoperators as our multitime observables.

The two-time correlation function of operators A and B is

$$\langle \mathcal{T}\hat{A}_+(t_a)\hat{B}_+(t_b) \rangle = \langle \mathcal{T}\hat{A}_+(t_a)\hat{\mathcal{U}}(t_a, t_b)\hat{B}_+(t_b)\hat{\mathcal{U}}(t_b, -\infty) \rangle_0 \quad (1.31a)$$

$$= \langle \mathcal{T}\hat{A}_+(t_a)\hat{B}_+(t_b)\hat{\mathcal{U}}(t_a, -\infty) \rangle_0. \quad (1.31b)$$

In going from Eq. 1.31a to Eq. 1.31b we switched the order of $\hat{B}_+(t_b)$ and $\hat{\mathcal{U}}(t_a, t_b)$ (allowed by the \mathcal{T}), and then used the identity $\hat{\mathcal{U}}(t_a, t_b)\hat{\mathcal{U}}(t_b, -\infty) = \hat{\mathcal{U}}(t_a, -\infty)$. As with the single-time measurements, Eq. 1.31b is evaluated by expanding $\hat{\mathcal{U}}$ (Eq. 1.22) in powers of $\hat{V}_-(t')$. The series expansion is

$$\begin{aligned} \langle \mathcal{T}\hat{A}_+(t_a)\hat{B}_+(t_b) \rangle &= \langle \mathcal{T}\hat{A}_+(t_a)\hat{B}_+(t_b) \rangle_0 + \left(\frac{-i}{\hbar}\right) \int dt_1 \langle \mathcal{T}\hat{A}_+(t_a)\hat{B}_+(t_b)\hat{V}_-(t_1) \rangle_0 \\ &\quad + \frac{1}{2!} \left(\frac{-i}{\hbar}\right)^2 \int dt_2 \int dt_1 \langle \mathcal{T}\hat{A}_+(t_a)\hat{B}_+(t_b)\hat{V}_-(t_2)\hat{V}_-(t_1) \rangle_0 \\ &\quad + \dots \end{aligned} \quad (1.32)$$

It is not necessary to specify the limits of integration in Eq. 1.32 because the \mathcal{T} operator guarantees that the integrand is zero for $\max(t_2, t_1) > \max(t_a, t_b)$.

The response of a three-point correlation function may similarly be expanded as

$$\begin{aligned} \langle \mathcal{T}\hat{A}_+(t_a)\hat{B}_+(t_b)\hat{C}_+(t_c) \rangle &= \langle \mathcal{T}\hat{A}_+(t_a)\hat{B}_+(t_b)\hat{C}_+(t_c) \rangle_0 + \\ &\quad \left(\frac{-i}{\hbar}\right) \int dt_1 \langle \mathcal{T}\hat{A}_+(t_a)\hat{B}_+(t_b)\hat{C}_+(t_c)\hat{V}_-(t_1) \rangle_0 + \\ &\quad \frac{1}{2!} \left(\frac{-i}{\hbar}\right)^2 \int dt_2 \int dt_1 \langle \mathcal{T}\hat{A}_+(t_a)\hat{B}_+(t_b)\hat{C}_+(t_c)\hat{V}_-(t_2)\hat{V}_-(t_1) \rangle_0 \\ &\quad + \dots \end{aligned} \quad (1.33)$$

The equivalent Hilbert space expressions are far more involved because the integrals

must be broken into separate branches corresponding to each ordering of the time-arguments.

For a system where the perturbation may be decomposed as $V(t) = -\sum_j q_j f_j(t)$, we define the generalized response functions (GRFs)

$$R_{i,j}^{+-}(t_2, t_1) = \left(\frac{i}{\hbar}\right) \langle \mathcal{T} \hat{q}_{i+}(t_2) \hat{q}_{j-}(t_1) \rangle_0 \quad (1.34a)$$

$$R_{i,j}^{++}(t_2, t_1) = \langle \mathcal{T} \hat{q}_{i+}(t_2) \hat{q}_{j+}(t_1) \rangle_0, \quad (1.34b)$$

$$R_{i,j,k}^{+--}(t_3, t_2, t_1) = \frac{1}{2!} \left(\frac{i}{\hbar}\right)^2 \langle \mathcal{T} \hat{q}_{i+}(t_3) \hat{q}_{j-}(t_2) \hat{q}_{k-}(t_1) \rangle_0 \quad (1.35a)$$

$$R_{i,j,k}^{++-}(t_3, t_2, t_1) = \left(\frac{i}{\hbar}\right) \langle \mathcal{T} \hat{q}_{i+}(t_3) \hat{q}_{j+}(t_2) \hat{q}_{k-}(t_1) \rangle_0 \quad (1.35b)$$

$$R_{i,j,k}^{+++}(t_3, t_2, t_1) = \langle \mathcal{T} \hat{q}_{i+}(t_3) \hat{q}_{j+}(t_2) \hat{q}_{k+}(t_1) \rangle_0, \quad (1.35c)$$

and so on. The prefactor for each GRF is $\frac{1}{n_-!} \left(\frac{i}{\hbar}\right)^{n_-}$, where n_- is the number of $(-)$ superoperators in the multitime correlation function. The GRFs tell us how a perturbation affects correlations within the system. The series expansions of a one-, two-, and 3-point correlation function are:

$$\begin{aligned} \langle q_i(t) \rangle &= \langle q_i \rangle_0 + \int dt_1 R_{i,j}^{+-}(t, t_1) f_j(t_1) + \\ &\int dt_2 \int dt_1 R_{i,j,k}^{+--}(t, t_2, t_1) f_j(t_2) f_k(t_1) + \dots \end{aligned} \quad (1.36a)$$

$$\begin{aligned} \langle \mathcal{T} \hat{q}_{i+}(t_b) \hat{q}_{j+}(t_a) \rangle &= R_{i,j}^{++}(t_b, t_a) + \int dt_1 R_{i,j,k}^{++-}(t_b, t_a, t_1) f_k(t_1) + \\ &\int dt_2 \int dt_1 R_{i,j,k,l}^{+++-}(t_b, t_a, t_2, t_1) f_k(t_2) f_l(t_1) + \dots \end{aligned} \quad (1.36b)$$

$$\begin{aligned} \langle \mathcal{T} \hat{q}_{i+}(t_c) \hat{q}_{j+}(t_b) \hat{q}_{k+}(t_a) \rangle &= R_{i,j,k}^{+++}(t_c, t_b, t_a) + \int dt_1 R_{i,j,k,l}^{+++-(t_c, t_b, t_a, t_1) f_l(t_1) + \\ &\int dt_2 \int dt_1 R_{i,j,k,l,m}^{++++-(t_c, t_b, t_a, t_2, t_1) f_l(t_2) f_m(t_1) \\ &+ \dots, \end{aligned} \quad (1.36c)$$

where summation over repeated indices is implied. Henceforth we omit the coordinate indices i, j, k, \dots

Time-ordered Liouville space correlation functions of the form $+-$, $+-$, $+-$, etc. are related to response functions, $R^{(n)}$; correlation functions of the form $++$, $+++$, $++++$, etc. are related to fluctuations in the initial state; and correlation functions of the form $++-$, $++--$, $+++$, $++++$, etc. are related to changes in the fluctuations brought on by a perturbation.

Appendix A has a discussion of the symmetry properties of the GRFs in the time domain and in the frequency domain.

Chapter 2

Two-Body Interactions

In the previous chapter we showed that generalized response functions (GRFs) provide a compact description of an open quantum system subject to a perturbation. In this chapter we consider two quantum systems interacting with each other and with a bath. The GRFs of the coupled system are expressed in terms of the GRFs of the individual components.

2.1 Introduction

Computing the time-evolution of a system composed of many interacting particles is a difficult problem in both classical and quantum physics. Standard perturbation theory provides one approach by expressing the eigenstates of the coupled system in terms of the eigenstates of the isolated systems. Response functions of the interacting system can then be expressed as sums over states. However, there are several reasons to work directly with response functions, making no reference to eigenstates. 1) Application of perturbation theory presupposes a knowledge of the eigenstates of the isolated systems, but experiments probe response functions. 2) Standard perturbation

theory is unable to accommodate degrees of freedom associated with a thermal bath without treating them explicitly. For systems coupled to a bath, eigenstates are not good variables but response functions are. 3) The computational effort required to calculate single-particle response functions (via e.g. time-dependent density functional theory) is less than that required to calculate eigenstates. 4) The formulation in terms of response functions has a clear semiclassical dynamical interpretation. It provides model-independent results, which may then be applied either to models of single-particle response functions or to experimental measurements of such quantities.

Response-function formulations of many-body theory have been developed at varying levels of approximation. One popular approach is to focus on a limited number of degrees of freedom, the “particle”, and to treat the rest of the system as a “bath.” The designation of particle and bath is formally arbitrary, but makes a big difference in practice. Once this designation is made, projection operator techniques allow one to formulate reduced equations of motion for the particle, in which the interaction with the bath is incorporated through a complex self-energy in an effective Hamiltonian. This procedure is exact with respect to the particle, but sacrifices information about the state of the bath.

Willis and Picard developed a more symmetric treatment for the time evolution of two particles interacting with each other and with a bath [200, 145]. They wrote a reduced equation of motion for the direct product of the single particle density matrices, that includes the interparticle correlations in an effective Hamiltonian. However, this procedure renders the information about correlations inaccessible: the joint density matrix contains more information than the direct-product of the single-particle

density matrices. Thus the method of Willis and Picard can only calculate single-particle observables. Dispersion forces, which depend on interparticle correlations, cannot be calculated by this method.

Another common approach is to write the field at each particle as the sum of applied fields and the fields due to its neighbors. The fields can then be found self-consistently in terms of single-particle response functions. This technique is called the local field approximation (LFA). When a system consists of many identical particles, it is commonplace to focus on one, and to introduce an average field due to all the other particles. This mean-field approximation is the basis of the Clausius-Mossotti model of dielectrics, the Curie-Weiss model of ferromagnetism, and the Hartree and Hartree-Fock approaches to electronic structure. Local field techniques are approximate because they treat the polarization of each particle as a classical quantity with a single well-defined value, when the polarization is actually an operator. The LFA reproduces many aspects of interacting systems, but misses some important effects due to correlations. Even if the system starts with no correlations (i.e. its density matrix can be expressed as a direct product of single-particle density matrices) the interactions between particles lead to correlations at later times.

In this chapter I develop a perturbation theory for the time-evolution of two interacting systems that is formally exact, that treats both systems on an equal footing, and that relates joint observables of the coupled system to single-particle observables of the isolated systems. This procedure includes the effects of correlations in the time-evolution and allows one to calculate observables that depend on correlations. The price of keeping this additional information is that the time-evolution can only be expressed as an infinite series. However, for many physical systems this series can

be truncated at low order.

The starting point of my theory is a density matrix that at time $-\infty$ was in a direct-product state. The Liouville space time-evolution operator transforms this state into a correlated state. However, I show how to factorize the time-evolution operator into a sum of terms that individually preserve the purity of the direct-product form. The terms that act in the single-particle space are the generalized response functions (GRFs) calculated in Chapter 1. This result provides a systematic procedure for adding quantum corrections to the local field approximation.

In chapters 3, 4, and 5 we apply this technique to study intermolecular forces.

2.2 Factorization of two-body response function

The Hamiltonian of two interacting systems, a and b , can always be partitioned as:

$$H = H_a(\mathbf{Q}_a) + H_b(\mathbf{Q}_b) + H_{ab}(\mathbf{Q}_a, \mathbf{Q}_b, t), \quad (2.1)$$

where $\mathbf{Q}_j \equiv (\mathbf{q}_j, \mathbf{p}_j)$, is the vector of the generalized coordinates, \mathbf{q}_j , and momenta \mathbf{p}_j , of system j ($j = a, b$). The Hamiltonians of the individual systems, H_a and H_b , are time-independent. The perturbation, $H_{ab}(\mathbf{Q}_a, \mathbf{Q}_b, t)$, includes interactions between the two systems as well as any time-dependent driving force on either system. Interaction between each system and a bath may be included in H_a and H_b , provided that the two baths are uncorrelated. For convenience we refer to the two systems as “molecules” a and b , but it should be noted that the derivation is completely general: the systems could be a molecule and the radiation field, electronic and nuclear coordinates within a molecule, two nuclear spins, etc.

We wish to express the linear and nonlinear response functions of any operator, $B_{ab}(\mathbf{Q}_a, \mathbf{Q}_b)$, to an arbitrary perturbation, $H_{ab}(\mathbf{Q}_a, \mathbf{Q}_b, t)$, in terms of the response functions of single-molecule Hermitian operators, $B_a(\mathbf{Q}_a)$ and $B_b(\mathbf{Q}_b)$, to single-molecule perturbations $V_a(\mathbf{Q}_a, t)$ and $V_b(\mathbf{Q}_b, t)$.

The time-evolution of B_{ab} is given by (Eqs. 1.22 and 1.23)

$$\langle B_{ab}(t) \rangle = \left\langle \mathcal{T} \hat{B}_{ab+}(t) \exp \left(-\frac{i}{\hbar} \int_{-\infty}^t \hat{H}_{ab-}(t') dt' \right) \right\rangle_0, \quad (2.2)$$

where quantities with a $(\hat{\ })$ are expressed in the interaction picture (Eq. 1.21), with $H_0 \equiv H_a + H_b$. The initial density matrix, ρ_0 is assumed to be a direct product of the noninteracting steady state density matrices of the individual molecules, ρ_{a0} and ρ_{b0} . Expanding Eq. 2.2 in powers of \hat{H}_{ab-} yields the n^{th} order response of B_{ab} :

$$\langle B_{ab}^{(n)}(t) \rangle = \frac{1}{n!} \left(\frac{-i}{\hbar} \right)^n \int dt_n \cdots \int dt_1 \left\langle \mathcal{T} \hat{B}_{ab+}(t) \hat{H}_{ab-}(t_n) \cdots \hat{H}_{ab-}(t_1) \right\rangle_0. \quad (2.3)$$

We now express Eqs. 2.2 and 2.3, in terms of products of single-molecule GRFs. The perturbation $H_{ab}(\mathbf{Q}_a, \mathbf{Q}_b, t)$ and the observable $B_{ab}(\mathbf{Q}_a, \mathbf{Q}_b)$ are each expressed in a basis whose coordinates are direct products of single-molecule operators:

$$H_{ab}(\mathbf{Q}_a, \mathbf{Q}_b, t) = \sum_{i,j} c_{ij}(t) V_{ai}(\mathbf{Q}_a) V_{bj}(\mathbf{Q}_b) \quad (2.4a)$$

$$B_{ab}(\mathbf{Q}_a, \mathbf{Q}_b) = \sum_{i,j} d_{ij} B_{ai}(\mathbf{Q}_a) B_{bj}(\mathbf{Q}_b) \quad (2.4b)$$

The decomposition of Eq. 2.4 is not unique; in fact any convenient basis in phase space may be chosen. For instance, in Chapter 3 we show how the nonretarded interaction Hamiltonian for two molecules with nonoverlapping charge distributions can be expressed in terms of charge density operators [129], dipole density operators [49], or electric multipole operators [86]. Each expression is naturally in the form of Eq. 2.4. When carried to infinite order, all expansions of the Hamiltonian yield

identical results. However, the sum in Eq. 2.4 is typically truncated and the physical approximation implied by this truncation depends on the basis. External forcing of one particle, (e.g. by classical radiation) may also be included in this expansion: the operator for the noninteracting particle is simply the identity matrix.

To keep the notation simple, we assume Eqs. 2.4a and 2.4b each have only a single term, so $H_{ab} = -c(t)V_a(\mathbf{Q}_a)V_b(\mathbf{Q}_b)$ and $B_{ab} = B_a(\mathbf{Q}_a)B_b(\mathbf{Q}_b)$. There is no conceptual difficulty in extending the results to multiple terms in each sum. Converting Eq. 2.4 to the interaction picture yields

$$\hat{H}_{ab}(t) = -c(t)\hat{V}_a(t)\hat{V}_b(t) \quad (2.5a)$$

$$\hat{B}_{ab}(t) = \hat{B}_a(t)\hat{B}_b(t). \quad (2.5b)$$

Because the operators on the r.h.s. of Eq. 2.5 each act in a single-molecule basis, their interaction picture only requires the single-molecule reference Hamiltonian. That is

$$\begin{aligned} \hat{V}_a(t) &\equiv \exp\left(\frac{i}{\hbar}H_a t\right)V_a \exp\left(-\frac{i}{\hbar}H_a t\right) \\ \hat{V}_b(t) &\equiv \exp\left(\frac{i}{\hbar}H_b t\right)V_b \exp\left(-\frac{i}{\hbar}H_b t\right), \end{aligned} \quad (2.6)$$

and similarly for $\hat{B}_a(t)$ and $\hat{B}_b(t)$.

Finally, products of ordinary operators may be converted into products of superoperators using the following identities:

$$\boxed{\begin{aligned} (XY)_- &= X_-Y_+ + X_+Y_- \\ (XY)_+ &= X_+Y_+ + \frac{1}{4}X_-Y_-, \end{aligned}} \quad (2.7)$$

which can easily be verified by applying the definitions of the superoperators. Thus

the Liouville superoperator becomes

$$\begin{aligned}\hat{H}_{ab-}(t) &= -c(t)[\hat{V}_a(t)\hat{V}_b(t)]_- \\ &= -c(t)[\hat{V}_{a+}(t)\hat{V}_{b-}(t) + \hat{V}_{a-}(t)\hat{V}_{b+}(t)]\end{aligned}\quad (2.8)$$

Similarly the observable B_{ab} becomes

$$\hat{B}_{ab+}(t) = \hat{B}_{a+}(t)\hat{B}_{b+}(t) + \frac{1}{4}\hat{B}_{a-}(t)\hat{B}_{b-}(t).\quad (2.9)$$

Because \hat{B}_{ab+} is the leftmost superoperator in Eqs. 2.2 and 2.3, all $(-)$ terms in its expansion vanish when the trace is evaluated. We are thus free to neglect the second half of Eq. 2.9. The expansion of \hat{H}_{ab-} has $(+)$ and $(-)$ terms, both of which must be kept.

Inserting Eqs. 2.8 and 2.9 into Eq. 2.2 yields

$$\boxed{\langle B_{ab}(t) \rangle = \left\langle \mathcal{T} \hat{B}_{a+}(t) \hat{B}_{b+}(t) \exp \left[\frac{i}{\hbar} \int_{-\infty}^t dt' c(t') [\hat{V}_{a+}(t') \hat{V}_{b-}(t') + \hat{V}_{a-}(t') \hat{V}_{b+}(t')] \right] \right\rangle_0}.\quad (2.10)$$

Eq. 2.10 is an exact formal expression and contains only single-molecule superoperators which act either only on system a or only on system b . As discussed in chapter 1, a $(+)$ superoperator corresponds to a measurement and a $(-)$ superoperator corresponds to a time-evolution of the density matrix. Thus the term $\hat{V}_{a+}(t')\hat{V}_{b-}(t')$ represents system b evolving under the influence of system a ; the term $\hat{V}_{a-}(t')\hat{V}_{b+}(t')$ represents system a evolving under the influence of system b .

Expanding the exponent in Eq. 2.10, the n^{th} order response can be written as a

sum of 2^n terms:

$$\begin{aligned} \langle B_{ab}^{(n)}(t) \rangle &= \frac{1}{n!} \left(\frac{i}{\hbar} \right)^n \int_{-\infty}^t dt_n \cdots \int_{-\infty}^t dt_1 \sum_{\{\nu_\alpha\}} \\ &\quad \left\langle \mathcal{T} [\hat{B}_{a+}(t) \hat{B}_{b+}(t)] [\hat{V}_{a\nu_n}(t_n) \hat{V}_{b\bar{\nu}_n}(t_n)] \cdots [\hat{V}_{a\nu_1}(t_1) \hat{V}_{b\bar{\nu}_1}(t_1)] \right\rangle_0 \\ &\quad c(t_n) \cdots c(t_1) \quad \nu_\alpha = +, -, \end{aligned} \quad (2.11)$$

where $\bar{\nu} \equiv -\nu$, and the sum is over all n -element sequence (ν_n, \dots, ν_1) .

The integrand of Eq. 2.11 has the structure of a response function, where the bimolecular coordinate $\langle B_{ab}(t) \rangle$, responds to the history of time-dependent intermolecular couplings, $c(t')$, with the symmetric kernel given by

$$R_{ab}^{(n)}(t, t_n, \dots, t_1) = \frac{1}{n!} \left(\frac{i}{\hbar} \right)^n \sum_{\{\nu_\alpha\}} \left\langle \mathcal{T} \hat{B}_{a+}(t) \hat{B}_{b+}(t) \hat{V}_{a\nu_n}(t_n) \hat{V}_{b\bar{\nu}_n}(t_n) \cdots \hat{V}_{a\nu_1}(t_1) \hat{V}_{b\bar{\nu}_1}(t_1) \right\rangle_0. \quad (2.12)$$

We have nearly accomplished our goal, because the superoperators inside the $\langle \cdots \rangle_0$ of Eq. 2.12 each act only on a or only on b . Because the initial density matrix is a direct product, we can factor the correlation function into a product of single-molecule correlation functions:

$$\begin{aligned} R_{ab}^{(n)}(t, t_n, \dots, t_1) &= \frac{1}{n!} \left(\frac{i}{\hbar} \right)^n \sum_{\{\nu_\alpha\}} \left(\left\langle \mathcal{T} \hat{B}_{a+}(t) \hat{V}_{a\nu_n}(t_n) \cdots \hat{V}_{a\nu_1}(t_1) \right\rangle_{a0} \times \right. \\ &\quad \left. \left\langle \mathcal{T} \hat{B}_{b+}(t) \hat{V}_{b\bar{\nu}_n}(t_n) \cdots \hat{V}_{b\bar{\nu}_1}(t_1) \right\rangle_{b0} \right). \end{aligned} \quad (2.13)$$

Thus the n^{th} order response of $\langle B_{ab} \rangle$ may be written as a sum of 2^n products of *single-molecule* multitime correlation functions of Liouville space superoperators.

In the expansion 2.13, if the term $\langle \cdots \rangle_{a0}$ has m (+) superoperators and $n - m$ (-) superoperators (not counting the initial \hat{B}_{a+} which is fixed), then it is multiplied by a term $\langle \cdots \rangle_{b0}$ with $n - m$ (+) superoperators and m (-) superoperators. Making

use of the \mathcal{T} , we may collect all the products $\langle \cdots \rangle_{a0} \langle \cdots \rangle_{b0}$ characterized by a given value of m , and write them as

$$\frac{n!}{(n-m)!m!} \left\langle \mathcal{T} \hat{B}_{a+}(t) \underbrace{\hat{V}_{a+}(t_n) \cdots \hat{V}_{a+}(t_{n-m+1})}_{m \text{ terms}} \underbrace{\hat{V}_{a-}(t_{n-m}) \cdots \hat{V}_{a-}(t_1)}_{n-m \text{ terms}} \right\rangle_{a0} \times \left\langle \mathcal{T} \hat{B}_{b+}(t) \underbrace{\hat{V}_{b+}(t_1) \cdots \hat{V}_{b+}(t_{n-m})}_{n-m \text{ terms}} \underbrace{\hat{V}_{b-}(t_{n-m+1}) \cdots \hat{V}_{b-}(t_n)}_{m \text{ terms}} \right\rangle_{b0}. \quad (2.14)$$

The multitime correlation functions in Eq. 2.14 are the same as in the definitions of the GRFs. When Eq. 2.14 is inserted into Eq. 2.13, the factors of $n!$ cancel and the prefactor may be written as $\frac{1}{m!} \left(\frac{i}{\hbar}\right)^m \frac{1}{(n-m)!} \left(\frac{i}{\hbar}\right)^{n-m}$. Noting that the prefactor for each GRF is $\frac{1}{n-!} \left(\frac{i}{\hbar}\right)^{n-}$ we arrive at the result

$$R_{ab}^{(n)}(t, t_n, \dots, t_1) = \sum_{m=0}^n R_a^{+\cdots+ \overbrace{-\cdots-}^{n-m}}(t, t_n, \dots, t_1) R_b^{+\cdots+ \overbrace{-\cdots-}^m}(t, t_1, \dots, t_n). \quad (2.15)$$

As advertised, the joint nonlinear response function of the coupled system is expressed in terms of the GRFs of the constituents. The single-molecule GRFs can be computed at many levels of theory, or may be determined directly from measurements on the *individual* molecules.

It is noteworthy that the joint response function $R_{ab}^{(n)}$ is *not* expressed in terms of the single-molecule response functions; rather the entire set of single-molecule GRFs is required. The discussion of the KMS condition in Appendix section A.2 suggests that there may exist a way to express all n^{th} order GRFs in terms of the n^{th} order response function. If such a relation exists, then the joint response may be expressed in terms of the single-molecule responses alone, but for now we must be satisfied with Eq. 2.15.

2.3 Factorization in the L, R representation

Sometimes it is more convenient to work directly with the single-molecule Liouville space pathways rather than the single-molecule GRFs. Towards that end we factor the joint time-evolution superoperator in the L, R representation. The results of this section are equivalent to those of the preceding section, although they paint a different physical picture.

The point of departure from the preceding discussion is Eq. 2.5. Rather than factoring $\hat{H}_{ab-}(t)$ and $\hat{B}_{ab+}(t)$ in the $+, -$ representation, we factor them in the L, R representation:

$$\begin{aligned}\hat{H}_{ab-}(t) &= -c(t)[(\hat{V}_a(t)\hat{V}_b(t))_L + (\hat{V}_a(t)\hat{V}_b(t))_R] \\ &= -c(t)[\hat{V}_{aL}(t)\hat{V}_{bL}(t) + \hat{V}_{aR}(t)\hat{V}_{bR}(t)].\end{aligned}\quad (2.16)$$

Similarly B_{ab} is expanded to

$$\hat{B}_{abL} = \hat{B}_{aL}(t)\hat{B}_{bL}(t).\quad (2.17)$$

Inserting Eqs. 2.16 and 2.17 into Eq. 2.2 yields

$$\langle B_{ab}(t) \rangle = \left\langle \mathcal{T} \hat{B}_{aL}(t) \hat{B}_{bL}(t) \exp \left[\frac{i}{\hbar} \int_{-\infty}^t dt' c(t') [\hat{V}_{aL}(t') \hat{V}_{bL}(t') + \hat{V}_{aR}(t') \hat{V}_{bR}(t')] \right] \right\rangle_0. \quad (2.18)$$

Eq. 2.10 expressed in the \pm notation and Eq. 2.18 expressed in the L, R notation have very similar structures. However, there is a subtle difference between these equations. In the exponent of Eq. 2.10, every $+$ superoperator that acts on a is paired with a $-$ superoperator that acts on b , and *vice versa*, which leads to the interpretation of a evolving under the influence of b and b evolving under the influence of a . In the exponent of Eq. 2.18, every L superoperator that acts on a is paired with another L

superoperator that acts on b , and similarly for the R superoperators. The reason is that each term represents the perturbation acting simultaneously on either the bras of a and b , or on the kets of a and b . The \pm expression and the L, R expression are both exact and equivalent, but lead to different physical pictures. Depending on the situation one may be more convenient than the other.

Expanding Eq. 2.18 in powers of H_{ab} , the n^{th} order response can be written as a sum over Liouville space pathways:

$$\begin{aligned} \left\langle B_{ab}^{(n)}(t) \right\rangle &= \frac{1}{n!} \left(\frac{i}{\hbar} \right)^n \int_{-\infty}^t dt_n \cdots \int_{-\infty}^t dt_1 \sum_{\{\eta_\alpha\}} \\ &\quad \left\langle \mathcal{T}[\hat{B}_{aL}(t)\hat{B}_{bL}(t)][\hat{V}_{a\eta_n}(t_n)\hat{V}_{b\eta_n}(t_n)] \cdots [\hat{V}_{a\eta_1}(t_1)\hat{V}_{b\eta_1}(t_1)] \right\rangle_0 \\ &\quad c(t_n) \cdots c(t_1) \qquad \eta_\alpha = L, R, \end{aligned} \quad (2.19)$$

where $\{\eta_\alpha\}$ denotes a particular choice of the n -element sequence (η_n, \dots, η_1) .

Each term in Eq. 2.19 factors into a product of single-molecule Liouville space pathways:

$$\begin{aligned} &\left\langle \mathcal{T}\hat{B}_{aL}(t)\hat{B}_{bL}(t)\hat{V}_{a\eta_n}(t_n)\hat{V}_{b\eta_n}(t_n) \cdots \hat{V}_{a\eta_1}(t_1)\hat{V}_{b\eta_1}(t_1) \right\rangle_0 = \\ &\left\langle \mathcal{T}\hat{B}_{aL}(t)\hat{V}_{a\eta_n}(t_n) \cdots \hat{V}_{a\eta_1}(t_1) \right\rangle_{a0} \times \left\langle \mathcal{T}\hat{B}_{bL}(t)\hat{V}_{b\eta_n}(t_n) \cdots \hat{V}_{b\eta_1}(t_1) \right\rangle_{b0}, \end{aligned} \quad (2.20)$$

so that the joint response function is

$$\begin{aligned} R_{ab}^{(n)}(t, t_n, \dots, t_1) &= \frac{1}{n!} \left(\frac{i}{\hbar} \right)^n \sum_{\{\eta_\alpha\}} \left(\left\langle \mathcal{T}\hat{B}_{aL}(t)\hat{V}_{a\eta_n}(t_n) \cdots \hat{V}_{a\eta_1}(t_1) \right\rangle_{a0} \times \right. \\ &\quad \left. \left\langle \mathcal{T}\hat{B}_{bL}(t)\hat{V}_{b\eta_n}(t_n) \cdots \hat{V}_{b\eta_1}(t_1) \right\rangle_{b0} \right). \end{aligned} \quad (2.21)$$

The objects $\langle \cdots \rangle_{a0}$ and $\langle \cdots \rangle_{b0}$ that appear in Eq. 2.21 are exactly the Liouville space pathways that occur in the definition of the *single molecule* nonlinear response functions, Eq. 1.27. If the Liouville space pathways of the individual molecules have

been computed in order to determine the single-molecule response functions, then no further effort is required to calculate the joint response of the coupled molecules. However, if *only* the single-molecule response functions are known, and *not* their Liouville space pathways, then there is not enough information to calculate the joint response. Thus we need either all the GRFs of each molecule, or all the Liouville space pathways of each molecule to calculate the joint response.

The parallel between the expression for the joint response function, Eq. 2.21 and the expressions for the individual response functions, Eq. 1.27 suggests an interpretation of Eq. 2.21 in terms of double-sided Feynman diagrams. The photon lines in standard double-sided Feynman diagrams are replaced by “coupling lines”, which represent the coupling H_{ab} acting simultaneously on the a and b density matrices. Figure 2.1 shows the double-sided Feynman diagram for the linear response of a dimer to a time-dependent intermolecular coupling.

Suppose we are given two separate quantum systems, and we probe the response of each to a set of arbitrary perturbations. Can we then predict the response when the two systems are coupled? In this section I have shown that the answer is no. However, if we also measure the *fluctuations* of the individual systems, and how these fluctuations change in response to a perturbation, then we can predict the behavior of the coupled system. This result is exact and independent of any model for the matter. In the next three chapters we treat the two systems as molecules, and apply the formalism to calculate intermolecular forces.

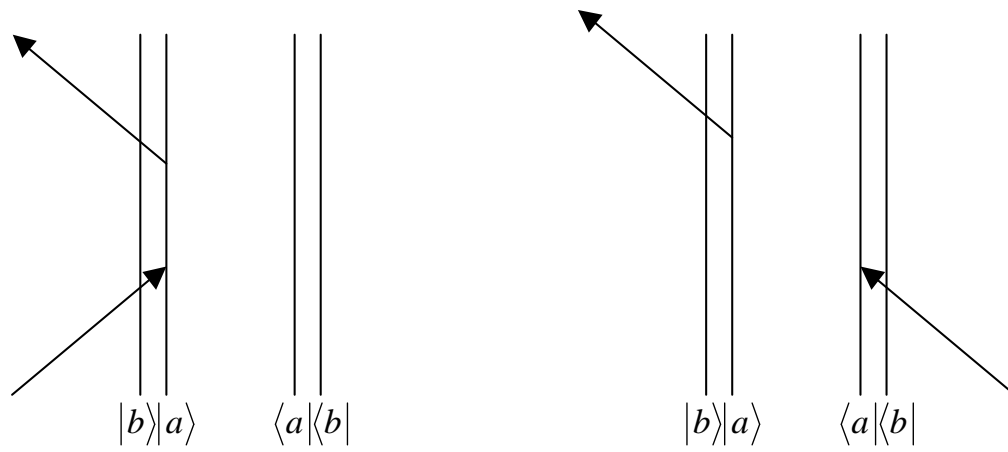


Figure 2.1: Double-sided Feynman diagram for the linear response of an intermolecular correlation, $\langle q_a(t)q_b(t) \rangle$ to a time-dependent intermolecular coupling, $c(t)q_aq_b$. Each Liouville space pathway for the dimer is the product of the corresponding Liouville space pathways for the individual molecules.

Chapter 3

Nonequilibrium van der Waals Forces

The formalism of the preceding chapter is applied to calculate the van der Waals force between molecules at different temperatures and subject to time-dependent coupling. In contrast to attractive equilibrium forces, nonequilibrium forces may be attractive or repulsive, exhibit chemically specific resonances, are far stronger, and may be nonconservative (with either positive or negative dissipation). The force also shows significant fluctuations, especially at high temperature.

3.1 Introduction

Fluctuation-induced long-range forces are widespread and have been well studied for systems in thermodynamic equilibrium [88, 124, 109, 120]. These forces were first calculated for electromagnetic fluctuations, leading to the van der Waals and Casimir forces. Recently, analogous forces have been predicted for phononic fluctuations [20] and for bodies immersed in correlated fluids, such as superfluid He, liquid crystals, and binary mixtures near a critical point [94]. At low temperature the force is entirely due

to zero-point fluctuations, while at finite temperatures thermal fluctuations contribute as well.

Consider two bodies, each with a characteristic resonant frequency ω_0 , interacting in vacuum at absolute zero. As the distance, r , between the bodies increases, the force goes through two qualitatively different regimes, corresponding to $r < c/\omega_0$ and $r > c/\omega_0$. In the nonretarded limit, $r \ll c/\omega_0$, the force is determined solely by the fluctuation properties of the bodies. The electromagnetic coupling between the bodies is “rigid”, in the sense that it would require an energy $\gg \hbar\omega_0$ to excite a radiation mode of wavelength $\lambda \sim r$. London showed that in this regime the van der Waals energy scales as r^{-6} , and arises from correlated zero-point fluctuations of molecular dipole moments [118]. For most interactions of small and midsized molecules, a nonretarded calculation of the force is adequate.

In the retarded limit, $r \gg c/\omega_0$, the lowest-energy mode of the (particles plus intervening vacuum) system belongs to the vacuum. Thus the particles may be approximated as “rigid”, and the force depends only on the electrodynamic properties of the vacuum. Casimir and Polder [30] showed that the retarded interaction energy scales as r^{-7} . Casimir provided the interpretation that this force arises from the zero-point fluctuations of the *vacuum* [29]. Casimir forces depend only on the geometry of the objects and on the boundary conditions they impose on the field. Li and Kardar developed sophisticated path-integral techniques for calculating these Casimir forces [113], both in vacuum and in correlated fluids.

Roughly speaking, Casimir forces probe the spectral density of the vacuum, while van der Waals forces probe the spectral density of the interacting objects. Casimir forces have been of interest to physicists because of their “universal” nature: like

gravity, they are independent of the composition of the bodies. van der Waals forces have been of interest to chemists for precisely the opposite reason: they provide a means for understanding and controlling the assembly of a wide range of nanoscale objects.

In both nonretarded and retarded regimes, there is the possibility of thermal excitation. In the nonretarded case, McLachlan showed that for $k_B T > \hbar\omega_0$ (i.e. when the molecules may be thermally excited), the force depends only on the zero-frequency polarizabilities and scales as r^{-6} (Eq. 3.13 below) [130]. Lifshitz [115] and Dzyaloshinskii, Lifshitz, and Pitaevskii [54] studied the retarded force for $k_B T > \hbar c/r$ (i.e. when the vacuum gap may be thermally excited) and showed that this force too depends only on the zero-frequency polarizabilities and scales as r^{-6} . Since for any temperature $T > 0$ there exists an r large enough that $k_B T > \hbar c/r$, the interaction energy for two molecules follows the unusual dependence $r^{-6} \rightarrow r^{-7} \rightarrow r^{-6}$ as r is increased. Recent studies have sought to unify the formalisms for zero-temperature and finite-temperature, retarded and nonretarded interactions [73, 133, 135, 155], although in Chapter 5 we show that some of these works are incorrect.

Work on nonequilibrium van der Waals-Casimir forces has focussed on the retarded regime, in which the specific material properties are irrelevant. A range of studies has considered the forces accompanying motion or deformation of objects in a vacuum [9, 89, 190, 139, 74]. The principal finding is that there is a “friction of the vacuum” that accompanies relative motion of two noncontacting objects. The dissipated energy goes into exciting electromagnetic modes of the intervening vacuum. Thus it is possible to generate light from the vacuum merely by modulating the boundary conditions [163]. Neto and Reynaud pointed out that the friction of the vacuum must be associated

with a fluctuating vacuum force, by the fluctuation-dissipation theorem [139], and Bartolo and coworkers recently considered the fluctuations in the classical Casimir force in correlated fluids [8]. For an excellent and readable review of dynamic Casimir forces, see [94].

These dynamic Casimir effects are of theoretical interest and are reminiscent of the Hawking effect (radiation from black holes) and the Unruh effect (radiation from accelerated bodies), which suggest deep connections between quantum mechanics, relativity and cosmology. However, on the laboratory scale there is little hope of detecting dynamic Casimir effects.

Dynamic van der Waals forces are another story. Many interesting systems are not in equilibrium when they interact. Cells run on interactions between molecules that have been chemically excited, e.g. by conversion of ATP. Optically excited molecules interact during photosynthesis [189], photochemical reactions [127], excitonic processes in molecular aggregates [189], and experiments using fluorescence resonance energy transfer (FRET) [168, 38]. Furthermore, the coupling between molecules is rarely constant in time. Molecules in a gas undergo fleeting encounters, while the coupling between molecules in a liquid may oscillate at bond vibrational frequencies. Nonequilibrium van der Waals forces are not “universal” the way Casimir forces are, but we can turn this to our advantage, to find a whole zoo of *chemically specific* effects.

Here we consider time-dependent nonretarded interactions between molecules. Since the vacuum is rigid in the nonretarded limit, the lowest available mode corresponds to molecular excitation. We examine the effects of temperature and a thermal bath, and find that nonequilibrium van der Waals forces show a much richer range of

behaviors than their equilibrium cousins.

3.2 Interaction Hamiltonian

Consider the Hamiltonian of two coupled molecules, a and b , each with a single internal coordinate q_j and momentum p_j ($j = a, b$)

$$H = H_a(q_a, p_a) + H_b(q_b, p_b) - J(z(t))q_aq_b, \quad (3.1)$$

The coupling, $J(z(t))$, is an externally driven parameter modulated by e.g. the intermolecular separation, $z(t)$. Assuming we know the trajectory $z(t)$, we can write the coupling either as $J(z)$ or $J(t)$, as is convenient. The bilinear perturbation, $H_{ab}(q_a, q_b, t) = -J(t)q_aq_b$, is paradigmatic of intermolecular forces: most two-body interactions can be written as a sum of terms of the form of Eq. 3.1. For example, if q_a and q_b represent charge density operators, ρ_a and ρ_b , respectively, then the interaction Hamiltonian is

$$H_{ab} = \frac{1}{2} \int \int \frac{\rho_a(\mathbf{r}_a)\rho_b(\mathbf{r}_b)}{4\pi\epsilon_0 r} d\mathbf{r}_a d\mathbf{r}_b, \quad (3.2)$$

where $\mathbf{r} \equiv \mathbf{r}_a - \mathbf{r}_b$ is the separation between points in molecules a and b . If both molecules are neutral, then at long range $H_{ab} \propto r^{-3}$, while Eq. 3.2 might give the erroneous impression that $H_{ab} \propto r^{-1}$. To avoid calculating contributions to H_{ab} that end up cancelling, it is possible to work with *dipole densities*, $\boldsymbol{\mu}(\mathbf{r})$, rather than charge densities. Integrating Eq. 3.2 by parts yields

$$H_{ab} = -\frac{1}{2} \int \int J_{ij}(\mathbf{r})\mu_{ai}(\mathbf{r}_a)\mu_{bj}(\mathbf{r}_b)d\mathbf{r}_a d\mathbf{r}_b. \quad (3.3)$$

where repeated indices are summed over and the nonretarded interaction tensor is

$$J_{ij}(\mathbf{r}) = \frac{1}{4\pi\epsilon_0} \nabla_i \nabla_j \frac{1}{r} = \frac{3r_i r_j - \delta_{ij}}{4\pi\epsilon_0 r^3}. \quad (3.4)$$

The dipole distribution function and the charge density are related by $\rho = \nabla \cdot \boldsymbol{\mu}$. For an arbitrary vector function \mathbf{f} , the gauge transformation $\boldsymbol{\mu} \rightarrow \boldsymbol{\mu} + \nabla \times \mathbf{f}$ leaves ρ , and hence H_{ab} , unchanged. The choice of gauge for the dipole distribution function is formally arbitrary, but may affect the severity of errors introduced in numerical calculations.

In the point-dipole approximation we associate a single dipole with each molecule, so the relevant coordinates are $\mathbf{q}_a = \boldsymbol{\mu}_a$, $\mathbf{q}_b = \boldsymbol{\mu}_b$. The interaction is approximated as $H_{ab} = -J_{ij}(\mathbf{r})\mu_{ai}\mu_{bj}$. It is almost always acceptable to make the point-dipole approximation for molecule-light interactions because an optical-frequency plane wave is spatially homogeneous over most molecules. This is less often the case for molecule-molecule interactions. The relevant intermolecular spacings are typically comparable to the molecular size (e.g. typical Förster radii are 10 - 50 Å), and thus the field produced by one molecule may vary significantly over its neighbor.

For closely spaced molecules, the point-dipole approximation may be improved by including higher multipole moments of each molecule. When this is done, the interaction becomes [124, 178]

$$\begin{aligned} H_{ab} = & -J_{ij}\mu_i^a\mu_j^b - \frac{1}{3}J_{ijk}(\mu_i^a\Theta_{jk}^b - \Theta_{ij}^a\mu_k^b) \\ & - J_{ijkl}\left(\frac{1}{15}\mu_i^a\Omega_{jkl}^b - \frac{1}{9}\Theta_{ij}^a\Theta_{kl}^b + \frac{1}{15}\Omega_{ijk}^a\mu_l^b\right) + \dots, \end{aligned} \quad (3.5)$$

where μ , Θ , and Ω are molecular dipole, quadrupole, and octupole moments, respectively. The quadrupole and octupole field propagators are defined in extension of Eq. 3.4 by

$$\begin{aligned} J_{ijk}(\mathbf{r}) &= \frac{1}{4\pi\epsilon_0}\nabla_i\nabla_j\nabla_k\frac{1}{r} \\ J_{ijkl}(\mathbf{r}) &= \frac{1}{4\pi\epsilon_0}\nabla_i\nabla_j\nabla_k\nabla_l\frac{1}{r}. \end{aligned} \quad (3.6)$$

The multipole expansion is most useful for analytical treatments of molecules with high symmetry. Rapid advances in quantum chemistry density functional theory (DFT) packages allow the computation of the entire charge distribution of a molecule, so it is not often necessary to resort to the multipole expansion to calculate electrostatic couplings.

All of the expressions for the interaction potential (Eq. 3.2, Eq. 3.3 and Eq. 3.5) are bilinear in single-molecule operators, and thus are already in the form of the generic expansion of a two-body interaction, Eq. 2.4a. We work with the Hamiltonian of Eq. 3.1 so that any model of the interaction can be substituted into our results.

3.3 McLachlan formalism

The van der Waals force is usually calculated in second order perturbation theory, under the assumptions that the intermolecular coupling J is independent of time and that both molecules are at thermal equilibrium. London showed that the ground state experiences a shift that is second order in the intermolecular coupling [118], given by

$$U = -\frac{1}{\hbar} J^2 \sum_{\{m,n\} \neq 0} \frac{|\mu_{0m}^a \mu_{0n}^b|^2}{\omega_{m0}^a + \omega_{n0}^b}, \quad (3.7)$$

where $\mu_{xy}^j \equiv \langle y | q_j | x \rangle$ is the transition dipole and $\omega_{xy}^j = (E_x^j - E_y^j)/\hbar$ is the transition frequency, both from state x to y of molecule j . The denominator, $\hbar(\omega_{m0}^a + \omega_{n0}^b)$, shows that the interaction arises from highly off-resonant virtual transitions from the ground state to states with both molecules excited.

The identity

$$\frac{1}{x+y} = \frac{2}{\pi} \int_0^\infty \frac{xy}{(x^2 + \xi^2)(y^2 + \xi^2)} d\xi \quad (3.8)$$

may be used to factor U into a product of terms that depend only on the coordinates of a or b :

$$U = -\frac{2}{\pi\hbar} J^2 \int_0^\infty d\xi \left(\sum_m \frac{\omega_{m0}^a |\mu_{0m}^a|^2}{(\omega_{m0}^a)^2 + \xi^2} \right) \left(\sum_n \frac{\omega_{n0}^b |\mu_{0n}^b|^2}{(\omega_{n0}^b)^2 + \xi^2} \right). \quad (3.9)$$

Meanwhile, the sum-over-states expression for the single-molecule polarizability is

$$\alpha_j(\omega) = \frac{2}{\hbar} \sum_n \frac{\omega_{n0}^j |\mu_{0n}^j|^2}{(\omega_{n0}^j)^2 - \omega^2}. \quad (3.10)$$

Thus each term in parentheses in Eq. 3.9 can be replaced by $\frac{\hbar}{2}\alpha_j(i\omega)$. The ground state energy becomes

$$U = -\frac{\hbar}{2\pi} J^2 \int_0^\infty \alpha_a(i\omega) \alpha_b(i\omega) d\omega. \quad (3.11)$$

A polarizability at imaginary frequency gives the response to an exponentially growing force, $f(t)$: $\langle q(t) \rangle = \alpha(i\omega) f e^{\omega t}$.

McLachlan showed that at finite temperature, the interaction free energy, ΔF is given by a generalization of Eq. 3.11 [129, 130]:

$$\Delta F = -k_B T J^2 \sum_{n=0}^{\infty} \prime \alpha_a(i\omega_n) \alpha_b(i\omega_n), \quad (3.12)$$

where the prime means that the $n = 0$ term is to be multiplied by 1/2, and $\omega_n \equiv 2\pi n k_B T / \hbar$ are the Matsubara frequencies. When applying McLachlan's formula, it should be noted that for all systems except the harmonic oscillator, the polarizability is a function of temperature too.

The lowest excitation energy in small molecules is typically $\hbar\omega_0 \gg k_B T$, in which case Eq. 3.12 reduces to Eq. 3.11. When there are excitations of energy less than $k_B T$ (such as rotations, vibrations, and conformational shifts), then Eq. 3.12 yields the classical expression

$$\Delta F = -\frac{1}{2} k_B T J^2 \alpha_a(0) \alpha_b(0). \quad (3.13)$$

Most molecules have modes with both high and low energies, relative to $k_B T$. For freely rotating dipolar molecules, the contribution to the van der Waals force from the high energy modes is called the dispersion interaction, while the contributions from the low energy rotational mode are called the Keesom interaction (molecular alignment) and the induction interaction (molecular polarization) [88]. McLachlan's formula provides a unified description of the three contributions to the van der Waals force.

The McLachlan formalism has been used to calculate van der Waals forces for many systems and at various levels of theory. In the dipole approximation, the α_j represent dipole susceptibilities and Eq. 3.12 yields a $1/r^6$ interaction energy. If Eq. 3.1 is expanded in charge densities, dipole densities, or multipole moments, then the α_j represent the corresponding single-particle susceptibilities. McLachlan also showed that Eq. 3.12 yields the fully retarded dispersion interaction when system a is a molecule and system b is the radiation field. The presence of a second molecule modifies the susceptibility of the radiation field and thus affects the self-energy of the first molecule.

The advantage of the McLachlan formula, Eq. 3.12, over the sum-over-states formula, Eq. 3.7, is that the McLachlan formula does not require a model of the internal dynamics of either body: it expresses the interaction free energy in terms of single-molecule linear response functions, which may be determined through experiment, simulation, or at various levels of theory.

The response function formalism developed in Chapter 2 allows us to generalize the McLachlan expression to include 1) time-dependent coupling, $J(t)$, associated with

relative motion; 2) nonequilibrium initial conditions corresponding to different temperatures or athermal distributions; 3) higher order corrections related to nonlinear single-molecule response functions; 4) fluctuations in the force about its equilibrium value. In Chapter 4 we consider the case of one molecule excited and in Chapter 5 we treat the effect of an incident radiation field. The McLachlan formula arises as a special case of our more general results.

3.4 Response function formalism

We now formulate intermolecular forces in terms of response functions. The operator

$$\boxed{B \equiv q_a q_b} \quad (3.14)$$

creates intermolecular correlations. The key quantities in my theory are response functions, $R_B^{(n)}(t, t_n, \dots, t_1)$, that relate the expectation value of the correlation, $\langle B(t) \rangle$, to the coupling at past times, $J(t')$, via:

$$\langle B(t) \rangle = B_0 + \int_{-\infty}^t dt_1 R_B^{(1)}(t, t_1) J(t_1) + \int_{-\infty}^t dt_2 \int_{-\infty}^t dt_1 R_B^{(2)}(t, t_2, t_1) J(t_2) J(t_1) + \dots, \quad (3.15)$$

where $B_0 \equiv \langle B \rangle_0$ is the expectation value of the correlation in the uncoupled state.

The n^{th} order response function is

$$R^{(n)}(t, t_n, \dots, t_1) = \frac{1}{n!} \left(\frac{i}{\hbar} \right)^n \left\langle \mathcal{T} \hat{B}_+(t) \hat{B}_-(t_n) \hat{B}_-(t_{n-1}) \dots \hat{B}_-(t_1) \right\rangle_0, \quad (3.16)$$

which can be expanded in single-molecule GRFs via Eq. 2.15. In the frequency domain, $\langle \tilde{B}(\omega) \rangle$ is given by

$$\langle \tilde{B}(\omega) \rangle = B_0 \delta(\omega) + \chi_B^{(1)}(\omega) \tilde{J}(\omega) + \int d\omega_2 \int d\omega_1 \chi_B^{(2)}(-\omega; \omega_2, \omega_1) \tilde{J}(\omega_2) \tilde{J}(\omega_1) + \dots, \quad (3.17)$$

where

$$\chi_B^{(n)}(-\omega_s; \omega_n, \dots, \omega_1) = \int d\tau_n \cdots \int d\tau_1 G^{(n)}(\tau_n, \dots, \tau_1) e^{i(\omega_n \tau_n + \dots + \omega_1 \tau_1)} \delta(\omega_s - \omega_n - \dots - \omega_1), \quad (3.18)$$

and $G^{(n)}$ is related to $R^{(n)}$ by Eq. 1.4.

Equations 3.15 and 3.16 are equivalent to the fundamental equations of nonlinear optics, with the polarization, p , replaced by the intermolecular correlation, B , the field, $E(t)$, replaced by the coupling, $J(t)$, and the time-domain optical response functions, $S^{(n)}$, replaced by the response function of the intermolecular correlation, $R_B^{(n)}$. This analogy allows us to apply many of the analytical techniques and results of nonlinear optics to the intermolecular force.

For instance, the linear response function, $\chi_B^{(1)}(\omega)$ has real and imaginary components, $\chi'_B(\omega)$ and $\chi''_B(\omega)$, which are even and odd functions of frequency, respectively. The parallel between $\chi_B^{(1)}(\omega)$ and the linear polarizability, $\alpha(\omega)$, allows us to write a Kramers Kronig relation connecting $\chi'_B(\omega)$ and $\chi''_B(\omega)$:

$$\chi'_B(\omega) = \frac{1}{\pi} \mathcal{P} \int_{-\infty}^{\infty} \frac{\chi''_B(\omega')}{\omega' - \omega} d\omega', \quad (3.19)$$

and its inverse

$$\chi''_B(\omega) = -\frac{1}{\pi} \mathcal{P} \int_{-\infty}^{\infty} \frac{\chi'_B(\omega')}{\omega' - \omega} d\omega'. \quad (3.20)$$

In the next section we show that $\chi'_B(\omega)$ is related to the conservative part of the force and $\chi''_B(\omega)$ is related to the dissipative part, and Eqs. 3.19 and 3.20 provide a connection between the two.

3.4.1 Forces and dissipation

Now we relate $\langle B(t) \rangle$ to the intermolecular force. The steady state van der Waals free energy is obtained by an adiabatic switching of the coupling, J . The work performed in this process is

$$W = \int \frac{\partial H}{\partial J} dJ = - \int \langle B \rangle dJ, \quad (3.21)$$

where $\langle B \rangle$ is given by Eq. 3.15 or Eq. 3.17. In an adiabatic process $W = \Delta F$, where ΔF is the change in free energy. For nearly constant J , it is most convenient to use the zero-frequency components of $\chi_B^{(n)}$ to calculate $\langle B \rangle$, whence the free energy is:

$$\Delta F = -B_0 J - \frac{1}{2} \chi_B^{(1)}(0) J^2 - \frac{1}{3} \chi_B^{(2)}(0; 0, 0) J^3 - \dots \quad (3.22)$$

The interaction force is given by $f = -\frac{\partial \Delta F}{\partial z}$. When $B_0 = 0$ (i.e. q_a and q_b are uncorrelated when $J = 0$), then $\Delta F = -\frac{1}{2} \chi_B^{(1)}(0) J^2$. This energy shift is analogous to the DC Stark shift, $\Delta F = -\frac{1}{2} \alpha(0) E^2$.

In order for ΔF to be well defined, the system must be in a steady state throughout the process of applying J . We will study several cases below which satisfy this constraint, but in which the states are *not* ones of thermal equilibrium. Nonequilibrium steady states are allowed in open quantum systems coupled to multiple heat baths. In such cases, ΔF is not the thermodynamic free energy, but it still plays the role of a “potential function” (i.e. a state-function whose gradient gives the force).

When J varies on a timescale comparable to or shorter than the slowest relaxation time of $G_B^{(1)}$, then the free energy is ill-defined but we can still calculate the interaction force. The classical force on molecule j is $f = \dot{p}_j$, where p_j is its classical momentum. We define a quantum mechanical force *operator* by $f \equiv \dot{p}_j$, where the operator $p_j \equiv$

$i\hbar\frac{\partial}{\partial z}$. The rate of change of momentum is given by the Heisenberg equation of motion

$$\dot{p}_j = \frac{i}{\hbar}[H, p_j]. \quad (3.23)$$

Evaluating the commutator yields $\dot{p}_j = -\partial H_{ab}/\partial z$. The intermolecular force operator is thus $f(t) = (\partial J/\partial z)B(t)$, with expectation value

$$\langle f(t) \rangle = \left. \frac{\partial J}{\partial z} \right|_{z(t)} \langle B(t) \rangle. \quad (3.24)$$

The quantity $\partial J/\partial z$ can come outside the brackets because we are treating J as a classical variable.

A second quantity of interest is the instantaneous power dissipation, given by

$$\begin{aligned} \langle P(t) \rangle &= f(t) \frac{\partial z}{\partial t} \\ &= \langle B(t) \rangle \frac{\partial J}{\partial t}. \end{aligned} \quad (3.25)$$

When the dominant contribution to the force comes from the linear susceptibility, $\chi_B^{(1)}(\omega)$, we may evaluate explicitly the conservative and dissipative components of the force. In the frequency domain, the coordinate B has two components: $\langle \tilde{B}(\omega) \rangle = \langle \tilde{B}'(\omega) \rangle + i\langle \tilde{B}''(\omega) \rangle$, where $\langle \tilde{B}'(\omega) \rangle \equiv \chi_B'(\omega)\tilde{J}(\omega)$ and $\langle \tilde{B}''(\omega) \rangle \equiv \chi_B''(\omega)\tilde{J}(\omega)$. $\langle \tilde{B}'(\omega) \rangle$ is in phase with $\tilde{J}(\omega)$ while $\langle \tilde{B}''(\omega) \rangle$ is phase-shifted by $\pi/2$. The components of $\langle \tilde{B}(\omega) \rangle$ lead to a force which has reversible and irreversible components, $\tilde{f}(\omega) = \tilde{f}_r(\omega) + \tilde{f}_i(\omega)$, where the Fourier transform of Eq. 3.24 yields:

$$\begin{aligned} \tilde{f}_r(\omega) &\equiv \int_{-\infty}^{\infty} \frac{\partial \tilde{J}(\omega - \omega_1)}{\partial z} \chi_B'(\omega_1) \tilde{J}(\omega_1) d\omega_1 \\ \tilde{f}_i(\omega) &\equiv \int_{-\infty}^{\infty} i \frac{\partial \tilde{J}(\omega - \omega_1)}{\partial z} \chi_B''(\omega_1) \tilde{J}(\omega_1) d\omega_1. \end{aligned} \quad (3.26)$$

The time-averaged force, $\tilde{f}(0)$, is due entirely to $\tilde{f}_r(0)$, because $\chi_B''(\omega)$ is odd so $\tilde{f}_i(0) = 0$. Making use of the fact that $\tilde{J}(-\omega) = \tilde{J}^*(\omega)$, we write $(\partial \tilde{J}(-\omega_1)/\partial z)\tilde{J}(\omega_1)$

as $(\partial/\partial z)\frac{1}{2}|\tilde{J}(\omega_1)|^2$. The time-averaged force is given by the gradient of an energy:

$$\boxed{\tilde{f}(0) = \frac{\partial}{\partial z} \frac{1}{2} \int_{-\infty}^{\infty} \chi'_B(\omega_1) |\tilde{J}(\omega_1)|^2 d\omega_1.} \quad (3.27)$$

We proceed along similar lines to calculate the power dissipation. Converting Eq. 3.25 into the frequency domain, the power separates into reversible and irreversible parts, $\tilde{P}(\omega) = \tilde{P}_r(\omega) + \tilde{P}_i(\omega)$, where

$$\begin{aligned} \tilde{P}_r(\omega) &\equiv \int_{-\infty}^{\infty} -i\omega_1 \tilde{J}(\omega - \omega_1) \chi'_B(\omega_1) \tilde{J}(\omega_1) d\omega_1 \\ \tilde{P}_i(\omega) &\equiv \int_{-\infty}^{\infty} \omega_1 \tilde{J}(\omega - \omega_1) \chi''_B(\omega_1) \tilde{J}(\omega_1) d\omega_1. \end{aligned} \quad (3.28)$$

The time-averaged power, $\tilde{P}(0)$, is entirely due to $\tilde{P}_i(\omega)$, because of the extra factor of ω_1 in Eq. 3.28 compared to Eq. 3.26:

$$\boxed{\tilde{P}(0) = \int_{-\infty}^{\infty} \omega_1 \chi''_B(\omega_1) |\tilde{J}(\omega_1)|^2 d\omega_1.} \quad (3.29)$$

Under steady state coupling ($dJ/dt = 0$), the force is fully reversible and there is no power dissipation.

When J changes slowly (but not infinitely slowly), then there should be a velocity-dependent dissipation associated with the relative motion of the molecules. We make the *ansatz* that the force has the form:

$$f = A(z) - \Gamma(z)\dot{z}, \quad (3.30)$$

where $A(z)$ is the conservative part of the force, and $\Gamma(z)$ is a friction coefficient. Now we evaluate $A(z)$ and $\Gamma(z)$. We may rewrite Eq. 3.24 as

$$f = \frac{\partial J}{\partial z} \int_0^{\infty} G_B^{(1)}(\tau) J(t - \tau) d\tau. \quad (3.31)$$

The function $G_B^{(1)}(\tau)$ is a rapidly decreasing function of τ . Thus in the integral of Eq. 3.31 we may expand $J(t - \tau)$ as

$$J(t - \tau) = J(t) - \tau \frac{\partial J}{\partial z} \dot{z}, \quad (3.32)$$

whereupon Eq. 3.31 becomes

$$f = \frac{\partial J}{\partial z} \left(J(t) \int_0^\infty G_B^{(1)}(\tau) d\tau - \frac{\partial J}{\partial z} \dot{z} \int_0^\infty \tau G_B^{(1)}(\tau) d\tau \right). \quad (3.33)$$

The first term in the parentheses of Eq. 3.33 only depends on the instantaneous value of J . Evaluating the integral yields

$$A(z) = \frac{\partial}{\partial z} \frac{1}{2} \chi_B'(0) J^2, \quad (3.34)$$

a result we obtained previously. The second integral may be evaluated by integration by parts, and yields a velocity-dependent force

$$\Gamma(z) = \left(\frac{\partial J}{\partial z} \right)^2 \frac{\partial \chi_B''(\omega)}{\partial \omega} \Big|_{\omega=0}. \quad (3.35)$$

Thus the nonconservative part of the van der Waals force depends on the slope of the imaginary part of $\chi_B^{(1)}(\omega)$ at $\omega = 0$. The most surprising result of this thesis is that when the interacting molecules are out of equilibrium, $\Gamma(z)$ may be either positive or negative, implying that the possibility of *negative friction*. We will show this in the next section.

3.5 Examples

We now calculate the interaction force for molecules in various nonequilibrium situations. For consistency with other treatments we classify the effects by their order in J

rather than by their order in perturbation theory, e.g. the van der Waals force which is second order in J depends on the *linear* response function, $\chi_B^{(1)}(\omega)$. We examine modifications to the van der Waals force when the molecules are at different temperatures or subject to time-dependent coupling. For equilibrium interactions, the forces to third and fourth order in J are rarely of interest (although they are important for matter-antimatter interactions.¹). Third and fourth order forces may be significant for nonequilibrium interactions.

3.5.1 First order interaction

Interactions that are first order in the coupling may arise in two ways: either both molecules may have permanent moments, $\langle q_a(t) \rangle_{a0} \neq 0$ and $\langle q_b(t) \rangle_{b0} \neq 0$, or an external perturbation such as an optical field may impose correlated fluctuations in $\langle q_a(t) \rangle$ and $\langle q_b(t) \rangle$.

If there are permanent moments, then the zeroth order value of B is

$$\begin{aligned} \langle B^{(0)}(t) \rangle &= \langle \hat{B}_+(t) \rangle_0 \\ &= \langle \hat{q}_a(t) \rangle_{a0} \langle \hat{q}_b(t) \rangle_{b0}, \end{aligned} \quad (3.36)$$

whence the first order interaction energy is

$$\Delta F^{(1)}(t) = -J(t) \langle \hat{q}_a(t) \rangle_{a0} \langle \hat{q}_b(t) \rangle_{b0}. \quad (3.37)$$

This static energy is easily accounted for e.g. by summing the Coulomb interactions between fixed charges. The case of an external field that imposes correlated fluctuations is the subject of Chapter 5.

¹The dispersion force between two hydrogen atoms is the same as that between a hydrogen and an antihydrogen, up to third order in perturbation theory. The first term for which these interactions differ is proportional to r^{-11} . [124, 33]

3.5.2 Second order interaction, different temperatures

Now we calculate contributions to the intermolecular force arising from the linear response function, $R_B^{(1)}(t, t_1)$, when each molecule is at thermal equilibrium (although the molecules may be at different temperatures). In the absence of permanent moments or externally applied fields, this second order interaction is the dominant contribution to the intermolecular force.

In the notation of Chapter 1, $R_B^{(1)}(t, t_1) = R_B^{+-}(t, t_1)$. Using Eq. 2.15 we factor the first order joint response function in terms of single-molecule GRFs:

$$\boxed{R_B^{+-}(t, t_1) = R_a^{+-}(t, t_1)R_b^{++}(t, t_1) + R_a^{++}(t, t_1)R_b^{+-}(t, t_1).} \quad (3.38)$$

The function $R_j^{+-}(t, t_1)$ gives the response of coordinate $\langle q_j(t) \rangle$ to a perturbation $-f(t_1)q_j$. The function $R_j^{++}(t, t_1)$ is the two-time autocorrelation function of operator $\hat{q}_j(t)$. We thus arrive at the physical picture that R_B^{+-} arises from molecule b responding to fluctuations of a and *vice versa*. This picture is the rigorous basis for the semiclassical notion that the van der Waals force arises from fluctuating dipole-induced dipole interactions.

When both molecules are at their respective thermal equilibria, then the correlation functions of the individual molecules are time-translation invariant, so we may use the Green functions $G_j^{+-}(\tau_1)$ and $G_j^{++}(\tau_1)$. Thus the joint response function is also time-translation invariant: $G_B^{+-}(\tau_1) = G_a^{+-}(\tau_1)G_b^{++}(\tau_1) + G_a^{++}(\tau_1)G_b^{+-}(\tau_1)$. The

single-molecule GRFs are related to single-molecule susceptibilities by

$$G_j^{+-}(\tau_1) = \frac{i}{\pi} \theta(\tau_1) \int_{-\infty}^{\infty} \alpha_j''(\omega) e^{-i\omega\tau_1} d\omega \quad (3.39a)$$

$$= \frac{1}{2\pi} \int_{-\infty}^{\infty} \alpha_j(\omega) e^{-i\omega\tau_1} d\omega \quad (3.39b)$$

$$G_j^{++}(\tau_1) = \frac{\hbar}{2\pi} \int_{-\infty}^{\infty} \alpha_j''(\omega) \coth\left(\frac{\hbar\omega\beta_j}{2}\right) e^{-i\omega\tau_1} d\omega, \quad (3.39c)$$

where $\beta \equiv 1/k_B T$ and the single-molecule susceptibility is $\alpha_j(\omega) \equiv \alpha_j'(\omega) + i\alpha_j''(\omega)$. The equivalence of Eqs. 3.39a and 3.39b can be established by application of a Kramers-Kronig relation. Eq. 3.39c is a statement of the fluctuation dissipation theorem for molecule j at its local temperature. The operator $\hat{q}_j(t)$ fluctuates because 1) q_j does not commute with the free-particle Hamiltonian and 2) each molecule is subject to thermal disturbances. It is noteworthy that although the system as a whole need not have a temperature, we can divide it into thermalized pieces on which we can apply the fluctuation dissipation theorem.

Converting $G_B^{+-}(\tau_1)$ (Eq. 3.38) to the frequency domain, we get

$$\chi_B^{(1)}(\omega) = \frac{\hbar}{2\pi} \int_{-\infty}^{\infty} d\omega_1 \left[\coth\left(\frac{\hbar\beta_b\omega_1}{2}\right) \alpha_b''(\omega_1) \alpha_a(\omega - \omega_1) + \coth\left(\frac{\hbar\beta_a\omega_1}{2}\right) \alpha_a''(\omega_1) \alpha_b(\omega - \omega_1) \right]. \quad (3.40)$$

Eq. 3.40 is the most general form of the van der Waals susceptibility for systems at local thermal equilibrium. From it we can calculate the force and dissipation for arbitrary time-dependent coupling.

Constant coupling

Eq. 3.40 exhibits several subtle features so we now explore its limits in detail. To calculate the interaction energy for constant coupling we need only $\chi_B^{(1)}(0)$, in which case the symmetry properties of $\alpha_a(\omega)$ and $\alpha_b(\omega)$ can be used to simplify Eq. 3.40.

The product $\coth(\hbar\beta\omega/2)\alpha''(\omega)$ is an even function of ω , so only the even (real) components of $\alpha_a(\omega)$ and $\alpha_b(\omega)$ survive the integral. Making use of the fact that $\alpha'(\omega) = \alpha'(-\omega)$ we get

$$\chi_B^{(1)}(0) = \frac{\hbar}{2\pi} \int_{-\infty}^{\infty} d\omega \left[\coth\left(\frac{\hbar\beta_b\omega}{2}\right) \alpha'_a(\omega)\alpha''_b(\omega) + \coth\left(\frac{\hbar\beta_a\omega}{2}\right) \alpha'_b(\omega)\alpha''_a(\omega) \right]. \quad (3.41)$$

Eq. 3.41 has a simple physical interpretation. In the first term of the integrand, the quantity $\coth(\hbar\beta_b\omega/2)\alpha''_b(\omega)$ represents the fluctuations of b . $\alpha'_a(\omega)$ is the in-phase response of a to these fluctuations. In the second term of the integrand the roles of a and b are reversed.

A delicate cancellation in Eq. 3.41 occurs in the case of global thermal equilibrium ($\beta_a = \beta_b = \beta$) that does not occur when $\beta_a \neq \beta_b$. This cancellation leads to an equilibrium force that is, in general, much weaker than the nonequilibrium force. In the equilibrium case we can factor out $\coth(\hbar\omega\beta/2)$ to get

$$\chi_B^{(1)}(0) = \frac{\hbar}{2\pi} \int_{-\infty}^{\infty} d\omega \coth\left(\frac{\hbar\beta\omega}{2}\right) [\alpha'_a(\omega)\alpha''_b(\omega) + \alpha''_a(\omega)\alpha'_b(\omega)]. \quad (3.42)$$

McLachlan showed how to transform this integral by analytic continuation to complex frequencies. The polarizabilities in the integrand can be written $\text{Im}(\alpha_a\alpha_b)$. However, $\text{Re}(\alpha_a\alpha_b)$ is an even function of frequency, so it gives no contribution to the integral, except for the pole of $\coth(\hbar\beta\omega/2)$ at $\omega = 0$. Taking the principal value of the integral eliminates this contribution. Thus

$$\chi_B^{(1)}(0) = \frac{\hbar}{\pi i} \mathcal{P} \int_{-\infty}^{\infty} d\omega \frac{1}{2} \coth\left(\frac{\hbar\beta\omega}{2}\right) \alpha_a(\omega)\alpha_b(\omega). \quad (3.43)$$

Extending the contour as shown in Figure 3.1, the integral picks up contributions from the poles of $\frac{1}{2} \coth(\hbar\beta\omega/2)$, located at the Matsubara frequencies $\omega_n = n2\pi i/\beta\hbar$. Each

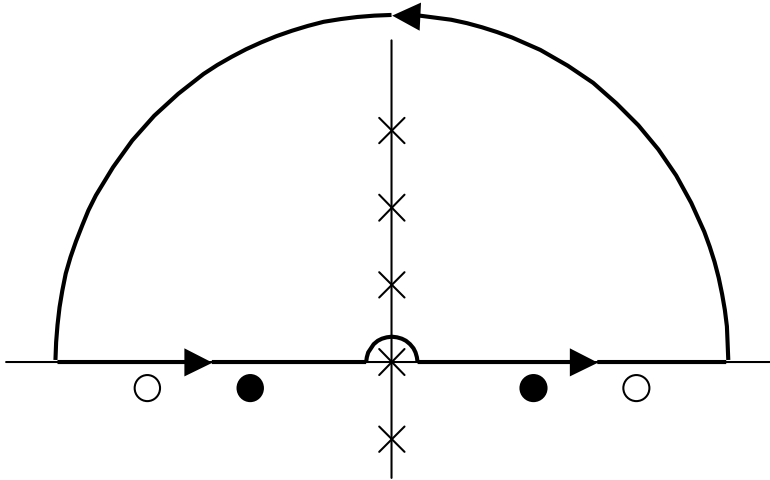


Figure 3.1: Contour used to evaluate Eq. 3.41. The integrand has poles coming from the coth function (\times), α_a (\circ) and α_b (\bullet).

pole has a residue of $(\beta\hbar)^{-1}$, so the contribution from all the poles is

$$\chi_B^{(1)}(0) = 2k_B T \sum'_{n=0} \alpha_a(i\omega_n) \alpha_b(i\omega_n), \quad (3.44)$$

where the prime indicates a half contribution from the pole at $\omega = 0$. The change in free energy $\Delta F = -\frac{1}{2} \chi_B^{(1)}(0) J^2$ reproduces the McLachlan formula, Eq. 3.12.

The methods of analytic continuation and contour integration do not yield any simplification when $\beta_a \neq \beta_b$. However, $\chi_B^{(1)}(0)$ can be evaluated directly from Eq. 3.41, provided a model is specified for the single-molecule polarizabilities, $\alpha_j(\omega)$. We consider two interacting simple harmonic oscillators, with resonant frequencies ω_a and ω_b . For simplicity we assume they both have the same damping constant, $\gamma \ll \omega_a, \omega_b$. The polarizabilities in this model are

$$\alpha_j(\omega) = -\frac{\mu_j^2}{\hbar} \left(\frac{1}{\omega - \omega_j + i\gamma} - \frac{1}{\omega + \omega_j + i\gamma} \right), \quad (3.45)$$

where μ_j is the transition dipole strength of oscillator j . If the oscillators are at the

same temperature, β , then in the limit $\gamma \rightarrow 0^+$, Eq. 3.41 (or Eq. 3.44) evaluates to

$$\chi_B^{(1)}(0) = \frac{2\mu_a^2\mu_b^2}{\hbar(\omega_a^2 - \omega_b^2)} \left[\omega_a \coth\left(\frac{\hbar\omega_b\beta}{2}\right) - \omega_b \coth\left(\frac{\hbar\omega_a\beta}{2}\right) \right]. \quad (3.46)$$

When the resonance frequencies are equal (i.e. $\omega_a = \omega_b \equiv \omega_0$) a cancellation prevents divergence of Eq. 3.46, which becomes

$$\chi_B^{(1)}(0) = \frac{\mu_a^2\mu_b^2}{2\hbar\omega_0} \operatorname{csch}^2\left(\frac{\hbar\omega_0\beta}{2}\right) [\hbar\omega_0\beta + \sinh(\hbar\omega_0\beta)]. \quad (3.47)$$

For $\omega_a \approx \omega_b$, Eq. 3.47 gives $\chi_B^{(1)}(0) \propto (\omega_a + \omega_b)^{-1}$, so the force has no special features at $\omega_a = \omega_b$.

Now we consider oscillators at different temperatures. In the limit $\gamma \rightarrow 0^+$, $\alpha_j''(\omega)$ takes the simple form:

$$\alpha_j''(\omega) = \frac{\pi\mu_j^2}{\hbar} [\delta(\omega - \omega_j) - \delta(\omega + \omega_j)]. \quad (3.48)$$

Inserting this expression into Eq. 3.41 yields

$$\chi_B^{(1)}(0) = \frac{2\mu_a^2\mu_b^2}{\hbar(\omega_a^2 - \omega_b^2)} \left[\omega_a \coth\left(\frac{\hbar\omega_b\beta_b}{2}\right) - \omega_b \coth\left(\frac{\hbar\omega_a\beta_a}{2}\right) \right], \quad (3.49)$$

which differs from Eq. 3.46 in the temperature arguments. If $\beta_a \neq \beta_b$, then the cancellation no longer occurs in Eq. 3.49 as $\omega_a \rightarrow \omega_b$. $\chi_B^{(1)}(0) \propto (\omega_a - \omega_b)^{-1}$ diverges, in a direction determined by the sign of $\beta_a - \beta_b$ and $\omega_a - \omega_b$: If particle a is hotter and $\omega_a < \omega_b$, then $\chi_B^{(1)}(0)$ diverges positively (corresponding to a strong *attractive* force). Switching the temperature difference or the relative frequencies reverses the direction of the divergence, leading to a strong *repulsive* force. The sign of the divergence can be easily understood by picturing the field from the hotter oscillator driving the cooler oscillator. If the hotter oscillator has the lower resonance frequency, then the cooler oscillator can respond almost instantaneously to the driving force, and the motion

of the two is correlated, leading to an attractive force. If the hotter oscillator has the higher resonance frequency, then the response of the cooler oscillator is 180° out of phase—it can never “catch up”—and so their motion is anticorrelated, leading to a repulsive force. In physical systems damping will prevent a true divergence in $\chi_B^{(1)}(0)$. Figure 3.2 illustrates the cancellation that occurs when $\beta_a = \beta_b$ for the interaction of two simple harmonic oscillators with closely spaced resonant frequencies, and how the force becomes resonant when $\beta_a \neq \beta_b$.

Figure 3.3 shows the steady state interaction force ($f \propto \chi_B^{(1)}(0)$) as a function of the resonant frequencies of the oscillators ω_a and ω_b and their inverse temperatures β_a and β_b . The equilibrium force ($\beta_a = \beta_b$) displays no resonance at $\omega_a = \omega_b$, since it depends only on $(\omega_a + \omega_b)^{-1}$. The nonequilibrium force ($\beta_a \neq \beta_b$) has a contribution proportional to $(\omega_a - \omega_b)^{-1}$. This contribution yields a *chemically specific* force, in the sense that the force diverges if the two molecule have closely spaced resonant frequencies. The divergent force can be either attractive or repulsive, and is accompanied by a resonance in the rate of heat transfer from the hotter particle to the colder particle.

Time-dependent coupling

When the intermolecular coupling depends on time, there is the possibility of energy dissipation associated with the van der Waals force. First we study the dissipation at zero temperature, and then with the molecules at finite, different temperatures.

At zero temperature all the population resides in the ground state, while the coupling J connects the ground state to the state with both molecules excited. The zero-temperature van der Waals response function in the harmonic oscillator model

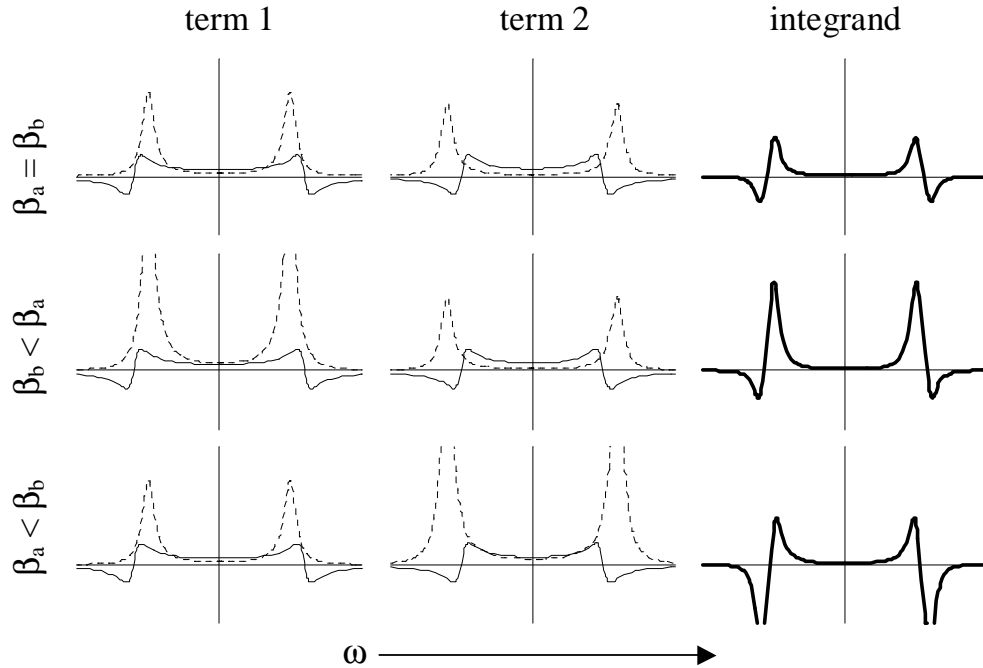


Figure 3.2: Contributions to the integral of Eq. 3.41 for the interaction of two simple harmonic oscillators with closely spaced resonant frequencies, $\omega_b < \omega_a$. Left column: fluctuations of b ($\coth(\hbar\beta_b\omega/2)\alpha_b''(\omega)$; dashed), and the response of a ($\alpha_a'(\omega)$; solid). Center column: fluctuations of a ($\coth(\hbar\beta_a\omega/2)\alpha_a''(\omega)$; dashed), and the response of b ($\alpha_b'(\omega)$; solid). Right column: integrand of Eq. 3.41. Top row: global thermal equilibrium. The contributions from the first two columns lead to an integrand in which the positive and negative parts nearly cancel. Middle row: oscillator b is hotter ($\beta_b < \beta_a$). The fluctuations of b have a larger impact on a than the fluctuations of a on b . The positive contribution to the integrand dominates, so $\chi_B^{(1)}(0)$ is large and positive, and the force is strongly attractive. Bottom row: oscillator a is hotter. The strong fluctuations of a occur at a frequency where $\alpha_b'(\omega)$ is negative. The negative contribution to the integrand dominates, so $\chi_B^{(1)}(0)$ is large and negative, and the force is strongly repulsive.

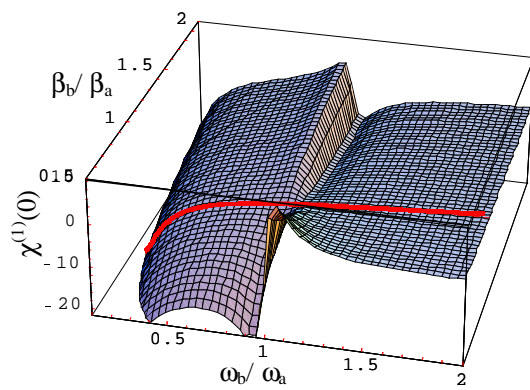


Figure 3.3: Interaction force of two harmonic oscillators as a function of their resonant frequencies, ω_b/ω_a and their temperatures, β_b/β_a . The red line indicates the isothermal case, for which the interaction energy is continuous at $\omega_b = \omega_a$. When the oscillators are at different temperatures there is a resonance in the force at $\omega_b = \omega_a$. The steady state force may even become *repulsive*. The dimensionless resonant frequency of oscillator a is $\beta_a \hbar \omega_a = 1$, and its linewidth is $\beta_a \hbar \gamma = .03$

is

$$\chi_B^{(1)}(\omega) = -\frac{\mu_a^2 \mu_b^2}{\hbar} \left(\frac{1}{\omega - (\omega_a + \omega_b) + 2i\gamma} - \frac{1}{\omega + (\omega_a + \omega_b) + 2i\gamma} \right). \quad (3.50)$$

The dissipative component of the force reaches a maximum when the coupling $\tilde{J}(\omega)$ has a component at frequency $\omega_a + \omega_b$. When the coupling is driven above resonance, the intermolecular force switches sign and becomes *repulsive*. The dissipated energy goes into exciting internal modes of the molecules. In molecular beam experiments or high temperature gasses, the duration of a close-encounter of two molecules may be comparable to the inverse excitation frequency. A close-encounter may leave both molecules excited, with a concomitant decrease in the translational kinetic energy, even without any electron-electron overlap between the molecules.

Except for the case of high-energy gas-phase collisions, the optical frequency $\omega_a + \omega_b$ is typically much higher than any frequency component of the coupling that arises from relative motion (this is the basis of the Born-Oppenheimer approximation). However, the present formalism also includes contributions to the single-molecule polarizabilities, and hence the force, from low-frequency vibrational modes, which could readily couple to intermolecular motions in condensed matter.

Now we consider a time-dependent interaction when the molecules are at finite, different temperatures. $\chi_B^{(1)}(\omega)$ may be evaluated in the harmonic oscillator model in the limit $\gamma \rightarrow 0^+$. The resulting complicated expression is noteworthy for its denominator:

$$\chi_B^{(1)}(\omega) = - \left(\frac{2\mu_a^2 \mu_b^2}{\hbar} \right) \frac{\omega_b(\omega^2 + \omega_a^2 - \omega_b^2) \coth\left(\frac{\hbar\omega_a\beta_a}{2}\right) + \omega_a(\omega^2 - \omega_a^2 + \omega_b^2) \coth\left(\frac{\hbar\omega_b\beta_b}{2}\right)}{(\omega - \omega_a - \omega_b)(\omega + \omega_a - \omega_b)(\omega - \omega_a + \omega_b)(\omega + \omega_a + \omega_b)}. \quad (3.51)$$

The denominator has resonances at $\omega = \pm\omega_a \pm \omega_b$, so for $\omega_a \approx \omega_b$, a resonance in the force (and an accompanying dissipation) may occur at very low frequencies. These

difference-frequency resonances arise because at finite temperature, there is some population in the first excited state of each oscillator and the coupling J connects the two singly excited states. For finite γ , there is no analytical expression for $\chi_B^{(1)}(\omega)$, but we can evaluate it numerically from Eq. 3.40. The result is plotted in Figure 3.4.

When $\beta_a = \beta_b$, the imaginary part of the joint response function, $\chi_B''(\omega)$, is positive for all $\omega > 0$. This implies that there is viscous dissipation associated with a rapid change in the intermolecular separation. However, if $\omega_a > \omega_b$ and $\beta_a\omega_a < \beta_b\omega_b$, then $\frac{\partial\chi_B''}{\partial\omega}|_{\omega=0}$ is *negative*, which implies that the friction coefficient, $\Gamma(z)$ is also negative. Energy is transferred from the oscillators to motion along the intermolecular coordinate. We thus have a heat engine, in which the van der Waals force is the energy transducer. Extraction of energy from the system is accompanied by heat flow from the hotter particle to the colder particle. The dissipative component of the van der Waals force allows for conversion between *intramolecular* excitation and *intermolecular* work, mediated purely by the fluctuating electromagnetic field. Such a mechanism is required for the system to reach thermal equilibrium.

One of the principal results of the theory of dynamic Casimir forces is that there is a friction associated with tangential motion of two noncontacting plates in vacuum. The dissipated energy goes into exciting electromagnetic modes of the intervening vacuum [94]. Dynamic Casimir forces have only been considered for plates at the same temperature. Consider two parallel plates, each composed of the harmonic oscillator “molecules” we studied in this last section. If the density of each plate is low, then the interaction between the plates may be approximated by pairwise summation of interactions between the molecules in each plate. Our results suggest that when the two plates are held at sufficiently different temperatures, then the vacuum friction

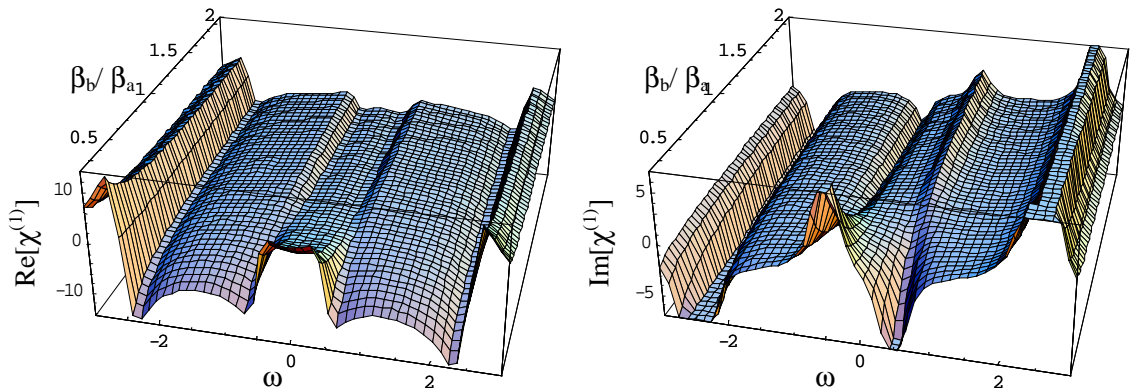


Figure 3.4: Reversible ($f_r \propto \chi'(\omega)$) and irreversible ($f_i \propto \chi''(\omega)$) components of the intermolecular force for coupling that oscillates at frequency ω . Resonances in the force occur at $\omega = \pm\omega_a \pm \omega_b$. The positive-frequency dissipation may be *negative* if the higher frequency particle is hot enough. The dimensionless resonant frequencies are $\beta_a \hbar \omega_a = 1$, $\beta_a \hbar \omega_b = 1.5$ and the linewidths are $\beta_a \hbar \gamma = 0.08$

can be made to vanish, or even become negative! This negative friction is entirely consistent with thermodynamics, because it is accompanied by a flow of heat from the hotter plate to the colder plate.

Fluctuations in the force

In Chapter 2 we developed a procedure for expressing the joint multitime correlation function $\langle \mathcal{T} \hat{B}_+(t) \hat{B}_-(t_n) \hat{B}_-(t_{n-1}) \dots \hat{B}_-(t_1) \rangle_0$ in terms of multitime correlation functions of the individual molecules in either the \pm or L, R representations. We were interested in a \hat{B}_+ followed by a string of \hat{B}_- superoperators because this sequence appears in the definition of the response function $R_B^{(n)}$. However, we can also consider a \hat{B}_+ superoperator followed by an arbitrary time-ordered string of \hat{B}_+ and

\hat{B}_- superoperators. The same factorization procedure can be applied to any such sequence.

Of particular interest is the two-point correlation function of B , $R_B^{++}(t, t_1) \equiv \langle \mathcal{T} \hat{B}_+(t) \hat{B}_+(t_1) \rangle_0$, or

$$G_B^{++}(\tau_1) \equiv \langle \mathcal{T} \hat{B}_+(\tau_1) \hat{B}_+(0) \rangle_0. \quad (3.52)$$

This correlation function is a measure of the fluctuations in B , which may lead to significant fluctuations of the force. Using the identity $B_+ = [q_a q_b]_+ = q_{a+} q_{b+} + \frac{1}{4} q_{a-} q_{b-}$, we factor $G_B^{++}(\tau_1)$ using the single-molecule Green functions:

$$\boxed{G_B^{++}(\tau_1) = G_a^{++}(\tau_1) G_b^{++}(\tau_1) + \left(\frac{\hbar}{2i}\right)^2 (G_a^{+-}(\tau_1) G_b^{+-}(\tau_1) + G_a^{+-}(-\tau_1) G_b^{+-}(-\tau_1))}. \quad (3.53)$$

Thus the same single-molecule quantities that determine the van der Waals response function also determine the fluctuations in B .

In the preceding section we considered the case of molecules at different temperatures to calculate $G_B^{+-}(\tau_1)$. Here we apply the same Green functions (Eqs. 3.39a - 3.39c) to calculate $G_B^{++}(\tau_1)$. Taking the Fourier transform of Eq. 3.53 yields,

$$\tilde{G}_B^{++}(\omega) = \frac{\hbar^2}{4\pi^2} \left[\left(\alpha_a''(\omega) \coth \frac{\hbar\omega\beta_a}{2} \right) * \left(\alpha_b''(\omega) \coth \frac{\hbar\omega\beta_b}{2} \right) + \alpha_a''(\omega) * \alpha_b''(\omega) \right] \quad (3.54a)$$

$$= \frac{\hbar^2}{4\pi^2} \int_{-\infty}^{\infty} d\omega_1 \alpha_a''(\omega_1) \alpha_b''(\omega - \omega_1) \left[\coth \frac{\hbar\omega_1\beta_a}{2} \coth \frac{\hbar(\omega - \omega_1)\beta_b}{2} + 1 \right] \quad (3.54b)$$

where the $*$ operator denotes a convolution.

In the low temperature limit, the operator B undergoes zero-point fluctuations, whose origin is the zero-point fluctuations of \hat{q}_a and \hat{q}_b of the individual molecules. The term in the brackets in Eq. 3.54b is zero for $\omega_1 < 0$ and $\omega_1 > \omega$, and is equal to 2 for $0 < \omega_1 < \omega$. Thus

$$\tilde{G}_B^{++}(\omega) = \frac{\hbar^2}{2\pi^2} \int_0^\omega d\omega_1 \alpha_a''(\omega_1) \alpha_b''(\omega - \omega_1) \quad k_B T \ll \hbar\omega_0. \quad (3.55)$$

In the high temperature limit, \hat{q}_a and \hat{q}_b each act as independent fluctuating classical quantities. The fluctuation term dominates Eq. 3.53, so we have the classical relation

$$G_B^{++}(\tau_1) = G_a^{++}(\tau_1)G_b^{++}(\tau_1) \quad k_B T \gg \hbar\omega_0. \quad (3.56)$$

The fluctuations of the coordinate B are given by $\langle B^2 \rangle = G_B^{++}(0)$, and the individual Green functions are given by the classical fluctuation dissipation relation

$$G_j^{++}(0) = \langle q_j^2 \rangle = k_B T_j \alpha'_j(0). \quad (3.57)$$

Substituting Eq. 3.57 into Eq. 3.56 we see that for systems at the same temperature the fluctuations in B are given by:

$$\langle B^2 \rangle = (k_B T)^2 \alpha'_a(0) \alpha'_b(0). \quad (3.58)$$

Contrast this with the average value of B for constant coupling J , derived from the high temperature limit of Eq. 3.44:

$$\langle B \rangle = J k_B T \alpha'_a(0) \alpha'_b(0). \quad (3.59)$$

By assumption $J \ll k_B T$, or the perturbative approach here would be invalid, so the fluctuations in the intermolecular force are far larger than the force itself:

$$\frac{\langle B \rangle}{\langle B^2 \rangle^{1/2}} = \frac{J \langle q_a^2 \rangle^{1/2} \langle q_b^2 \rangle^{1/2}}{k_B T}. \quad (3.60)$$

That is, the mean force is less than its fluctuations by the ratio of the mean interaction energy to $k_B T$.

Bartolo and coworkers recently studied fluctuations in the Casimir-like forces that arise between plates in correlated fluids [8]. They found significant fluctuations, but only considered the classical (high-temperature) limit. The present results describe

the fluctuations throughout the classical and quantum regime, albeit for the nonretarded interaction.

An alternative method to evaluate the fluctuations in B is to apply to fluctuation-dissipation theorem directly to the van der Waals response function. Namely, if there is dissipation from motion along coordinate B , then, by the fluctuation dissipation theorem, there are spontaneous fluctuations in that coordinate. While the approach of the previous section only required local thermal equilibrium, this approach requires global thermal equilibrium, i.e. the molecules must be at the same temperature.

The fluctuation dissipation theorem applied to the van der Waals response functions states

$$\tilde{G}_B^{++}(\omega) = \frac{\hbar}{2\pi} \chi_B''(\omega) \coth\left(\frac{\hbar\omega\beta}{2}\right). \quad (3.61)$$

Taking $\chi_B''(\omega)$ from Eq. 3.40, should lead to an expression for $\tilde{G}_B^{++}(\omega)$ that is equivalent to Eq. 3.54b in the limit $\beta_a = \beta_b$. Unfortunately I did not find a simple way to prove this. Low-frequency fluctuations in the van der Waals force may be significant in reaction kinetics where the rate depends not on the mean force but on its extrema.

3.6 Higher order forces

The Liouville space superoperator formalism enables us to calculate contributions to the intermolecular force beyond second order in J . From Eq. 2.15, the second-order response function of the joint coordinate B to coupling J is

$$\begin{aligned} R_B^{(2)}(t, t_2, t_1) &= R_a^{+-}(t, t_2, t_1) R_b^{+++}(t, t_1, t_2) \\ &\quad + R_a^{++-}(t, t_2, t_1) R_b^{+-}(t, t_1, t_2) \\ &\quad + R_a^{+++}(t, t_2, t_1) R_b^{+--}(t, t_1, t_2). \end{aligned} \quad (3.62)$$

This expression contains the second order response functions of the individual molecules (R_a^{+-} and R_b^{+-}), the third moment of the fluctuations of each molecule (R_a^{+++} and R_b^{+++}), and the response of the second moment of the fluctuations to a perturbation (R_a^{++-} and R_b^{++-}). Similar expressions may be generated to arbitrary order.

3.7 Discussion

In this chapter we studied the forces between idealized “molecules,” coupled to baths at different temperatures and subject to a time-dependent coupling. By varying the temperatures we could make the force attractive or repulsive, and we could make the friction positive or negative. Of course it is implausible to hold two molecules in solution at different temperatures. Furthermore, the temperatures must be comparable to the excitation energies, which would be unreasonably hot for most electronic transitions. However, the above results also apply to closely spaced micromechanical components, which may exist at different temperatures and have lower frequency electronic modes. There has recently been interest in using van der Waals-Casimir forces to actuate microelectromechanical systems (MEMs) [32]. These efforts have been hindered by the fact that the force is always one-way: it can bring two elements together, but a separate force is needed to take them apart. The results of this section show that it is possible to reverse the sign of the force through careful choice of materials and by applying temperature gradients. Friction is a second major obstacle in building MEMs devices. The ability to generate negative friction under a sufficiently strong temperature gradient could, in principle, solve this problem. In the next chapter I consider the forces between molecules in athermal distributions, where one molecule is in an excited state.

Chapter 4

Excited state forces

We calculate the nonretarded interaction force between two molecules, one of which is excited. Previous calculations of this force have focused on few-level gaseous atoms, in which case the Hamiltonian may be diagonalized exactly [177, 149, 150, 203]. These calculations show that optical excitation can dramatically alter the long-range force. However, it is not clear how or whether these formal calculations apply to real multilevel molecules in the presence of relaxation and dephasing.

We show that the coupling responsible for fluorescence resonance energy transfer (FRET) generates a mechanical force that is distinct from the van der Waals force between ground-state molecules and can be either attractive or repulsive. The underlying potential has the same $1/r^6$ distance-dependence as the rate of FRET and the two are connected by a Kramers-Kronig relation. Just as the rate of FRET can be derived either classically or quantum mechanically, so too can the interaction potential. Because of the FRET-force, time-resolved FRET measurements contain information on the mechanical stiffness of the matrix containing donor and acceptor. The FRET force is ~ 50 times stronger than the ground state van der Waals force.

4.1 Eigenstate picture

Intermolecular forces with one molecule excited were first studied via perturbation theory in the 1930's by Eisenschitz and London [58] and by King and Van Vleck [98]. The eigenstate approach is based on diagonalizing the Hamiltonian of the interacting molecules, either exactly or approximately via perturbation theory. Once the global eigenstates are known, the distance-dependent energy of each eigenstate determines the intermolecular force when the system is in that state.

For dissimilar molecules, the energy can be calculated to second order in perturbation theory via a variant of Eq. 3.7. Suppose molecule b is excited to state i . Then

$$U = -\frac{1}{\hbar} J^2 \sum_{\{m,n\}} \frac{|\mu_{0m}^a \mu_{in}^b|^2}{\omega_{m0}^a + \omega_{ni}^b}. \quad (4.1)$$

Some terms in Eq. 4.1 involve downward transitions of molecule b , in which case ω_{ni}^b is negative. If molecule a has a transition frequency $\omega_{m0}^a \approx -\omega_{ni}^b$, then there is a resonant contribution to the denominator, which may be positive or negative. For molecules with closely spaced transitions, these resonant denominators dominate the interaction, leading to strongly attractive or repulsive forces.

If the coupling energy, $V = J\mu_a\mu_b$, is larger than the splitting between interacting levels (e.g. for any interaction of identical molecules with one excited), then the perturbative assumption underlying Eq. 4.1 is invalid and it is necessary to use degenerate perturbation theory. For interaction of identical molecules, the dipole-dipole coupling splits the doubly degenerate first excited state in *first* order. The corresponding eigenstates have a delocalized excitation (called a Frenkel exciton) in a

symmetric or antisymmetric configuration over both molecules. Note that the intermolecular interaction is dipole-dipole, and not due to electron overlap. Thus, while excitons are delocalized, electrons are firmly bound to the individual molecules.

4.1.1 Two-level system

As a simple application of the eigenstate picture, consider the interaction of two identical two-state fluorophores, one excited and the other in the ground state. Each molecule has a resonant frequency of ω_0 , and the coupling between the molecules is $V = J\mu_a\mu_b$. Eq. 3.7 shows that the ground state shift is $U = -\frac{1}{2}V^2/\hbar\omega_0$. The singly excited states of the dimer are split by the coupling, and have energies $U = \hbar\omega_0 \pm V$. These states are illustrated in Figure 4.1. For dipole-dipole coupling ($J \propto r^{-3}$), a dimer in the lower one-exciton state experiences a r^{-3} attraction and a dimer in the upper one-exciton state experiences a r^{-3} repulsion.

Niemax detected these first-order forces between excited atoms in the gas phase [142]. He found the force to be up to four orders of magnitude stronger than the ground state force. However, it is an experimental fact that in condensed matter there is rapid thermalization within the one-exciton manifold. A system in the repulsive upper state quickly relaxes to the attractive ground state on a timescale of picoseconds, so the repulsive first-order force is not detectable in solution.

We may patch the eigenstate model by assuming thermal equilibrium between the two one-exciton states on a timescale short compared to radiative decay to the ground state. Considering just the states with energy $U = \hbar\omega_0 \pm V$, the partition function is $Z = 2e^{-\beta\hbar\omega_0} \cosh(\beta V)$, whence the free energy of the excited dimer, $F = -k_B T \ln Z$

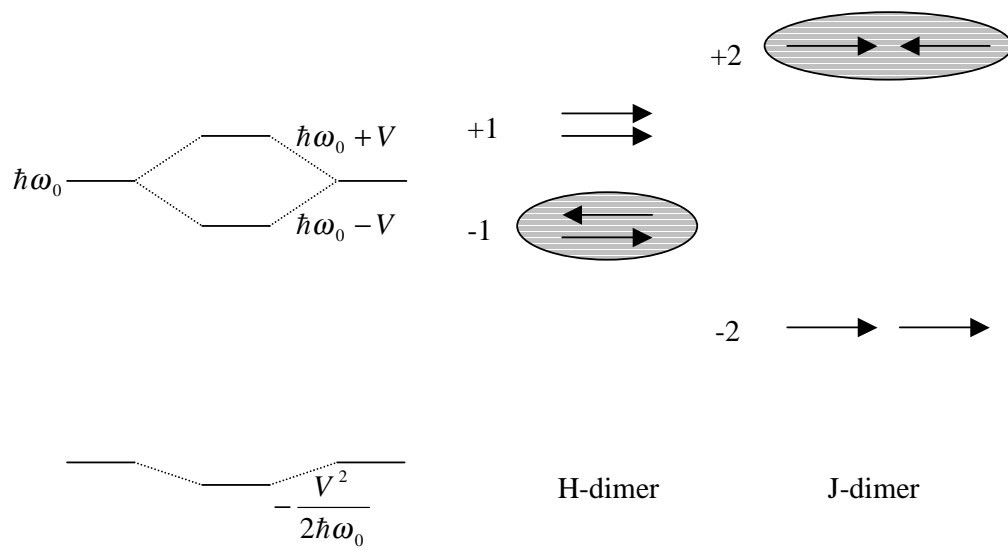


Figure 4.1: Level-splitting of identical 2-level molecules coupled through a dipole-dipole interaction. In an H-dimer the transition dipoles are side-by-side. The level shifts are ± 1 in units of $\mu_a\mu_b/4\pi\epsilon_0r^3$. The lower one-exciton state (shaded) has zero dipole strength and thus does not absorb or emit light. In a J-dimer the transition dipoles are end-to-end. The level shifts are ± 2 in units of $\mu_a\mu_b/4\pi\epsilon_0r^3$. The upper one-exciton state (shaded) has zero dipole strength.

is

$$F = \hbar\omega_0 - k_{\text{B}}T \ln[2 \cosh(V/k_{\text{B}}T)]. \quad (4.2)$$

In this case the force is always attractive because at any finite temperature there is a greater population in the lower one-exciton state than in the upper one-exciton state. As the intermolecular separation increases, the interaction free energy switches from first-order ($\Delta F \propto -V$ for $V > k_{\text{B}}T$) to second-order ($\Delta F \propto -V^2/k_{\text{B}}T$ for $V < k_{\text{B}}T$). Figure 4.2 illustrates this transition. Thermalization typically occurs over several picoseconds in water. On a much longer timescale (several nanoseconds) the one-exciton states decay via spontaneous emission or a nonradiative process, and the interaction free energy returns to its equilibrium value, $\Delta F \propto -V^2/\hbar\omega_0$, assuming $k_{\text{B}}T \ll \hbar\omega_0$. Typically $\hbar\omega_0 \sim 50k_{\text{B}}T$, so the excited-state force is roughly 50 times stronger than the ground state force, even in the weak-coupling regime $V < k_{\text{B}}T$. We will see that this enhancement of excited state forces persists in the more detailed models considered below.

The eigenstate picture has a number of shortcomings for calculating intermolecular forces. Excited state forces should be time dependent: a sequence of optical pulses puts the system in a time-dependent superposition of excited states, which eventually relax back to the ground state. Yet the eigenstate picture is, by definition, time-independent. The source of this problem is that the eigenstates calculated above are not the true system eigenstates. Each molecule has a vast number of modes in its environment that are coupled to its principle electronic coordinates. Relaxation arises from a slow leakage of energy from the modes explicitly considered to the continuum of environmental modes.

The environmental modes introduce fluctuations in the energy of each eigenstate

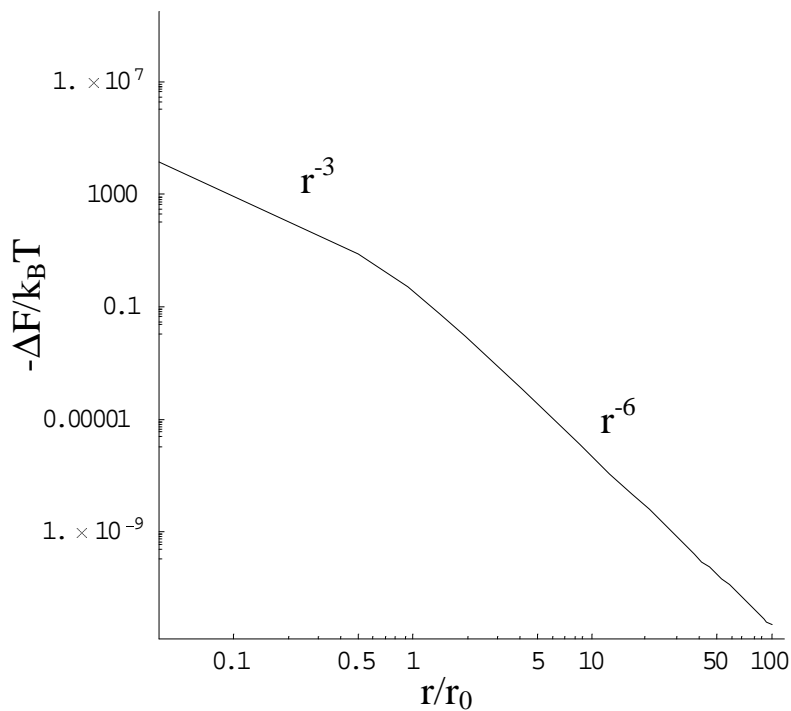


Figure 4.2: Log-log plot of the free energy of a dipole-dipole coupled dimer within the one-exciton manifold as a function of the intermolecular separation. The critical separation, r_0 , corresponds to the solution of $V(r) = k_B T$, where $V(r) = J(r)\mu_a\mu_b$. When $r \ll r_0$ ($V \gg k_B T$), essentially all of the population is in the lower excitonic state, so the free-energy is first-order in V . When $r \gg r_0$ ($V \ll k_B T$), the population is split roughly equally between the lower and upper states. The excess in the lower state is proportional to $V/k_B T$, so the free-energy is proportional to $V^2/k_B T$.

of magnitude $\sim k_B T$. These fluctuations, which affect the denominators of Eq. 3.7 and Eq. 4.1 are unimportant for the ground state force because for most electronic transitions, $k_B T \ll \hbar\omega_0$. In fact, it is common to replace the denominator for each term in the sum in Eq. 3.7 by an “average” excitation energy, without much loss in accuracy. However, for near-resonant excited-state forces, interactions with the environment are crucial because the denominator of Eq. 4.1 may be very small. Interactions with the environment also play a crucial role in spectroscopy: they cause spectral broadening, fluorescence Stokes shifts, and spontaneous emission. Building a microscopic model that incorporates these environmental effects is a challenging and complicated task, which we do not attempt here. Rather, we seek relations between spectroscopic quantities and mechanical forces that are independent of the details of the structure of the molecule or its interactions with the environment.

4.2 FRET force

In this section we study the force with one molecule excited for arbitrary donor and acceptor spectra, in the limit where the intermolecular coupling is weak compared to the coupling to the bath. This limit corresponds to the regime of validity of the Förster theory of fluorescence resonance energy transfer (FRET). There is an intimate connection between force and the rate of FRET.

FRET from an excited donor molecule to a nearby acceptor plays a major role in photosynthesis, carrying energy from chlorophyll molecules to the photosynthetic reaction center [189]. FRET also provides a nanoscale ruler: when donor and acceptor are attached to a biomolecule, the rate of FRET indicates the donor-acceptor distance [76, 181]. A process analogous to FRET involving vibrational excitations

and energy transfer may play an important role in transport of energy within and between proteins [112] and was recently observed experimentally for OH stretches in water [201]. There has been a resurgence of interest in FRET in connection with single-molecule studies as a probe for conformations of polymers and biomolecules [197].

FRET and long-range dispersion forces both arise from a coupling between the transition-dipoles of two molecules. Thus it is reasonable to expect a change in the long-range intermolecular force to accompany the process of FRET. This FRET force (FF) has implications both for photosynthesis and for biophysical FRET studies. A force accompanying photosynthetic FRET may lead to functionally significant conformational changes in the protein scaffold around chlorophyll molecules. Biophysical FRET studies usually assume that the FRET pair does not affect the molecule under study. While FF tends to be weak, corresponding to an interaction free-energy of $\sim 0.1k_B T$ at a donor-acceptor separation of 1 nm, this is still ~ 50 times *stronger* than the ground state van der Waals force. Small changes in intermolecular force can have a macroscopic effect near a critical point, where all other forces along a conformational coordinate vanish. Polymer solutions can be brought near a critical point by adjusting temperature and solvent composition [67]. Moreover, the force creates the possibility to use light to *control* the conformation of a biomolecule and to probe its mechanical response.

One way to think about the FF is as a generalization of optical trapping. A polarizable particle (atom, molecule, colloid, etc.) experiences a force along an electric field gradient. In laser tweezers, tight focusing of the laser beam creates the field-gradient [37]. It has been proposed to use sharp metal tips to enhance optical fields and field-gradients [27]. Consider the limit in which the sharp metal tip is shrunk

down to a single molecule. The near-field of an excited molecule has strong fields and strong field-gradients. Thus the FF can be thought of as optical trapping of the acceptor by the near-field of the excited donor.

This electrodynamic picture can be formally established by using the multipolar Hamiltonian in which all intermolecular interactions are mediated by photons, so there is no explicit donor-acceptor coupling in the Hamiltonian [146]. The Coulomb force is recovered in the near-field limit, where retardation is neglected. This picture can be obtained classically because the Hamiltonian for a harmonic oscillator is identical in classical and quantum mechanics. By modelling the acceptor as a collection of harmonic oscillators, and then lumping this response into the complex polarizability function, $\alpha(\omega)$, the system appears to be completely classical [109, 132].

A second way to understand the FRET-force is to consider the eigenstates of the donor and acceptor in the minimal coupling Hamiltonian, with the Coulomb coupling included explicitly [100, 101]. In this picture the force arises from a radiative shift in the energy levels of the donor induced by its coupling to the acceptor. The minimal coupling and multipolar Hamiltonians are related by a canonical gauge transformation and the two descriptions are both exact and equivalent, even though they offer completely different physical pictures [100, 101, 132, 137].

A third way to calculate the FRET-force is with the superoperator techniques developed in Chapters 1 and 2. The intermolecular dipole-dipole correlation is factored in terms of single-molecule absorption and emission spectra. This approach yields the same results as the other two.

4.2.1 Electrodynamic derivation

Molecule in a field

A spatially uniform electric field

$$E(t) = E_0 \sin \omega t \quad (4.3)$$

induces an oscillating dipole moment, $p_a(t)$, in a molecule

$$p_a(t) = \alpha'_a(\omega) E_0 \sin(\omega t) - \alpha''_a(\omega) E_0 \cos(\omega t) \quad (4.4)$$

where the frequency-dependent complex polarizability is $\alpha(\omega) = \alpha'(\omega) + i\alpha''(\omega)$.

The molecule absorbs power P :

$$\begin{aligned} P &= \overline{E\dot{p}_a} \\ &= \frac{1}{2} E_0^2 \omega \alpha''_a(\omega), \end{aligned} \quad (4.5)$$

where the average is taken over many optical cycles. If the electric field has a power spectral density, $f(\omega)$, where $\int f(\omega) d\omega = 1$, then the molecule absorbs a power per unit frequency

$$P(\omega) = \frac{1}{2} E_0^2 \omega \alpha''_a(\omega) f(\omega) \quad (4.6)$$

and the total power absorbed is $P = \int_0^\infty P(\omega) d\omega$.

The molecule also experiences a change in its mean free-energy, U :

$$\begin{aligned} U &= -\frac{1}{2} \overline{E p_a} \\ &= -\frac{1}{4} E_0^2 \alpha'_a(\omega). \end{aligned} \quad (4.7)$$

If the field has a power spectral density $f(\omega)$, then the change in free-energy per unit frequency is

$$U(\omega) = -\frac{1}{4} E_0^2 \alpha'_a(\omega) f(\omega), \quad (4.8)$$

and the total free energy shift is $U = \int_0^\infty U(\omega) d\omega$.

Comparison of Eqs. 4.6 and 4.8 shows that the change in free-energy and rate of excitation (both per unit frequency) are related:

$$\boxed{U(\omega) = -\frac{1}{2} \left(\frac{\alpha'_a(\omega)}{\alpha''_a(\omega)} \right) \hbar K(\omega)} \quad (4.9)$$

where we have replaced the power absorbed by the rate of excitation, $K(\omega) = P(\omega)/\hbar\omega$.

Field gradients cause the rate of excitation, and hence the free-energy, to depend on molecular position, \mathbf{r} . Molecular anisotropy causes the rate of excitation to depend on the angle, θ , between the molecular axis and the local field. Making note of these effects, we get a position and orientation dependent free-energy $U(\mathbf{r}, \theta)$, which leads to a force $\mathbf{F} = -\nabla U(\mathbf{r}, \theta)$ and to a torque $\tau = -\partial U(\mathbf{r}, \theta)/\partial\theta$.

The electric field, $E(t)$, could come from a light source, or it could be produced by a nearby excited donor molecule: the acceptor, a , responds the same way regardless of the source of the field. When the electric field comes from laser light, the \mathbf{r} and θ dependence of $U(\mathbf{r}, \theta)$ lead to optical trapping[37] and the optical Kerr effect, respectively [203, 176]. In this case the \mathbf{r} dependence comes from the tight focusing of the laser beam. When the electric field comes from an excited donor molecule, the spatial dependence originates from the near-field variation of the field created by the donor and Eq. 4.9 gives the intermolecular potential associated with FRET. In principle there is also a torque that seeks to align anisotropic molecules participating in FRET. This torque will not be considered here.

4.2.2 Application to FRET

Forster showed that the rate of FRET is[5]

$$k_{FRET} = \frac{9c^4\kappa^2}{8\pi\tau_d r^6} \int_0^\infty \frac{f_d(\omega)\sigma_a(\omega)}{n^4(\omega)\omega^4} d\omega, \quad (4.10)$$

where τ_d is the lifetime of the donor, r is the distance between donor and acceptor, $f_d(\omega)$ is the normalized emission spectrum of the donor, $\sigma_a(\omega)$ is the absorption cross-section of the acceptor, and $n(\omega)$ is the refractive index of the medium surrounding the donor and acceptor [143]. The factor $\kappa \equiv 3(\hat{n}_a \cdot \hat{r})(\hat{n}_d \cdot \hat{r}) - \hat{n}_a \cdot \hat{n}_d$ takes into account the relative orientation of donor and acceptor transition dipoles, where \hat{n}_a and \hat{n}_d are unit vectors oriented along the transition dipoles of the acceptor and donor, respectively. To express k_{FRET} in terms of the polarizability we make the substitution

$$\sigma_a(\omega) = \frac{\omega\alpha_a''(\omega)}{3c\epsilon_0 n(\omega)}, \quad (4.11)$$

so that

$$k_{FRET} = \int_0^\infty \frac{3c^3\kappa^2}{8\pi\epsilon_0\tau_d r^6} \frac{f_d(\omega)\alpha_a''(\omega)}{n^5(\omega)\omega^3} d\omega. \quad (4.12)$$

The integrand of Eq. 4.12 is precisely the $K(\omega)$ in Eq. 4.9. Combining Eqs. 4.9 and 4.12, we find the interaction free-energy associated with FRET

$$U_{FRET} = -\frac{3\hbar c^3\kappa^2}{16\pi\epsilon_0\tau_d r^6} \int_0^\infty \frac{f_d(\omega)\alpha_a'(\omega)}{n^5(\omega)\omega^3} d\omega. \quad (4.13)$$

4.2.3 Kramers-Kronig relations

Both the real and imaginary parts of the molecular polarizability can be readily computed for models and at various levels of theory. Absorption experiments give the imaginary part, but the real part is harder to measure. To eliminate $\alpha'(\omega)$ in the

expression for U_{FRET} , we use the Kramers-Kronig formula:

$$\alpha'_a(\omega) = \frac{2}{\pi} \wp \int_0^\infty \frac{\omega' \alpha''_a(\omega')}{\omega'^2 - \omega^2} d\omega', \quad (4.14)$$

where \wp indicates the principal value of the integral. Thus

$$U_{FRET} = -\frac{3\hbar c^3 \kappa^2}{16\pi \epsilon_0 \tau_d r^6} \int_0^\infty \frac{2}{\pi} \wp \int_0^\infty \frac{f_d(\omega) \omega' \alpha''_a(\omega')}{n^5(\omega) \omega^3 (\omega'^2 - \omega^2)} d\omega' d\omega \quad (4.15)$$

This expression *almost* contains $K(\omega)$, except that $f_d(\omega)$ and $\alpha''(\omega')$ occur at different frequencies. We thus define a new quantity, $K(\omega, \omega')$:

$$K(\omega, \omega') \equiv \frac{3c^3 \kappa^2}{8\pi \epsilon_0 \tau_d r^6} \frac{f_d(\omega) \alpha''_a(\omega')}{n^5(\omega) \omega^3}. \quad (4.16)$$

This two-dimensional transition density corresponds to the rate of FRET that would occur if the spectrum of the acceptor were shifted along the frequency axis relative to the spectrum of the donor. While this shift cannot be easily realized experimentally (i.e. it is hard to make a family of molecules with shifted spectra but the same spectral lineshape), it is easy to compute $K(\omega, \omega')$ from a known donor emission spectrum and acceptor absorption spectrum. In terms of $K(\omega, \omega')$,

$$K_{FRET} = \int_0^\infty \int_0^\infty K(\omega, \omega') \delta(\omega' - \omega) d\omega' d\omega \quad (4.17)$$

and

$$U_{FRET} = -\frac{\hbar}{\pi} \int_0^\infty \wp \int_0^\infty \frac{\omega' K(\omega, \omega')}{\omega'^2 - \omega^2} d\omega' d\omega. \quad (4.18)$$

4.2.4 Eigenstate derivation

In the previous section we considered a molecule with arbitrary polarizability, $\alpha(\omega)$, and focused on how $\alpha(\omega)$ mediates the response to an electric field. This corresponds to the multipolar Hamiltonian. In the alternative approach, based on the minimal

coupling Hamiltonian, we consider the internal eigenstates of the donor and acceptor molecules, and include the dipole-dipole coupling as a perturbation to these states. Then the question is, how does the coupling affect the expectation value of the energy? This calculation closely follows Förster's original paper on FRET,[153, 2] and yields the same results as the previous calculation.

In the Wigner-Weiskopff model, when a state, i , is coupled to a broad continuum, $\{j\}$, an effective Hamiltonian arises which adds a self energy to the energy of the isolated state: $E_i \rightarrow E_i + R_i$ [137]. Here

$$R_i = \lim_{\eta \rightarrow 0^+} \sum_j \frac{|V_{ij}|^2}{E_i - E_j + i\eta} \quad (4.19)$$

where V_{ij} is the matrix element coupling states i and j , and E_i and E_j are the energies of these states. This self energy is partitioned as,

$$R_i = U_i - \frac{i\hbar}{2}k_i, \quad (4.20)$$

where the real part, U_i , gives the level shift of state i , and the imaginary part, k_i , gives the rate of decay of state i . The Kramers-Kronig relation between the two follows immediately from the analytic properties of the self energy, which are a direct consequence of causality.

Let the initial state, i , correspond to the excited donor and ground state acceptor. The manifold of final states, $\{j\}$, corresponds to the ground state donor and excited acceptor (we assume that the acceptor has densely distributed levels). Replacing the sum in Eq. 4.19 by an integral over acceptor states, we find that the rate of energy transfer is given by Fermi's golden rule

$$k_i = \frac{2\pi}{\hbar} \int |V_{ij}|^2 \rho(E_j) \delta(E_i - E_j) dE_j \quad (4.21)$$

where $\rho(E_j)$ is density of transitions of energy E_j .

The coupling to a continuum also produces an energy-shift, U_i , of the initial state:

$$U_i = \wp \int \frac{|V_{ij}|^2 \rho(E_j)}{E_i - E_j} dE_j. \quad (4.22)$$

Förster used Eq. 4.21 to calculate the rate of FRET. We follow his procedure but apply it to Eq. 4.22 to calculate the energy shift.

The wavefunctions of the donor-acceptor system in its initial and final states are:

$$\begin{aligned} \Psi_i &= \phi_d^* \phi_a \Phi_d^* \Phi_a \\ \Psi_j &= \phi_d \phi_a^* \Phi_d \Phi_a^*, \end{aligned} \quad (4.23)$$

where ϕ_a and ϕ_d are the electronic wavefunctions and Φ_a and Φ_d are the nuclear wavefunctions. The matrix element for the transition is

$$\begin{aligned} V_{ij} &= \langle \Psi_j | \frac{e^2}{4\pi\epsilon_0 n^2 r} | \Psi_i \rangle \\ &= V_e \langle \Phi_d | \Phi_d^* \rangle \langle \Phi_a^* | \Phi_a \rangle. \end{aligned} \quad (4.24)$$

The nuclear components of V_{ij} are the Franck-Condon factors $S_d(E_d^*, E_d) \equiv \langle \Phi_d | \Phi_d^* \rangle$ and $S_a(E_a, E_a^*) \equiv \langle \Phi_a^* | \Phi_a \rangle$.

There are many ways to arrive at the electronic component of the matrix element, $V_e \equiv \langle \phi_d \phi_a^* | e^2 / (4\pi\epsilon_0 n^2 r) | \phi_d^* \phi_a \rangle$. Note that to calculate forces, it is necessary to know the *gradient* in V_e at the equilibrium donor-acceptor separation. If the molecules are neutral and their separation is large compared to their size, then the point dipole approximation is appropriate:

$$V_e = \frac{\mu_a \mu_d^k}{4\pi\epsilon_0 n^2 r^3}. \quad (4.25)$$

For molecules where the separation is small compared to the size, but there is still negligible electronic overlap (e.g. chlorophyll molecules in the bacterial photosynthetic

antenna complex), then the point dipole approximation breaks down and V_e must be calculated numerically, using one of the expansions of Section 3.2 [185]. Standard quantum chemistry codes exist to do this at varying levels of theory. The coupling can also be extracted from spectroscopic data: the Davydov splitting in the donor-acceptor pair is twice the electronic coupling energy [41]. It may be possible to obtain the gradient of V_e from the pressure-dependence of the the Davydov splitting.

Typically the donor in its excited state occupies a distribution of vibrational energy levels with probability $g_d(E_d^*)$. Similarly, the acceptor in its ground state occupies a distribution of vibrational energy levels with probability $g_a(E_a)$. The total rate of FRET is given by the rate for each microstate (E_d^*, E_a) weighted by the probability for the system to be in that microstate, and summed over all microstates. If $g_d(E_d^*)$ and $g_a(E_a)$ are statistically independent (i.e. they arise from different vibrational modes), then this sum factors into two components. One component depends only on the emission spectrum of the donor; the other depends only on the absorption spectrum of the acceptor. We apply this procedure to compute the energy-shift.

From Eq. 4.22, the total energy shift for all initial states of the donor is:

$$U_{FRET} = \int \wp \int \frac{\rho(E_i) |V_{ij}|^2 \rho(E_j)}{E_i - E_j} dE_j dE_i. \quad (4.26)$$

The numerator of the integrand of Eq. 4.26 can be expanded to yield

$$\begin{aligned} \rho(E_i) |V_{ij}|^2 \rho(E_j) &= |V_e|^2 \left(\int g_d(E_d^*) S_d^2(E_d^*, E_d^* - E_i) dE_d^* \right) \times \\ &\quad \left(\int g_a(E_a) S_a^2(E_a, E_a + E_j) dE_a \right), \end{aligned} \quad (4.27)$$

which contains separate integrals over the donor and acceptor coordinates. Each integral gives an observable. The donor integral is related to the normalized donor

emission spectrum, $f_d(\omega_i)$, (measured in photons per unit frequency) via[144]

$$\int g_d(E_d^*) S_d^2(E_d^*, E_d^* - E_i) dE_d^* = \frac{3\pi\epsilon_0\hbar c^3}{\omega_i^3 n(\omega_i) \mu_d^2 \tau_d} f_d(\omega_i). \quad (4.28)$$

The acceptor integral is related to the acceptor absorption cross-section, $\sigma_a(\omega_j)$, via

$$\int g_a(E_a) S_a^2(E_a, E_a + E_j) dE_a = \frac{3\epsilon_0\hbar c n(\omega_j)}{\pi\omega_j \mu_a^2} \sigma_a(\omega_j). \quad (4.29)$$

If we assume that the index of refraction is weakly dependent on frequency, then $n(\omega_j)/n(\omega_i)$ cancels in the product of Eqs. 4.28 and 4.29. Combining Eqs. 4.26, 4.27, 4.28 and 4.29 and converting to integrals over frequency gives U_{FRET} in terms of experimentally accessible parameters:

$$U_{FRET} = -\frac{|V_e|^2 9\hbar\epsilon_0^2 c^4}{\mu_a^2 \mu_d^2 \tau_d} \int \wp \int \frac{f_d(\omega_i) \sigma_a(\omega_j)}{\omega_i^3 \omega_j (\omega_j - \omega_i)} d\omega_j d\omega_i. \quad (4.30)$$

Substituting $\alpha''(\omega_j)$ for $\sigma(\omega_j)$ (Eq. 4.11) gives

$$U_{FRET} = -\frac{|V_e|^2 3\hbar\epsilon_0 c^3}{\mu_a^2 \mu_d^2 \tau_d} \int \wp \int \frac{f_d(\omega_i) \alpha_a''(\omega_j)}{n(\omega_j) \omega_i^3 \omega_j - \omega_i} d\omega_j d\omega_i. \quad (4.31)$$

Eq. 4.31 contains a Kramers-Kronig relation for $\alpha_a'(\omega_i)$, so making this substitution and inserting the point dipole approximation for V_e (Eq. 4.25) yields

$$U_{FRET} = -\frac{3\hbar c^3 \kappa^2}{16\pi\epsilon_0 r^6 \tau_d} \int_0^\infty \frac{f_d(\omega) \alpha_a'(\omega)}{n^5(\omega) \omega^3} d\omega, \quad (4.32)$$

which is exactly the same as the classically derived Eq. 4.13.

4.2.5 Superoperator derivation

Finally, we derive the FF within the superoperator formalism developed in Chapters 1 and 2. We treat the molecular dipole moments, μ_a and μ_d , as operators, and define the dipole-dipole correlation operator $B \equiv \mu_d \mu_a$. The bimolecular perturbation is

$H_{da}(t) = -J(t)\mu_d\mu_a$. We seek the Green function $G_B^{+-}(\tau_1)$ that connects $\langle B(t) \rangle$ to $J(t - \tau_1)$ via

$$\langle B(t) \rangle = \int G_B^{+-}(\tau_1)J(t - \tau_1)d\tau_1. \quad (4.33)$$

As in Chapter 3 we apply Eq. 3.38 to factor $G_B^{+-}(\tau)$ in terms of single-molecule quantities: $G_B^{+-}(\tau_1) = G_a^{+-}(\tau_1)G_d^{++}(\tau_1) + G_a^{++}(\tau_1)G_d^{+-}(\tau_1)$. The Förster theory typically neglects reverse energy transfer from the acceptor to the donor. This is equivalent to neglecting the term $G_a^{++}(\tau_1)G_d^{+-}(\tau_1)$. Using Eq. 3.39b for $G_a^{+-}(\tau_1)$ we have in the frequency domain:

$$\chi_B^{(1)}(\omega) = \int_{-\infty}^{\infty} \alpha_a(\omega')\tilde{G}_d^{++}(\omega - \omega')d\omega'. \quad (4.34)$$

The fluctuations of the donor are related to the donor emission spectrum via

$$\tilde{G}_d^{++}(\omega) = \frac{3\pi\epsilon_0\hbar c^3}{\omega^3 n(\omega)\tau_d} \left[\frac{1}{2}(f_d(\omega) + f_d(-\omega)) \right]. \quad (4.35)$$

When calculating $\chi_B^{(1)}(0)$ from Eq. 4.34, only the real part of $\alpha_a(\omega')$ survives the integral because $\tilde{G}_d^{++}(\omega')$ is an even function of frequency. We may rewrite the integral over the positive ω' -axis only. Under steady-state coupling, the interaction energy is given by $U_{FRET} = -\frac{1}{2}\chi_B^{(1)}(0)J^2$. The coupling J is given by:

$$J = \frac{\kappa}{4\pi\epsilon_0 n^2 r^3}. \quad (4.36)$$

Making these substitutions into Eq. 4.34 gives the same expression for the U_{FRET} as Eqs. 4.13 and 4.32.

4.2.6 Examples

Lorentzian lineshapes

The Lorentzian lineshape describes the response of a damped harmonic oscillator (classical or quantum mechanical), and also the linear response of a quantum mechanical two-level system. Consider the case where both the acceptor and donor are characterized by a Lorentzian response, with resonant frequencies ω_a and ω_d , respectively:

$$\begin{aligned}\alpha'_a(\omega) &= \frac{\mu_a^2}{\hbar} \frac{\omega_a - \omega}{(\omega_a - \omega)^2 + \gamma_a^2} \\ \alpha''_a(\omega) &= \frac{\mu_a^2}{\hbar} \frac{\gamma_a}{(\omega_a - \omega)^2 + \gamma_a^2},\end{aligned}\tag{4.37}$$

and

$$f_d(\omega) = \frac{\gamma_d/\pi}{(\omega_d - \omega)^2 + \gamma_d^2}.\tag{4.38}$$

Further assume that the index of refraction is weakly dependent on frequency in the region of interest and the spectra are narrow enough to replace $1/\omega^3$ by $1/\omega_0^3$, where $\omega_0 \sim (\omega_a + \omega_d)/2$. The integrals in Eqs. 4.12 and 4.13 then evaluate to

$$k_{FRET} = \frac{3c^3 \mu_a^2 \kappa^2}{8\pi\epsilon_0 \tau_d n^5 \hbar \omega_0^3 r^6} \frac{\gamma_a + \gamma_d}{(\omega_a - \omega_d)^2 + (\gamma_a + \gamma_d)^2}\tag{4.39}$$

and

$$\begin{aligned}U_{FRET} &= \frac{3c^3 \mu_a^2 \kappa^2}{16\pi\epsilon_0 \tau_d n^5 \omega_0^3 r^6} \frac{\omega_d - \omega_a}{(\omega_a - \omega_d)^2 + (\gamma_a + \gamma_d)^2} \\ &= \frac{\omega_d - \omega_a}{2(\gamma_d + \gamma_a)} \hbar k_{FRET}.\end{aligned}\tag{4.40}$$

Eq. 4.40 shows that U_{FRET} vanishes on resonance ($\omega_d = \omega_a$) and in the absence of spectral overlap ($|\omega_d - \omega_a| \gg \gamma_d + \gamma_a$). It is maximized for $\omega_d - \omega_a = \pm(\gamma_d + \gamma_a)$. If $\omega_d > \omega_a$, then U_{FRET} is positive and the force is repulsive.

The direction of the FF may be rationalized in the same way as the direction of the van der Waals force between molecules at different temperatures. If the driving frequency of the excited donor is below the resonant frequency of the acceptor, then the polarization of the acceptor is in-phase with the driving field and the force is attractive. If the driving frequency of the donor is greater than the resonant frequency of the acceptor, then the acceptor is never able to “catch up” with the quickly varying driving field and the interaction is repulsive. For homotransfer the FF is always attractive because the Stokes shift guarantees that $\omega_d < \omega_a$.

Lineshapes are usually Lorentzian near the center, but have much shorter wings (and finite second and higher moments). In many cases the wings are Gaussian. The Voigt profile (convolution of a Gaussian and a Lorentzian) or the stochastic model of Kubo (also known as the Brownian oscillator model) are commonly used models that interpolate between the two profiles [137, 107], and may be used for more realistic simulations of the FRET force.

4.2.7 Sample calculation

The FF can easily be calculated from experimental spectra via the relation

$$U_{FRET} = \frac{-\int f_d(\omega)\alpha'_a(\omega)\omega^{-3} d\omega}{\int f_d(\omega)\alpha''_a(\omega)\omega^{-3} d\omega} \frac{\hbar k_{FRET}}{2}. \quad (4.41)$$

The imaginary polarizability, $\alpha''_a(\omega)$, can be extracted from an absorption spectrum and Eq. 4.11 (there is no need to worry about multiplicative constants because they cancel in the ratio). The Kramers-Kronig relation then gives $\alpha'_a(\omega)$. If the Förster radius,¹ r_F , and the lifetime of the donor are known, k_{FRET} can easily be calculated

¹The Förster radius is defined as the donor-acceptor separation at which the rate of FRET and the rate of spontaneous emission by the donor are equal. Typical Förster radii are ~ 5 nm.

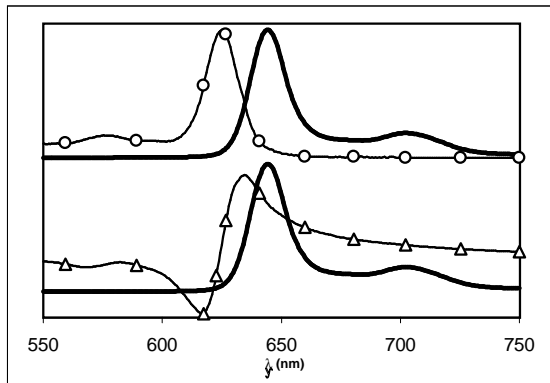


Figure 4.3: Spectral properties of Chlorophyll *b* in diethylether used for calculating the rate of homotransfer FRET (top) and the accompanying FRET force (bottom). Top: (—) emission spectrum, $f_d(\lambda)$; (—○—) absorption spectrum, $\alpha''(\lambda)$. The overlap integral yields the rate of FRET. ($\alpha''(\lambda)$ was padded with zeros for $\lambda = (700\text{nm} - 750\text{nm})$ to have absorption and emission spectra over comparable wavelengths.) Bottom: (—) same emission spectrum, $f_d(\lambda)$, as above; (—△—) real polarizability, $\alpha'(\lambda)$. The overlap integral yields the interaction energy. To calculate the real polarizability, the Kramers-Kronig relations were applied to α'' over the region $\lambda = (220\text{nm} - 750\text{nm})$.

from

$$k_{FRET} = \frac{1}{\tau_d} \left(\frac{r_F}{r} \right)^6. \quad (4.42)$$

The ratio of integrals in Eq. 4.41 is typically of order 1, and is calculated for some common FRET pairs in Table 4.1. Figure 4.3 shows the emission spectrum and calculated values of $\alpha'(\lambda)$ and $\alpha''(\lambda)$ for Chlorophyll *b*. Calculations were performed by numerically integrating spectra available over the internet [1]. Integrations and the Kramers-Kronig calculation were carried out over the spectral window for which data was reported, with no extrapolation to high or low frequencies. When the ratio of integrals (labelled in the table as $2U_{FRET}/\hbar k_{FRET}$) is negative, then the FF is attractive. At a separation equal to the Förster radius $k_{FRET} \sim 1/\tau_d$, so $U_{FRET} \sim \hbar/\tau_d$, or the radiative linewidth of the donor. This miniscule shift in energy would be very difficult to detect. However, for separations typical of chlorophyll molecules in

Donor	Acceptor	$\frac{2U_{FRET}}{\hbar k_{FRET}}$	τ_d (ns)	R_0 (Å)
Ch a ^a	Ch a	-2.1		
Ch b ^b	Ch b	-6.3		
FITC ^c	FITC	-2.25	4.2	46
FITC	TMR ^d	0.14	4.2	55
AF594 ^e	QSY21 ^f	-0.088	3.9	77
FITC	AF532 ^g	0.087	4.2	63

Table 4.1: Parameters for calculating the interaction free-energy of some common FRET pairs. The quantity $2U_{FRET}/\hbar k_{FRET}$ is the the ratio of integrals from Eq 4.41. ^aChlorophyll *a* in MeOH, ^bChlorophyll *b* in diethyl ether, ^cfluorescein isothiocyanate, ^dtetramethylrhodamine, ^eAlexa Fluor 594, ^fNonfluorescent quencher, diarylrhodamine derivative, ^gAlexa Fluor 532.

the photosynthetic antenna complex, energy transfer occurs on a timescale of 100 fs to 1 ps, so $U_{FRET} \sim 0.1k_B T$.

4.3 Discussion

The ground state interaction energy given by the McLachlan formula (Eq. 3.11) is insensitive to the details of the spectral densities because it is highly off resonant, reminiscent of the off-resonant Stark shift. The interaction energy with one molecule excited, in contrast, (Eq. 4.13) depends on the overlap of absorption and resonant emission spectra at real frequencies, and thus is highly sensitive to the composition of the interacting molecules.

In all our calculations of interaction free energies, the leading term is of the form $\Delta F = -\frac{1}{2}V_e^2/\delta$, where δ is a measure of the detuning and V_e is a measure of the electronic coupling. For ground state interactions of identical two-level systems, $\delta = \hbar\omega_0$. For the interaction where one of the molecules is excited, the detuning is entirely due to interactions with a bath and is of order $\delta \approx k_B T$. Typically $\hbar\omega_0 \sim 50k_B T$,

so the excited state force far exceeds its ground state counterpart. However, if the molecules have very different resonant frequencies, then the excited state force may not be much stronger than the ground state force. These results are valid for times long compared to the relaxation time, Δ (typically picoseconds in water), but short compared to the spontaneous lifetime (typically nanoseconds). Also, our formalism holds only for $V_e < k_B T$. For stronger couplings, excitonic effects are important and the perturbation theory which is the basis of our approach is invalid.

Other studies of the van der Waals force with one molecule excited predict a $1/r^3$ interaction potential (i.e. first order in V_e) [177, 149, 150]. Why didn't our calculations reproduce this? To get such a first order excitonic effect requires coherent interaction of the two molecules. The Förster theory of FRET applies only in the case of *very weak coupling*; that is, the intermolecular coupling must be much weaker than the linewidth associated with coupling between each molecule and a thermal bath. Coupling to a bath destroys coherence, and so the interaction potential only arises in second order in V_e . Several pseudoisocyanine (PIC) dyes spontaneously form van der Waals-bonded aggregates in solution in which the intermolecular coupling is stronger than the coupling to the bath [189, 103, 152, 40]. These materials may demonstrate strong first-order forces.

The basic phenomena associated with the FRET force (strong attraction or repulsion, positive or negative dissipation) are the same as those that arise in the interaction between materials at different temperatures (Chapter 3). This should not be surprising, considering that a hotter particle is more likely to be in an excited state than a colder particle. Thus the thermal forces can be thought of as the FRET force, averaged over a thermal distribution of donor and acceptor populations.

How would one detect a force associated with FRET? Detection is simple if the donor and acceptor have some freedom of relative movement. The donor-acceptor separation and relative orientation both affect the dipolar coupling matrix element, V_e . This matrix element in turn affects the optical properties of the dimer: it determines the rate of FRET and the Davydov splitting. A time-dependence in either of these quantities indicates movement in the excited state. Since we assume conditions under which the Förster theory is valid, the Davydov splitting is much less than the linewidth of donor or acceptor. However, a small shift in the maximum of the donor emission spectrum may still be detectable.

Several studies have observed effects that can plausibly be interpreted in terms of FRET forces, although this explanation was not put forward. Whitten and coworkers [114, 119] studied the photophysical properties of a series of tethered bichromophores, as a function of the tether length and solvent viscosity. In these studies the chromophores on opposite ends of the tether were identical, so we would expect a strongly attractive interaction when one chromophore is excited. It was observed that optical excitation caused the molecules to collapse from their extended state to a folded state. This folding did not occur in rigid solutions or when the linker between the chromophores was rigid. Zeena and Thomas [204] performed similar experiments on a series of hemicyanine-based bichromophores, and also found optically induced folding transitions. By tailoring the polarity of the solvent, they could shift the equilibrium between the folded and unfolded conformations. When the two states were equally populated, the molecules were particularly sensitive to excitation. As discussed above, the Stokes shift guarantees that the FRET force between identical molecules is strongly attractive.

Consider a tethered bichromophore in which the two chromophores have slightly different resonant frequencies. The results of this section predict that if the lower frequency chromophore is excited, then the intermolecular force will be strongly attractive. If the higher frequency chromophore is excited, then the force will be strongly repulsive. Such a molecule would constitute a molecular actuator, which can be driven to either open or close depending on the color of the incident radiation.

For fluorophores freely diffusing in solution, the fluorescence quantum yield typically drops when the concentration surpasses a certain critical value, a phenomenon known as *concentration-quenching*. In the 1970s Beddard and Porter [12] proposed a model for concentration quenching in which excitations hop between fluorophores via FRET. At high concentrations, an excitation typically visits many fluorophores before decaying via spontaneous emission. To obtain concentration quenching, Beddard and Porter postulated that an excitation “dies” if it reaches a statistical pair of molecules spaced by less than a minimum radius of ~ 1 nm. This model is in quantitative agreement with quenching data for solutions of chlorophyll *a*, but does not address the ultimate question of what happens to the excitation in the statistical pair. 1 nm is too big a gap for electron-transfer interactions, and the mechanism of concentration quenching has remained unresolved to this day [102].

The theory of excited-state forces suggests a mechanism for concentration quenching. The attractive force when one molecule is excited far exceeds its ground state counterpart. For spacings of ~ 1 nm, the force may be strong enough to temporarily bind the two fluorophores together, just as it caused the tethered bichromophores to fold. For planar molecules such as chlorophyll *a*, the most likely geometry is for the molecules to stick face-to-face to form an H-dimer. In this conformation the lowest

excitonic state has zero transition dipole to the ground state. The excitation can only decay via a nonradiative process, whereafter the two molecules dissociate. This mechanism suggests that chemical modifications that sterically hinder face-to-face aggregation should inhibit concentration quenching. Such modifications may be useful in the design of dye lasers.

The ability to generate *resonant* van der Waals forces may be of practical use. For example, in a single-component gas, it is possible to excite selectively a subset of molecules characterized by a particular Doppler shift. These molecules are all moving in roughly the same direction. The excited molecules experience increased friction in their collisions with ground-state molecules, compared to collisions between two ground-state molecules. Thus the momentum of the excited molecules will gradually be transferred to the remaining molecules in the gas, and the gas will develop a net drift in the direction set by the detuning of the laser. This drift is in addition to the drift imposed by the direct action of the laser on the gas molecules, which is the basis of many optical trapping and cooling techniques.

As a second example we consider interactions within a cell. The mechanisms of biological specificity are currently not fully understood. The inside of a cell is roughly 25% proteins by weight, with many components present in minute amounts. How do enzymes and their substrates ever find each other? Charge-charge attraction, ground-state van der Waals forces, and the hydrophobic effect are all known to play some part [88], but none of these interactions is specific. Shape complementarity and charge-transfer interactions act only over a very short range. Might conversion of ATP leave molecules in a vibrationally excited state, whereupon the van der Waals forces are long-range and specific to molecules that have matching spectra?

Chapter 5

Optical Control of Intermolecular Forces

In the previous chapter we studied forces with one molecule excited, but we did not address how the molecule got to its excited state. In this chapter we study intermolecular forces in an arbitrary time-dependent optical field. In the dark we reproduce the ground state van der Waals force; any linear or nonlinear optical process leads to a new force which may be attractive or repulsive and which may show complex time-dependence. For instance, a photon-echo signal from closely spaced molecules is associated with a “force-echo” in the dipole-dipole interaction.

5.1 Introduction

Until this point, the only perturbation we have studied is a bilinear intermolecular coupling. We applied fictitious fields to the individual molecules to calculate the generalized response functions, but these fields were always set to zero when we calculated the force. Even when we calculated the force for one molecule excited, we assumed that whatever field originally excited the molecule had returned to zero by

the time we measured the force.

In this chapter we study molecules subject to a bilinear intermolecular coupling *and* to a time-dependent electric field. Two questions naturally arise: How does the intermolecular coupling affect the optical response? and how does the optical field affect the intermolecular force?

The first question has been addressed (albeit approximately) in the nonlinear optics literature. Many interesting and important optical effects arise from interactions of closely spaced molecules. Examples are density-dependent index of refraction, superradiance, pressure-induced resonances and the formation of delocalized Frenkel excitons. These effects all arise because molecules in close proximity experience not only the applied field, but also a perturbation due to the polarization of their neighbors.

The problems of calculating the optical response and calculating the intermolecular force are closely related. For molecules a and b and a polarization operator μ , the optical polarization is given by $p(t) = \langle \mu_a(t) \rangle + \langle \mu_b(t) \rangle$; the intermolecular force is related to $\langle \mu_a(t) \mu_b(t) \rangle$. It is tempting to assume that if we can calculate $\langle \mu_a \rangle$ and $\langle \mu_b \rangle$, then we can calculate $\langle \mu_a \mu_b \rangle$. Unfortunately, this is not the case because in general $\langle \mu_a \mu_b \rangle \neq \langle \mu_a \rangle \langle \mu_b \rangle$. In particular, if both molecules are in the ground state and subject to a bilinear coupling, then $\langle \mu_a \rangle \langle \mu_b \rangle = 0$ but $\langle \mu_a \mu_b \rangle > 0$. Calculating the intermolecular force is a subtler problem than calculating the optical response because the force depends on *correlations* of operators. There is no ready-made technique in the optical arsenal which would seamlessly interpolate between the van der Waals force in the dark and light-modified intermolecular forces.

The principle approach used in the literature to calculate intermolecular forces

in an optical field is the local field approximation (LFA) [133, 147, 132]. The linear LFA has been applied successfully by Jones to a theory of electromechanics of small particles ($1 \mu\text{m} - 1 \text{mm}$) [90] in low frequency fields (kHz - GHz), and by Chaumet and Nieto-Vesperinas to interactions between colloidal particles in intense laser fields [34]. Here we extend the theory to include Brownian motion and nonlinear optical effects. The LFA correctly yields the first-order forces in the light, but misses the ground-state van der Waals energy. We discuss several *ad hoc* procedures that have been developed to extract the van der Waals energy from the local field approximation and show that these procedures are incorrect. The Liouville space superoperator formalism developed in Chapters 1 and 2 allows us to calculate the force with and without the optical field in a manner that is quantum mechanically rigorous.

5.2 Local field approximation

In the local field approximation (LFA) we solve self-consistently for the electric field at each molecule and the resulting polarization. In order to do this, we must treat the molecular polarization as a classical quantity: it has a definite value at all times, and goes to a constant (usually zero) in the absence of an optical field. This approximation is equivalent to factoring the many-body density matrix into a direct-product of single-molecule density matrices. Within the LFA, each molecule is completely characterized by its set of response functions.

Consider a monochromatic plane-wave travelling through a vacuum. The electric field is

$$\mathbf{E}(\mathbf{r}, t) = \mathbf{E}_0 e^{-i(\omega t - \mathbf{k} \cdot \mathbf{r})} + c.c. \quad (5.1)$$

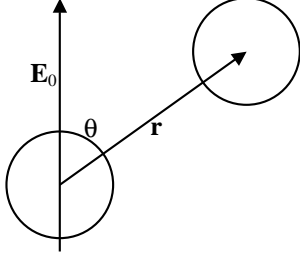


Figure 5.1: Two particles are immersed in a medium and subject to an optical field. We assume that $\mathbf{k} \cdot \mathbf{r} \ll 1$ so that the spatial variation of the applied field may be neglected.

Now introduce molecules a and b . Each molecule has a set of hyperpolarizabilities, $\alpha_j(\omega)$, $\beta_j(-\omega; \omega_1, \omega_2)$, $\gamma_j(-\omega; \omega_1, \omega_2, \omega_3)$, where the argument $-\omega$ of the hyperpolarizabilities is a reminder of the constraint $\omega_1 + \dots + \omega_n = \omega$. The n^{th} order hyperpolarizability is a tensor of rank $n + 1$ that connects n input vectors to one output vector. The polarization of molecule j is

$$\tilde{\mathbf{p}}_j(\omega) = \alpha_j(\omega)\tilde{\mathbf{E}}_j(\omega) + \int d\omega_2 \int d\omega_1 \beta_j(-\omega; \omega_2, \omega_1)\tilde{\mathbf{E}}_j(\omega_2)\tilde{\mathbf{E}}_j(\omega_1) + \dots, \quad (5.2)$$

where $\tilde{\mathbf{E}}_j$ is a Fourier component of the *local* field at molecule j .

Figure 5.1 illustrates the geometry. The vector \mathbf{r} joins the particles and forms an angle θ with the applied field. We assume $s \ll r \ll \lambda$, where s is the maximum dimension of either particle and λ is the wavelength of the incident light-wave. The first condition allows us to focus on dipole-dipole interactions to the exclusion of higher multipole interactions. The second condition allows us to ignore spatial variation in \mathbf{E} and also to ignore the effect of retardation in electromagnetic interactions between our two molecules.

5.2.1 Linear regime

For maximum generality we let the polarizability of each molecule, α_j , be a frequency dependent complex tensor. The polarization of each molecule is

$$\tilde{\mathbf{p}}_a = \alpha_a \tilde{\mathbf{E}}_a \quad (5.3a)$$

$$\tilde{\mathbf{p}}_b = \alpha_b \tilde{\mathbf{E}}_b, \quad (5.3b)$$

where we have omitted the frequency arguments and assumed that neither molecule has any permanent moments.

The local field is the sum of the incident field and the field due to the polarization of the neighboring molecule:

$$\tilde{\mathbf{E}}_a = \tilde{\mathbf{E}}_0 + \mathbf{J}\tilde{\mathbf{p}}_b \quad (5.4a)$$

$$\tilde{\mathbf{E}}_b = \tilde{\mathbf{E}}_0 + \mathbf{J}\tilde{\mathbf{p}}_a, \quad (5.4b)$$

where \mathbf{J} is the propagator that converts a polarization of one particle into an electric field at its neighbor, given by Eq. 3.4.

It is a matter of simple algebra to solve equations 5.3 and 5.4 for the four unknowns, $\tilde{\mathbf{E}}_a$, $\tilde{\mathbf{E}}_b$, $\tilde{\mathbf{p}}_a$, and $\tilde{\mathbf{p}}_b$. Doing so yields:

$$\tilde{\mathbf{E}}_a = (\mathbf{1} - \mathbf{J}\alpha_b\mathbf{J}\alpha_a)^{-1} (\mathbf{1} + \mathbf{J}\alpha_b) \tilde{\mathbf{E}}_0, \quad (5.5)$$

$$\tilde{\mathbf{p}}_a = (\mathbf{1} - \alpha_a\mathbf{J}\alpha_b\mathbf{J})^{-1} (\alpha_a + \alpha_a\mathbf{J}\alpha_b) \tilde{\mathbf{E}}_0. \quad (5.6)$$

Similar equations hold for $\tilde{\mathbf{E}}_b$ and $\tilde{\mathbf{p}}_b$ with the subscripts a and b interchanged.

The interaction free energy is given by an adiabatic switching of the coupling, \mathbf{J} (compare with Eq. 3.21):

$$U = - \int \tilde{\mathbf{p}}_a^* \tilde{\mathbf{p}}_b d\mathbf{J}, \quad (5.7)$$

and the interaction force is $\mathbf{F} = -\nabla U$. The imaginary part of the polarizability is typically negligible when the applied field is off-resonant, ($\alpha''(\omega)$ decays faster than ω^{-2} away from a resonance while $\alpha'(\omega)$ decays as ω^{-1}). Assuming that the polarizability is fully real, the free-energy of interaction, U is:

$$U = -\frac{1}{2}(1 - \alpha_a \mathbf{J} \alpha_b \mathbf{J})^{-1}(\alpha_a + \alpha_b + 2\alpha_a \mathbf{J} \alpha_b) |\tilde{\mathbf{E}}_0|^2 \quad (5.8)$$

For arbitrary anisotropic particles of fixed position and orientation, the distance-dependent part of Eq. 5.8 yields the free-energy of interaction. The force is a linear function of the intensity of the incident radiation.

We can gain physical insight into Eqs. 5.5, 5.6, and 5.8 by expanding them in powers of the coupling, $\alpha_a \mathbf{J} \alpha_b \mathbf{J}$. In the regime $|\alpha_a \mathbf{J} \alpha_b \mathbf{J}| < 1$ Eq. 5.6 becomes:

$$\tilde{\mathbf{p}}_a = \sum_{n=0}^{\infty} (\alpha_a \mathbf{J} \alpha_b \mathbf{J})^n (\alpha_a \tilde{\mathbf{E}}_0 + \alpha_a \mathbf{J} \alpha_b \tilde{\mathbf{E}}_0) \quad (5.9)$$

or

$$\tilde{\mathbf{p}}_a = \alpha_a \tilde{\mathbf{E}}_0 + \alpha_a \mathbf{J} \alpha_b \tilde{\mathbf{E}}_0 + \alpha_a \mathbf{J} \alpha_b \mathbf{J} \alpha_a \tilde{\mathbf{E}}_0 + \alpha_a \mathbf{J} \alpha_b \mathbf{J} \alpha_a \mathbf{J} \alpha_b \tilde{\mathbf{E}}_0 + \dots \quad (5.10)$$

This series expansion has a simple physical interpretation. The first term is the response of particle a to the incident field alone. The second term is a 's response to the dipole field from b 's response to the incident field. The third term is a 's response to b 's response to a 's response to the incident field, etc. An electric field propagates back and forth between the molecules, creating ever smaller corrections to the polarization.

The electric field at particle a is similarly expanded as:

$$\tilde{\mathbf{E}}_a = \tilde{\mathbf{E}}_0 + \mathbf{J} \alpha_b \tilde{\mathbf{E}}_0 + \mathbf{J} \alpha_b \mathbf{J} \alpha_a \tilde{\mathbf{E}}_0 + \mathbf{J} \alpha_b \mathbf{J} \alpha_a \mathbf{J} \alpha_b \tilde{\mathbf{E}}_0 + \dots, \quad (5.11)$$

and the interaction free energy is:

$$\boxed{U = -\frac{1}{2}\tilde{\mathbf{E}}_0^*(\boldsymbol{\alpha}_a + \boldsymbol{\alpha}_b)\tilde{\mathbf{E}}_0 - \tilde{\mathbf{E}}_0^*\boldsymbol{\alpha}_a\mathbf{J}\boldsymbol{\alpha}_b\tilde{\mathbf{E}}_0 - \frac{1}{2}\tilde{\mathbf{E}}_0^*(\boldsymbol{\alpha}_a\mathbf{J}\boldsymbol{\alpha}_b\mathbf{J}\boldsymbol{\alpha}_a + \boldsymbol{\alpha}_b\mathbf{J}\boldsymbol{\alpha}_a\mathbf{J}\boldsymbol{\alpha}_b)\tilde{\mathbf{E}}_0 - \dots}$$
(5.12)

The first term in equation 5.12 represents the free-energy of the individual molecules in a field. Its gradients and orientation-dependence are responsible for optical trapping and the optical Kerr effect, respectively. The second term, with a single factor of \mathbf{J} , represents direct dipole-dipole interaction. The third term represents dipole-induced dipole interactions: the field polarizes one particle; the dipole of this particle induces a dipole in its neighbor; these two dipoles interact.

It should be noted that Eq. 5.12 differs from the (incorrect) expression for the free energy given by Power and Thirunamachandran [148] and in Milonni's textbook on quantum electrodynamics [132]. These authors take the well-known formula for the free energy of a single molecule in a field, $U = -\frac{1}{2}\tilde{\mathbf{E}}^*\boldsymbol{\alpha}\tilde{\mathbf{E}}$, and reason that the free energy for two molecules should have the form:

$$U_{inc} = -\frac{1}{2}(\tilde{\mathbf{E}}_a^*\boldsymbol{\alpha}_a\tilde{\mathbf{E}}_a + \tilde{\mathbf{E}}_b^*\boldsymbol{\alpha}_b\tilde{\mathbf{E}}_b). \quad (5.13)$$

Expanding U_{inc} in powers of \mathbf{J} yields

$$\begin{aligned} U_{inc} = & -\frac{1}{2}\tilde{\mathbf{E}}_0^*(\boldsymbol{\alpha}_a + \boldsymbol{\alpha}_b)\tilde{\mathbf{E}}_0 - 2\tilde{\mathbf{E}}_0^*\boldsymbol{\alpha}_a\mathbf{J}\boldsymbol{\alpha}_b\tilde{\mathbf{E}}_0 \\ & -\frac{3}{2}\tilde{\mathbf{E}}_0^*(\boldsymbol{\alpha}_a\mathbf{J}\boldsymbol{\alpha}_b\mathbf{J}\boldsymbol{\alpha}_a + \boldsymbol{\alpha}_b\mathbf{J}\boldsymbol{\alpha}_a\mathbf{J}\boldsymbol{\alpha}_b)\tilde{\mathbf{E}}_0 - \dots \end{aligned} \quad (5.14)$$

Comparing Eq. 5.14 with Eq. 5.12 we see that Eq. 5.13 counts each n^{th} order interaction $n + 1$ times, while in Eq. 5.12 we only count each interaction once. It is easy to check by explicit differentiation that Eq. 5.12 yields the correct intermolecular force, and Eq. 5.14 does not.

The expression for the interaction free-energy simplifies if we consider isotropic particles (replacing each dielectric tensor by a frequency-dependent complex number). Then we can factor out the polarizabilities and write the series expansion for U (Eq. 5.12) as:

$$\begin{aligned}
 U = & -\frac{|\tilde{E}_0|^2}{2}(\alpha_a + \alpha_b) - \frac{|\tilde{E}_0|^2\alpha_a\alpha_b}{8\pi\epsilon_0r^3}(1 + 3\cos 2\theta) \\
 & - \frac{|\tilde{E}_0|^2(\alpha_a^2\alpha_b + \alpha_b^2\alpha_a)}{64\pi^2\epsilon_0^2r^6}(5 + 3\cos 2\theta) - \frac{|\tilde{E}_0|^2\alpha_a^2\alpha_b^2}{128\pi^3\epsilon_0^3r^9}(7 + 9\cos 2\theta) - \dots \quad (5.15)
 \end{aligned}$$

where we used equation 3.4 for the dipole field propagator.

The electric field induces parallel dipole-moments in the two particles, provided that α_a and α_b have the same sign. Thus if \hat{r} is parallel to \hat{E}_0 , then the dipoles are aligned head-to-tail, and the particles experience long-range $1/r^3$ attraction. If \hat{r} is perpendicular to \hat{E}_0 , then the dipoles are aligned head-to-head and tail-to-tail, and the particles experience long-range $1/r^3$ repulsion. The sign of the long-range force switches at $1 + 3\cos 2\theta = 0$, or $\theta = 54.7$ deg.

The force is reversed if α_a and α_b have opposite sign: the dipole moment of the particle with negative α' is *antiparallel* to the applied field. Since the sign of the real polarizability may differ at different frequencies, *for dissimilar particles it is possible to change the sign of the long-range force merely by changing the color of the illumination.*

In the discussion above we held \hat{E}_0 and \hat{r} fixed. In many physical situations, one or both of these will fluctuate randomly. If the illumination is isotropic, then we let \hat{E}_0 lie anywhere on the unit sphere. If the interparticle axis can tumble freely (the particles are in a fluid and $U \ll k_B T$), then we let \hat{r} lie anywhere on the unit sphere.

In either case we need to average U over all values of θ :

$$\overline{U} = \frac{\int_0^\pi U(\theta) \sin\theta \, d\theta}{\int_0^\pi \sin\theta \, d\theta}. \quad (5.16)$$

Since $\overline{\cos 2\theta} = -1/3$, the $1/r^3$ term in 5.15 averages to zero. The long-range behavior of the rotational average is dominated by the $1/r^6$ term:

$$\overline{U} = -\frac{|\tilde{E}_0|^2}{16\pi^2\epsilon_0^2 r^6}(\alpha_a^2\alpha_b + \alpha_b^2\alpha_a) + \mathcal{O}\left(\frac{|\tilde{E}_0|^2}{\epsilon_0^3 r^9}\right). \quad (5.17)$$

In 5.17 the distance-independent component of the free-energy has been omitted. Under isotropic conditions, light-induced forces have the same distance dependence as van der Waals forces.

When the illumination is unidirectional and polarized and the average in Eq. 5.17 is due to freedom of orientation of the molecules, then a Boltzmann factor favors those orientations with lower energy. Eq. 5.17 may be thought of as the infinite temperature approximation, in which all orientations of the intermolecular axis are equally likely. The partition function for two molecules of fixed intermolecular separation r but with orientational freedom is

$$Z(r) = \int_0^\pi e^{-U/k_{\text{B}}T} \sin\theta \, d\theta. \quad (5.18)$$

Assuming $U/k_{\text{B}}T \ll 1$, we may expand the exponential in Eq. 5.18 as $e^{-U/k_{\text{B}}T} = 1 - \frac{U}{k_{\text{B}}T} + \frac{1}{2}\left(\frac{U}{k_{\text{B}}T}\right)^2 + \dots$. The free energy, $F = -k_{\text{B}}T \ln Z$ then becomes

$$F = \overline{U} - \overline{U^2}/2k_{\text{B}}T + \dots \quad (5.19)$$

The first term in 5.19 corresponds to the infinite-temperature limit in which all orientations occur with equal probability and is given by Eq. 5.17. The second term introduces the fact that at finite temperature lower-energy orientations occur more frequently than higher-energy orientations.

As in the calculation of \overline{U} , we get terms proportional to $1/r^6$ from evaluating $\overline{U^2/2k_B T}$. The distance-dependent part is:

$$\overline{U^2/2k_B T} = \frac{|\tilde{E}_0|^4}{40k_B T \pi^2 \epsilon_0^2 r^6} \alpha_a^2 \alpha_b^2 + \frac{|\tilde{E}_0|^4}{160k_B T \pi^3 \epsilon_0^3 r^9} (\alpha_a^2 \alpha_b + \alpha_b^2 \alpha_a) + \dots \quad (5.20)$$

The derivation of Eq. 5.20 is analogous to the classical derivation of the Keesom interaction between molecules with permanent dipole moments. The chief difference here is that the dipole moments are induced by the applied field, rather than being intrinsic to the molecules. The temperature-dependent free-energy should be treated with some caution because it is proportional to E_0^4 , or the intensity squared. Some nonlinear optical effects contribute in the same order in the field and it is necessary to determine whether nonlinear effects significantly alter the free-energy of interaction.

5.2.2 Nonlinear regime

Now we turn to the case where the field is strong enough to induce nonlinear responses in the molecules. The local field equations must be solved iteratively in powers of the field and the intermolecular coupling, with the power of each determined by the strength of that perturbation.

The polarization of each particle depends on the applied field and the polarization of its neighbor:

$$\begin{aligned} \tilde{\mathbf{p}}_a(\omega) &= \boldsymbol{\alpha}_a(\omega)[\tilde{\mathbf{E}}_0(\omega) + \mathbf{J}\tilde{\mathbf{p}}_b(\omega)] \\ &+ \int d\omega_2 \int d\omega_1 \boldsymbol{\beta}_a(-\omega; \omega_2, \omega_1)[\tilde{\mathbf{E}}_0(\omega_2) + \mathbf{J}\tilde{\mathbf{p}}_b(\omega_2)][\tilde{\mathbf{E}}_0(\omega_1) + \mathbf{J}\tilde{\mathbf{p}}_b(\omega_1)] + \dots \end{aligned} \quad (5.21a)$$

$$\begin{aligned} \tilde{\mathbf{p}}_b(\omega) &= \boldsymbol{\alpha}_b(\omega)[\tilde{\mathbf{E}}_0(\omega) + \mathbf{J}\tilde{\mathbf{p}}_a(\omega)] \\ &+ \int d\omega_2 \int d\omega_1 \boldsymbol{\beta}_b(-\omega; \omega_2, \omega_1)[\tilde{\mathbf{E}}_0(\omega_2) + \mathbf{J}\tilde{\mathbf{p}}_a(\omega_2)][\tilde{\mathbf{E}}_0(\omega_1) + \mathbf{J}\tilde{\mathbf{p}}_a(\omega_1)] + \dots \end{aligned} \quad (5.21b)$$

Eqs. 5.21 may be solved iteratively by substituting Eq. 5.21b into the r.h.s. of Eq. 5.21a and Eq. 5.21a into the r.h.s. of Eq. 5.21b.

Here we consider only the interaction energy that is first-order in the intermolecular coupling, and arbitrary order in the field. We may then ignore the intermolecular coupling in calculating the time-evolution of each dipole moment, so the first-order interaction free energy is

$$U(t) = -\mathbf{p}_a(t)\mathbf{J}\mathbf{p}_b(t), \quad (5.22)$$

where the time-evolution of the dipole fields of the individual molecules may be calculated using response functions to arbitrary order, using the optical Bloch equations, or using any other method of calculating the single-molecule optical response.

As a nontrivial example of a force accompanying a nonlinear optical process, we consider the “force-echo” that accompanies a photon-echo experiment. Let a and b represent nominally identical two level systems subject to inhomogeneous broadening. Each molecule has a slightly different resonant frequency due to variations in its microenvironment. This model is a reasonably good description of molecules embedded in molecular crystals, glasses, and viscous liquids.

The system is characterized by two times: the *transverse relaxation time* T_2 , related to the rate of inhomogeneous dephasing (also known as decoherence), and the *longitudinal relaxation time* T_1 , related to the rate of spontaneous emission. Typically $T_2 \ll T_1$, so the inhomogeneous dephasing sets the linewidth. If the system is excited by an optical pulse, the emitted signal decays at a rate T_2 as the individual oscillators acquire different phases. However, if a second pulse is introduced after an interval $\tau \ll T_1$, it is possible to reverse the time-evolution of each oscillator, so that after a further interval τ all the oscillators are back in phase. The photon-echo describes the

burst of light that appears, as if from nowhere, 2τ after the original pulse.

Eq. 5.22 indicates that the *recoherence* that occurs in the photon echo experiment should be accompanied by an appearance of a first-order intermolecular force at the echo time, as $\mathbf{p}_a(t)$ and $\mathbf{p}_b(t)$ return to in-phase oscillation. This photon-echo force may be detectable as an *acoustical* pulse that accompanies the photon echo.

5.2.3 van der Waals forces within the LFA

The LFA predicts that when the applied field goes to zero, both molecules are quiescent and there is no intermolecular force. There have been several attempts to graft quantum mechanics onto the LFA in order to extract the ground state van der Waals force. The principle idea is to introduce zero-point fluctuations of the molecules and the radiation field as additional semiclassical sources in the local field equations.

Casimir and Polder first calculated the retarded van der Waals force using fourth order quantum electrodynamic perturbation theory [30] and found the potential to be:

$$U = -\frac{23\hbar c}{4\pi r^7}\alpha_a(0)\alpha_b(0). \quad (5.23)$$

The next year Casimir published a paper in French [29], showing that the retarded van der Waals force can be calculated from the second term of Eq. 5.12 if the field $\tilde{\mathbf{E}}_0$ is regarded as an operator and the fully retarded expression is used for the field propagator, \mathbf{J}^1

$$J_{ij} = [\nabla_i \nabla_j - \delta_{ij} \nabla^2] \frac{\exp(ikr)}{r}. \quad (5.24)$$

¹The first term in Eq. 5.12, which does not depend on the intermolecular separation, gives the nonrelativistic contribution to the Lamb shift when the field is treated quantum mechanically [133].

Casimir's approach was to sum the light-induced force over all wavevectors and polarizations of the zero-point field. The details of the calculation are clearly summarized in Refs. [132, 18, 147]. The result is that the retarded interaction potential is

$$U = -\frac{\hbar}{\pi c^6} \int_0^\infty d\omega \omega^6 \alpha_a(\omega) \alpha_b(\omega) G\left(\frac{\omega r}{c}\right), \quad (5.25)$$

where

$$G(x) \equiv \frac{\sin 2x}{x^2} + \frac{2 \cos 2x}{x^3} - \frac{5 \sin 2x}{x^4} - \frac{6 \cos 2x}{x^5} + \frac{3 \sin 2x}{x^6}. \quad (5.26)$$

For $\omega_0 r/c \gg 1$, where ω_0 is a characteristic resonant frequency of a and b , the polarizabilities may be taken outside of the integral. Evaluating the integral $\int \omega^6 G(\omega r/c) d\omega$ yields the Casimir formula, Eq. 5.23.

It is natural to consider the nonretarded limit of Eq. 5.25 as well, in the hopes of obtaining the r^{-6} potential. Milonni does this in his textbook on quantum electrodynamics [132], and similar attempts are widespread in the literature [133, 147, 134]. The procedure is to claim that for small r , the last term of Eq. 5.26 dominates:

$$\lim_{x \rightarrow 0} G(x) \stackrel{\text{claim}}{\implies} \frac{3 \sin 2x}{x^6}, \quad (5.27)$$

which does lead to the correct van der Waals energy. However, claim 5.27 is false. For small x , the r.h.s. of 5.27 is $\propto 1/x^5$, while the r.h.s. of 5.26 is $\propto 1/x$. The denominators in 5.26 are not indicative of the small x limit because, for instance, the terms $\frac{6 \cos 2x}{x^5}$ and $\frac{3 \sin 2x}{x^6}$ have the same small x limit. When limit is properly evaluated, the Casimir formula (Eq. 5.25) gives zero nonretarded force. This must be the case, because the rotational average of the second term of Eq. 5.12 is zero when the nonretarded propagator is used (Eq. 5.17).

So where does the nonretarded van der Waals force come from? Langbein rewrote

Eq. 5.12 as [109]

$$U = -\frac{1}{2}\tilde{\mathbf{E}}_0^*(\boldsymbol{\alpha}_a + \boldsymbol{\alpha}_b)\tilde{\mathbf{E}}_0 - \tilde{\mathbf{E}}_0^*\boldsymbol{\alpha}_a\mathbf{J}\boldsymbol{\alpha}_b\tilde{\mathbf{E}}_0 - \frac{1}{2}\tilde{\mathbf{p}}_a^*\mathbf{J}\boldsymbol{\alpha}_b\mathbf{J}\tilde{\mathbf{p}}_a - \frac{1}{2}\tilde{\mathbf{p}}_b^*\mathbf{J}\boldsymbol{\alpha}_a\mathbf{J}\tilde{\mathbf{p}}_b - \dots \quad (5.28)$$

The first term does not depend on the intermolecular spacing, so we neglect it. As we have shown, in the nonretarded limit, the orientational average of the second term is zero. Thus the third and fourth terms of Eq. 5.28 must give the nonretarded interaction.

The fluctuation-dissipation theorem relates the second moment of the dipole fluctuations of each molecule to the imaginary part of its susceptibility:

$$\langle \tilde{\mathbf{p}}_j^*(\omega)\tilde{\mathbf{p}}_j(\omega) \rangle = \frac{\hbar}{2\pi} \coth\left(\frac{\hbar\omega}{2k_B T}\right) \alpha_j''(\omega). \quad (5.29)$$

Substituting Eq. 5.29 into Eq. 5.28 and integrating over all frequencies gives

$$U = -\frac{\hbar}{4\pi} \int_{-\infty}^{\infty} d\omega \coth\left(\frac{\hbar\omega}{2k_B T}\right) [\alpha_a''(\omega)\alpha_b(\omega) + \alpha_b''(\omega)\alpha_a(\omega)]. \quad (5.30)$$

Only the real (even) parts of $\alpha_a(\omega)$ and $\alpha_b(\omega)$ survive the integral. Writing $[\alpha_a''(\omega)\alpha_b'(\omega) + \alpha_b''(\omega)\alpha_a'(\omega)]$ as $\text{Im}[\alpha_a\alpha_b]$ and performing a contour integration as in Chapter 3 yields the McLachlan formula for the van der Waals energy. We see again that the short-range van der Waals force depends on the fluctuation properties of the molecules, while the long-range Casimir force depends on the fluctuation properties of the vacuum. To obtain the full nonretarded and retarded van der Waals-Casimir energy it is necessary to keep all the terms in Eq. 5.28.

Contributions to the van der Waals energy higher order in the coupling depend on higher moments of the dipole fluctuations of each molecule. If the reference Hamiltonians of the molecules are harmonic, then the dipole fluctuations have a Gaussian distribution and all moments can be determined by the fluctuation dissipation theorem. However if the molecules have nonlinearities, as all molecules do, then the higher

moments of the dipole fluctuations are needed as well. There is currently no known analogue of the fluctuation dissipation theorem for the higher moments of the dipole fluctuations, so the Langbein theory cannot be extended beyond second order.

The shortcomings of the local field approximation in calculating *optical* effects have been addressed by the nonlinear exciton equations (NEE) [137], which keep track of collective variables related to intermolecular correlations. It can be shown that the local field approximation is exact in the linear response to an applied field, but that it misses certain resonances in the nonlinear response. It is tempting to apply the NEE to calculation of the intermolecular force as well. However, the NEE are based on the Heitler-London approximation for the intermolecular interaction, which neglects off-resonant interactions and thus completely misses the ground state van der Waals force. Thus neither the LFA, nor the more rigorous NEE is a good starting point for calculating light-modified intermolecular forces.

In the next section we introduce a procedure for calculating light-modified intermolecular forces that is quantum mechanically rigorous, is valid for arbitrary time-dependent light fields, is applicable to complex systems interacting with a bath, and yields the ground state van der Waals force in a seamless manner. The procedure uses the Liouville space superoperator formalism developed in Chapters 1 and 2.

5.3 Superoperator approach

Suppose we have a plane wave incident on a pair of molecules whose separation is much less than the wavelength. Then $E_a(t) = E_b(t) \equiv E(t)$. For simplicity we adopt the point-dipole approximation and neglect the vectorial nature of the fields

and polarizations. The perturbation then has three terms:

$$H_{ab} = -E(t)\mu_a - E(t)\mu_b - J(t)\mu_a\mu_b, \quad (5.31)$$

with J given by Eq. 3.4. We wish to calculate $\langle B(t) \rangle$, where $B \equiv \mu_a\mu_b$. Recall Eq. 2.2:

$$\langle B(t) \rangle = \left\langle \mathcal{T} \hat{B}_+(t) \exp \left(-\frac{i}{\hbar} \int_{-\infty}^t \hat{H}_{ab-}(t') dt' \right) \right\rangle_0. \quad (5.32)$$

We cannot say *a priori* whether the perturbation due to E or J is stronger—there are experiments corresponding to both scenarios. We wish to expand Eq. 5.32 to n^{th} order in J and m^{th} order in E , to calculate $\langle B^{(n,m)}(t) \rangle$. This is accomplished by factoring the exponential in Eq. 5.32. It is not normally possible to factor an exponentiated sum of operators: for operators A and B , $e^{A+B} \neq e^A e^B$. However the time-ordering operator on the left allows us to do this: $\mathcal{T} e^{A+B} = \mathcal{T} e^A e^B$. The time-evolution of $\langle B(t) \rangle$ becomes:

$$\begin{aligned} \langle B(t) \rangle = & \left\langle \mathcal{T} \hat{\mu}_{a+}(t) \hat{\mu}_{b+}(t) \exp \left[\frac{i}{\hbar} \int_{-\infty}^t dt' E(t') \hat{\mu}_{a-}(t') \right] \exp \left[\frac{i}{\hbar} \int_{-\infty}^t dt' E(t') \hat{\mu}_{b-}(t') \right] \right. \\ & \left. \exp \left[\frac{i}{\hbar} \int_{-\infty}^t dt' J(t') [\hat{\mu}_{a-}(t') \hat{\mu}_{b+}(t') + \hat{\mu}_{a+}(t') \hat{\mu}_{b-}(t')] \right] \right\rangle_0. \quad (5.33) \end{aligned}$$

The three exponentials in Eq. 5.33 represent the field interacting with molecule a , the field interacting with molecule b , and the interaction of molecules a and b , respectively. The term involving the intermolecular coupling was expanded using the identity $[\hat{\mu}_a \hat{\mu}_b]_- = \hat{\mu}_a \hat{\mu}_{b+} + \hat{\mu}_{a+} \hat{\mu}_b$ (see Eq. 2.9). Each exponential in Eq. 5.33 may be expanded to any desired order, or, if possible, treated exactly. Once expanded, Eq. 5.33 becomes a sum of products of single-molecule superoperators. Because the initial state is a direct-product, we may factor the resulting expression in terms of single-molecule multitime correlation functions.

We now evaluate $\langle B(t) \rangle$ to successive orders in $J(t)$ and $E(t)$. To zeroth order in $J(t)$ we can factor Eq. 5.33 to

$$\begin{aligned} \langle B^{(0)}(t) \rangle &= \left\langle \mathcal{T} \hat{\mu}_{a+}(t) \exp \left[\frac{i}{\hbar} \int_{-\infty}^t dt' E(t') \hat{\mu}_{a-}(t') \right] \right\rangle_{a0} \\ &\quad \left\langle \mathcal{T} \hat{\mu}_{b+}(t) \exp \left[\frac{i}{\hbar} \int_{-\infty}^t dt' E(t') \hat{\mu}_{b-}(t') \right] \right\rangle_{b0}. \end{aligned} \quad (5.34)$$

Each term in the brackets in Eq. 5.34 is simply the time-evolution of the dipole moment of an individual molecule interacting with the field. So the interaction energy to first order in J and to all orders in E is

$$U^{(1)}(t) = - \langle \mu_a(t) \rangle J(t) \langle \mu_b(t) \rangle. \quad (5.35)$$

This is the same as the result obtained using the local field approximation (Eq. 5.22), and leads to e.g. the force-echo that accompanies a photon-echo.

Expanding the intermolecular interaction term in Eq. 5.33 to first order in $J(t)$, we obtain

$$\begin{aligned} \langle B^{(1)}(t) \rangle &= \frac{i}{\hbar} \int_{-\infty}^t \sum_{\nu} \left\langle \mathcal{T} \hat{\mu}_{a+}(t) \hat{\mu}_{a\nu}(t_1) \exp \left[\frac{i}{\hbar} \int_{-\infty}^t dt' E(t') \hat{\mu}_{a-}(t') \right] \right\rangle_{a0} \\ &\quad \left\langle \mathcal{T} \hat{\mu}_{b+}(t) \hat{\mu}_{b\nu}(t_1) \exp \left[\frac{i}{\hbar} \int_{-\infty}^t dt' E(t') \hat{\mu}_{b-}(t') \right] \right\rangle_{b0} J(t_1) dt_1, \end{aligned} \quad (5.36)$$

where $\nu = +, -$. Now we may expand Eq. 5.36 to arbitrary order in the field. To zeroth order in the field it becomes:

$$\begin{aligned} \langle B^{(1,0)}(t) \rangle &= \frac{i}{\hbar} \int_{-\infty}^t \langle \mathcal{T} \hat{\mu}_{a+}(t) \hat{\mu}_{a-}(t_1) \rangle_{a0} \langle \mathcal{T} \hat{\mu}_{b+}(t) \hat{\mu}_{b+}(t_1) \rangle_{b0} J(t_1) dt_1 \\ &\quad + \frac{i}{\hbar} \int_{-\infty}^t \langle \mathcal{T} \hat{\mu}_{a+}(t) \hat{\mu}_{a+}(t_1) \rangle_{a0} \langle \mathcal{T} \hat{\mu}_{b+}(t) \hat{\mu}_{b-}(t_1) \rangle_{b0} J(t_1) dt_1 \\ &= \int_{-\infty}^t [R_a^{+-}(t, t_1) R_b^{++}(t, t_1) + R_a^{++}(t, t_1) R_b^{+-}(t, t_1)] J(t_1) dt_1 \end{aligned} \quad (5.37)$$

which was the starting point for our discussion of van der Waals forces in Chapter 3. Thus the superoperator approach naturally yields the ground state van der Waals force in the dark.

To first order in J and first order in E , the intermolecular correlation is:

$$\begin{aligned} \langle B^{(1,1)}(t) \rangle &= \int_{-\infty}^t dt_2 \int_{-\infty}^t dt_1 [2R_a^{+-}(t, t_2, t_1)R_b^{++}(t, t_2) + R_a^{+-}(t, t_2)R_b^{++-}(t, t_2, t_1) \\ &\quad + R_a^{++-}(t, t_2, t_1)R_b^{+-}(t, t_2) + 2R_a^{++}(t, t_2)R_b^{+-}(t, t_2, t_1)]J(t_2)E(t_1), \end{aligned} \quad (5.38)$$

where we have inserted the single-molecule GRFs for the corresponding single-molecule multitime correlation functions (the GRFs are defined in Eqs. 1.34 and 1.35). This expression describes modification of the second-order van der Waals force by light.

It is straightforward to continue the expansion of Eq. 5.33 to any desired order in J and E . For instance, the expansion to n^{th} order in J is

$$\begin{aligned} \langle B^{(n)}(t) \rangle &= \frac{1}{n!} \left(\frac{i}{\hbar} \right)^n \sum_{\{\nu_\alpha\}} \int_{-\infty}^t dt_n \cdots \int_{-\infty}^t dt_1 \\ &\quad \left\langle \mathcal{T} \hat{\mu}_{a+}(t) \hat{\mu}_{a\nu_n}(t_n) \cdots \hat{\mu}_{a\nu_1}(t_1) \exp \left[\frac{i}{\hbar} \int_{-\infty}^t dt' E(t') \hat{\mu}_{a-}(t') \right] \right\rangle_{a0} \\ &\quad \left\langle \mathcal{T} \hat{\mu}_{b+}(t) \hat{\mu}_{b\nu_n}(t_n) \cdots \hat{\mu}_{b\nu_1}(t_1) \exp \left[\frac{i}{\hbar} \int_{-\infty}^t dt' E(t') \hat{\mu}_{b-}(t') \right] \right\rangle_{b0} \\ &\quad J(t_n) \cdots J(t_1), \end{aligned} \quad (5.39)$$

where $\nu_\alpha = +, -$ and the sum is over all n -element sequences (ν_n, \dots, ν_1) . Each term in the expansion may be expressed in terms of single-molecule GRFs. For constant J (i.e. fixed intermolecular separation), the interaction free energy is given by $U = -\int \langle B \rangle dJ$, as in Eq. 3.21. In the presence of time-varying fields, neither molecule is in thermal equilibrium, so U does not correspond to a free energy in the

classical equilibrium sense. However, U is a potential function, whose gradient gives the intermolecular force.

5.4 Application to the van der Waals gas

In this section we calculate the effect of illumination on the density of a system obeying the van der Waals equation of state. Illumination may change the density through its effect on intermolecular forces. The index of refraction depends on the density, so materials obeying this equation of state should show an intensity-dependent index of refraction. Near the critical point there is a divergence in the sensitivity of the density and index of refraction to changes in the illumination. The van der Waals equation of state is a good model of many gases, solutions and polymer mixtures.

We model the material as hard spheres interacting via the pair-potential:

$$U(r) = \begin{cases} \infty & r < r_0 \\ U_0 \left(\frac{r_0}{r}\right)^6 & r > r_0 \end{cases} \quad (5.40)$$

where r_0 is the molecular radius. Normally the attractive component, U_0 , is given by the ground-state van der Waals interaction. Here we add to the dispersion energy the light-induced interaction, so $U_0 = U_{vdw} + U_{light}$, where U_{light} is taken from the first term of 5.17

$$U_{light} = -\frac{I\alpha^3}{4\pi^2 c \epsilon_0^3 r^6}, \quad (5.41)$$

where we assume molecules a and b are the same species and then make the substitution $|E_0|^2 = 2I/\epsilon_0 c$, where I is the intensity.

The van der Waals equation of state,

$$\left(p + \frac{a}{v^2}\right)(v - b) = RT \quad (5.42)$$

relates the pressure, p , molar volume, v and temperature, T , in a gas of interacting particles to the interaction-potential 5.40 via the constants a and b :

$$a = \frac{2\pi}{3} N_A^2 r_0^3 U_0 \quad (5.43a)$$

$$b = \frac{2\pi}{3} N_A r_0^3, \quad (5.43b)$$

where N_A is Avogadro's number.

Since the constant a is proportional to $U_{vdw} + U_{light}$, we can write $a = a_0 + a_1 I$. Substituting this expression back into the van der Waals equation of state, we evaluate the change in molar volume upon a change in intensity:

$$\left. \frac{\partial v}{\partial I} \right|_{p,T} = \frac{a_1 v (b - v)^2}{2a(b - v)^2 - RTv^3}. \quad (5.44)$$

Next we find the change in the index of refraction that results from this change in molar volume. The Lorentz-Lorenz equation relates the molecular polarizability, the index of refraction, and the molar volume of a material:

$$\alpha = \frac{3\epsilon_0 v}{N_A} \left(\frac{n^2 - 1}{n^2 + 2} \right), \quad (5.45)$$

whence the change in index of refraction upon a change in molar volume is:

$$\frac{\partial n}{\partial v} = -\frac{(n^2 - 1)(n^2 + 2)}{6nv}. \quad (5.46)$$

Combining results 5.46 and 5.44 we write:

$$\begin{aligned} \left. \frac{\partial n}{\partial I} \right|_{I=0} &= \frac{\partial n}{\partial v} \frac{\partial v}{\partial I} \\ &= -a_1 \frac{(n^2 - 1)(n^2 + 2)}{6n} \frac{(b - v)^2}{(2a_0(b - v)^2 - RTv^3)}. \end{aligned} \quad (5.47)$$

The critical point ($\left. \frac{\partial p}{\partial v} \right|_T = \left. \frac{\partial^2 p}{\partial v^2} \right|_T = 0$) occurs at $T_c = 8a_0/(27bR)$ and $v_c = 3b$. The denominator of 5.47 diverges at this point. Thus systems near a critical point

should show exceptionally large nonlinear optical response. Examples of such systems are single-component liquid-gas equilibria, polymers near the θ point, and binary solutions near the consolute critical point.

5.5 Discussion

The connection between optics and ground-state intermolecular forces dates to the beginning of the 20th century when it was noted that gases with a higher index of refraction tend to have a larger deviation from the ideal gas law [124]. The McLachlan formalism explains this connection by expressing the dispersion force (which affects the second virial coefficient) in terms of the molecular polarizability (which determines the index of refraction). In this section we have extended the formalism to relate optical effects to changes in intermolecular forces. For molecules with fixed orientation, a polarized light beam may generate $1/r^3$ forces, while for molecules with random orientations, light modifies the $1/r^6$ van der Waals potential.

In recent years there have been many observations and predictions of effects that are most plausibly interpreted in terms of light-modified intermolecular forces. Burns first observed light-induced crystallization of micron-sized colloidal particles [21, 22]. Xu [202] and Calander [27] both studied the forces in nanometer-sized metal particles. They showed that when the exciting light is tuned near an optical resonance (so that α is very large), then the fields may be strong enough to trap small molecules at room temperature. In all of the above studies, forces were calculated within the local-field approximation, so the ground state van der Waals interaction was ignored. This neglect of the ground state force is not justified, since excitonic splittings often exceed light-induced Stark shifts.

Polymers are good systems for investigating light-modified intermolecular forces because solutions can be tuned to the cusp of a phase transition, at which point they are exquisitely sensitive to small changes in intermolecular forces. Over the past six years a range of experimental studies has focussed on light-induced phase transitions in polymers [17, 83, 84, 85, 44, 45]. Recent experiments in this area have highlighted the absence of a good theory to explain the phenomena [170, 91]. Garetz and coworkers observed nonphotochemical light-induced nucleation of supersaturated solutions of glycine in water [71], and were able to control the crystal structure with the polarization of the light. To-date these light-induced phase transitions have been rationalized solely in terms of the first term of Eq. 5.12, i.e. density changes and molecular alignment induced by the light. One of the results of this section is that the light also modifies the forces between the molecules, and this too may play an important role in light-induced phase transitions. As one application of this, I suggest investigating the use of intense polarized light to facilitate the crystallization of proteins—a notoriously difficult problem of current biomedical interest.

The ability to use light to control interactions of biomolecules within a cell has tremendous potential. Just recently Ehrlicher and coworkers used a laser to direct the polymerization of actin within the growth-cone of a neuron, thereby steering the neuron towards their target [57]. Bruckner showed that light may also induce shape changes in vesicular membranes that have been doped with a fluorophore [151]. A fuller understanding of light-modified intermolecular forces may allow optical intervention in biochemical pathways.

Chapter 6

Biological Solitons

In this last chapter I study four examples of sine-Gordon solitons in filamentous biological and nanoscale materials. Soliton-like quasiparticles are widely applied in physics, but are more of a rarity in biological modelling. The systems studied are: an organelle in the sperm of the horseshoe crab, a multiwalled nanotube, a polymer in an AC electric field, and a polymer confined to a thin sheet.

6.1 Introduction

Small filamentous structures are common in biology, chemistry and condensed matter physics. The rich morphology that these structures exhibit arises from a combination of short and long range forces, often mediated by hydrodynamics, electrostatics and thermal fluctuations. While the chemistry of these materials may be complex, their physical properties can often be described by a few coarse-grained parameters. In organic and inorganic nanotubes as well as in semiflexible biopolymers, the mechanical properties depend mostly on bending and twisting moduli, while the complex interactions between filaments can be replaced by a simple short-range adhesive potential.

A simple polarizability per unit length provides a good description of the electrical response.

As we will see below, the material simplicity of these systems is well compensated for by geometrical complexity. The energy functionals for filamentous materials are nonlinear under even modest perturbations. The conformation of a filament is described by a unit tangent vector, $\mathbf{u}(s)$, where $s \in [0, L]$ is the contour length along the polymer. For the calculations below it is acceptable to replace $\mathbf{u}(s)$ by $\theta(s)$, where the angle θ is measured between the tangent to the filament and some reference orientation. The energy functional has the form

$$H = \int_0^L \frac{1}{2} K (\theta_s)^2 + V \sin(\chi\theta) ds, \quad (6.1)$$

where $K = YI$ is a measure of the bending stiffness, Y [N m⁻²] is the Young's modulus of the material and I [m⁴] is the area moment of inertia, given by the second moment of the mass distribution in a cross-section perpendicular to the axis of symmetry.¹ V and χ have different physical meanings in the different applications considered below. We will study free energy-minimizing solutions to Eq. 6.1.

6.2 Kinks in filamentous aggregates

We start by examining kinked helices in multiwalled carbon nanotubes (MWNTs) and in the acrosome of horseshoe crab (*Limulus*) sperm. MWNTs are fibers composed of concentric graphene tubules. They show promise as components of nanoelectronic devices, field-emission displays, and high-strength composites. MWNTs are usually fairly straight, but under some growth conditions tubes form with a corkscrew

¹For molecular-scale objects Y and I are not separately well-defined, but their product is.

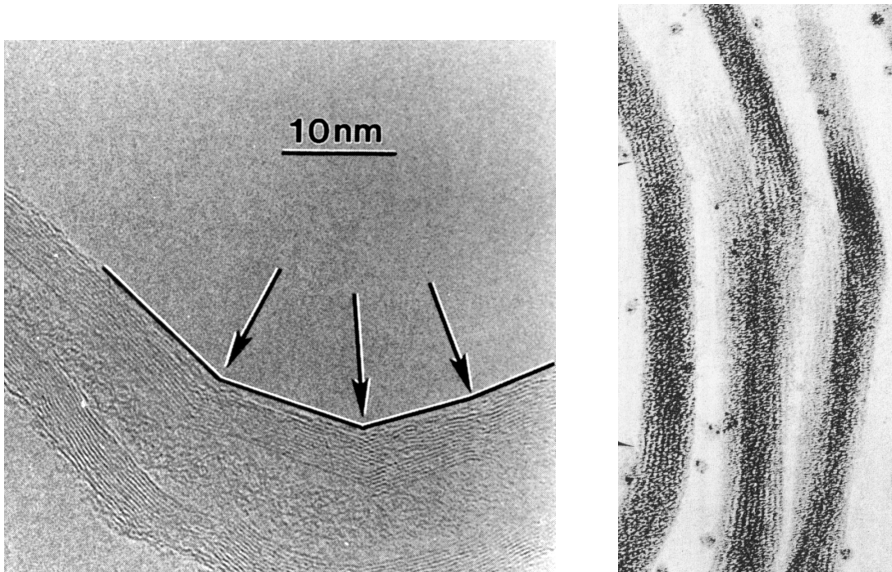


Figure 6.1: Kinks in bent fibrillar aggregates. a) MWNT [206], b) *Limulus* acrosome [46].

shape [70, 82, 205]. The tubes grow out of molten catalyst particles that have been supersaturated with carbon, and the corkscrew shape arises when there is a nonuniform rate of deposition of carbon around the circumference of the tube [4]. Close examination of a corkscrew MWNT often shows that the tube is composed of relatively straight sections joined at kinks [206, 14]. An example of this is shown in Figure 6.1.

The acrosomal process of a *Limulus* sperm is a $\sim 50 \mu\text{m}$ -long rod of bundled actin filaments. In a free-swimming sperm the acrosome is coiled around the base of the sperm. When the sperm encounters an egg, a calcium signal causes the acrosome to uncoil so that it juts out the front of the sperm and harpoons the egg [183]. Interestingly, the coiled acrosome is also composed of straight sections joined at kinks, as shown in Figure 6.1 [47].

The occurrence of a kinking instability in helices of these two seemingly dissimilar rods suggests that the kinks may arise through a common mechanism. Ihara and coworkers [87] and Dunlap [53, 52], have proposed a model of helix-formation in carbon nanotubes based on pentagon-heptagon paired defects (PHPDs). Putting a pentagon and heptagon of carbon atoms on diametrically opposite sides of a nanotube introduces a kink into the nanotube. Arrays of such kinks form a helix. Unlike the mechanism discussed in this section, forming PHPDs requires breaking covalent bonds. The PHPD mechanism also does not account for the observed periodicity of the kinks, nor why PHPDs should align in successive shells of a MWNT to produce localized kinks. Furthermore, it is not clear why kinked helices are observed in MWNTs but not in single walled nanotubes (SWNTs). Finally, the PHPD mechanism is specific to carbon nanotubes, and a different mechanism would be needed for the acrosome.

I propose a general model of kinking in fibrillar aggregates. Consider an aggregate of fairly inextensible fibers that are weakly coupled to each other. Both the concentric graphene shells in MWNTs and the actin filaments in the acrosome fit this description. Each fiber has corrugations along its length because it is composed of discrete molecular or atomic monomers; these corrugations reflect the periodic nature of the fiber and its interaction with its neighbors. Adjacent fibers are most stable when their corrugations are in registry, but this cannot occur everywhere along a bent aggregate. Bending or twisting introduces an *effective lattice mismatch* between fibers on the inside of the curve and those on the outside of the curve. Kinks develop where outer fibers slip one lattice constant behind their inner neighbors. The energy cost of introducing a kink is less than the energy gained by straightening segments

between kinks.

Simple geometry determines the angle each kink subtends. Let D be the distance between adjacent fibers, projected onto the plane of the curve, and S be the period of the corrugations along a fiber. Bending the aggregate through an angle $\theta_k = S/D$ leaves each fiber exactly one corrugation behind its inner neighbor. The interaction energy *per unit length* between adjacent fibers, $U_{int}(s)$, is a periodic function of their relative axial displacement, with period S . We approximate this interaction with a simple sinusoidal potential:

$$U_{int}(s) = -\frac{\Delta\gamma}{2} \cos\left(\frac{2\pi D}{S}\theta(s)\right), \quad (6.2)$$

where $\Delta\gamma$ measures the strength of the corrugations in the interaction potential and the contour of the aggregate is characterized by the angle, $\theta(s)$, between its orientation at position s and the orientation of one end. We take $\theta(0) = 0$ so that the corrugations are in registry at the beginning of the aggregate.

Each fiber experiences a bending energy as well as the interfacial energy, so the total energy *per unit length* is:

$$U(s) = \frac{K}{2}(\theta_s)^2 - \frac{\Delta\gamma}{2} \cos\left(\frac{2\pi D}{S}\theta(s)\right), \quad (6.3)$$

where K is the bending constant of a single fiber, and a s subscript indicates a derivative with respect to contour length. To find the function $\theta(s)$ that minimizes $H = \int_0^L U(s)ds$, where L is the total length of the aggregate, we set the variational derivative $\delta[H] = 0$. The equation of equilibrium for the aggregate is

$$K\theta_{ss} = \frac{\chi}{2}\Delta\gamma \sin(\chi\theta) \quad (6.4)$$

where the new variable $\chi \equiv 2\pi D/S$. This equation appears under many guises, and is variously known as the physical pendulum equation, the Frenkel-Kontorova

model [69, 66], or the steady-state sine-Gordon equation. Soliton-like solutions to this equation have been applied to solid-state diffusion [19], propagation of ultra-short optical pulses [108], field-theories of elementary particles [171, 172, 62], epitaxial growth of thin films [196, 105, 162], diffusion of flux in extended Josephson junctions [7], and pairing of complementary strands of DNA [61, 160]. The Frenkel-Kontorova model provides a nonlinear microscopic description of periodic dislocations that occur in lattice-mismatched epitaxial layers. Here the lattice-mismatch is replaced by a curvature-induced effective lattice mismatch. Srolovitz, Safran and Tenne [175, 159] used the concept of effective lattice mismatch to develop a mesoscopic continuum model of kinking in thin 2-dimensional films, but they did not consider the mechanics in the vicinity of the kink as I do here.

When $\chi = 1$ the solutions of 6.4 correspond to the standard elasticae of a homogeneous isotropic rod (or equivalently to solutions of the simple pendulum, with s being a time-like variable). In general $\chi \neq 1$ and a range of other interesting shapes results. For $\chi > 1$ we find *kinked aggregates*, where χ gives the number of kinks per loop of the aggregate. With the initial value $\theta(0) = 0$, the aggregate switches from being essentially straight, with small sinusoidal perturbations, to kinked at $\theta_s(0) \geq (2\Delta\gamma/K)^{1/2}$, where the equality corresponds to the separatrix solution of the elastica with a single loop (or equivalently, the solution for the pendulum that delineates the oscillatory solutions from the rotating solutions). As $\theta_s(0)$ increases beyond $(2\Delta\gamma/K)^{1/2}$ the aggregate adopts an ever more circular aspect.

When the kinks are far apart so that the sections between kinks are approximately straight, it is possible to solve analytically for the shape of a kink. Multiplying both sides of Eq. 6.4 by θ_s and integrating with the boundary conditions $\theta_s(-\infty) = 0 =$

$\theta_s(\infty)$ yields

$$\theta(s) = \frac{4}{\chi} \tan^{-1} \left[\exp \left(s\chi \sqrt{\frac{\Delta\gamma}{2K}} \right) \right]. \quad (6.5)$$

Eq. 6.5 shows that the kink occurs over a length

$$l_k \approx \frac{1}{\chi} \sqrt{\frac{2K}{\Delta\gamma}}, \quad (6.6)$$

as could be expected on dimensional grounds. The energy of a single kink is obtained by substituting the solution 6.5 into the energy functional 6.3 to yield

$$U_k = \frac{4}{\chi} \sqrt{2K\Delta\gamma} \quad (6.7)$$

Figure 6.2 shows the curve obtained for $\chi = 8$, and $\theta_s(0) = 1.0001 \times (2\Delta\gamma/K)^{1/2}$. In real systems the corrugation potential is not a perfect sinusoid, so kinks will in general have a shape slightly different from that described by Eq. 6.5.

Structural data obtained by electron-microscopy allows us to apply this model to the *Limulus* acrosome [169]. The crosslinks between fibers have a period of $S = 55 \text{ \AA}$ along a filament, and the separation between filaments is $D = 147 \text{ \AA}$. The ratio S/D gives a kink-angle of $\theta_k = 0.37 \text{ rad}$, or 21° , in reasonable agreement with the observed kink angle of 24° .

We can also estimate the distance between kinks from the molecular structure. A cross-section of the acrosome shows that the actin fibers are hexagonally packed. For all kinks to lie in the same plane, the acrosome must twist through a multiple of 60° between kinks. The actin monomers are spaced by 27 \AA , and the crosslinking protein *scruin* introduces a twist of 0.23° per monomer when the acrosome is coiled [46]. Thus, the spacing between kinks is roughly $27 \text{ \AA} \times 60^\circ / 0.23^\circ = 7000 \text{ \AA}$. From the kink-angle and the spacing between kinks we find that the coiled acrosome makes one loop every 10 \mu m of its length, to produce a coil with a diameter of 3.2 \mu m . This

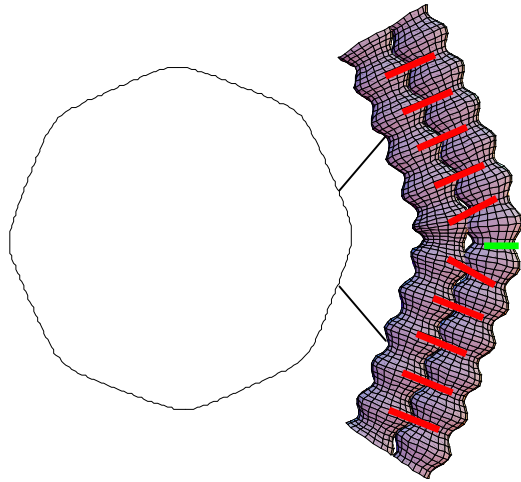


Figure 6.2: Energy-minimizing shape of a bent aggregate of corrugated fibers. The corrugation represents the periodicity of the inter-filament interactions. The fibers cannot maintain registry around a curve. Forming a kink minimizes the length that is out of registry but introduces an elastic penalty from the high curvature. Shown above is a kinked structure corresponding to the solution of Eq. 6.4 with $\chi = 8$, $\theta_s(0) = 1.0001 \times \left(\frac{2\Delta\gamma}{K}\right)^{1/2}$. The outer fiber has one additional corrugation at the kink, indicated by the green bar.

coil just fits inside the head of the sperm. Thus the molecular dimensions of the acrosomal constituents interact to set the size of the entire coiled acrosome.

The modified Frenkel-Kontorova model is more difficult to apply quantitatively to MWNTs because the constituent fibers (SWNTs) are concentric rather than adjacent. Nonetheless, similar reasoning applies. Thin graphite sheets form a kinked twin matrix boundary of $20^\circ 48'$ about $[1\bar{1}00]$ [96], which is very close to the kink-angle observed in MWNT helices. The surfaces of a MWNT on the inside and outside of a curve develop these kinks to relax strain. It is noteworthy that in cross-section MWNTs also often appear polygonal rather than circular. This polygonalization cannot be explained in terms of pentagon-heptagon defects, but arises naturally in a model based on curvature-induced lattice mismatch. The twin matrix boundary angle of $20^\circ 48'$ implies that a cross-section of a MWNT should have roughly 18 edges. In practice some of these edges are typically too short to observe. Polygonalization also occurs in nested fullerenes [174, 51] and WS_2 nanoparticles [165]. TEM pictures of MWNTs show that there is also some delamination of the graphene sheets and buckling in the popliteal region of each kink. These effects occur because of topological constraints on the graphene sheets in MWNTs, and are better explained in terms of buckling of a hollow tube.

Although we have focused on lattice-slip in the presence of spontaneous curvature as the source of mechanical nonlinearity leading to planar kinks, the same mechanisms will give rise to kinks in nonplanar fibrillar aggregates because of the competition between bend, twist and adhesion. More generally these localized structures arise in aggregates because of the presence of a non-convex bending energy functional or equivalently, by virtue of simple dimensional arguments that penalize kinks and bends

differently.

6.2.1 Finite temperature

At finite temperature thermal fluctuations may also nucleate kinks. The density of thermally activated kinks is proportional to $e^{-U_k/k_B T}$, where U_k is given by Eq. 6.7. For the present systems $U_k \gg k_B T$, so thermally activated kinks may be neglected. In other biological systems, the corrugations in the interfilament potential may be comparable to or less than $k_B T$. Consider a hexagonally packed bundle of corrugated filaments. The strength of the corrugations that any one filament feels is determined by the degree of longitudinal order among the six neighbors. If the neighbors are disordered, then the effect of their corrugations cancels. As the temperature increases, the disorder among filaments grows, which *decreases* the energetic cost of the disorder. These are the ingredients for a longitudinal melting phase transition.

The longitudinal melting transition should appear as a sharp decrease in bending stiffness of the aggregate. The bending stiffness of an aggregate in which the individual filaments maintain registry (coherent bending) scales as n^2 , where n is the number of filaments in the aggregate. When the individual filaments can slip relative to each other, the bending stiffness scales as n . Kis and coworkers recently measured the bending stiffness of an aggregate of microtubule filaments. They observed an abrupt decrease in stiffness above 25° C [99], but did not provide a model to explain these effects. A project for future research will be to develop a quantitative model of the longitudinal melting phase transition.

6.3 Kinks on polymers

As a second example of kinks on biological filaments, we study the conformation and force-extension curve of a polymer in a spatially uniform AC electric field. The polymer backbone minimizes its energy by aligning with the field; entropy opposes this alignment. In a strong field, hairpin kinks develop between regions of opposite alignment. These kinks act as a 1-dimensional gas of particles and antiparticles that diffuse along the polymer backbone. We calculate the equation of state of the kink-gas. The Langevin equation of motion has the structure of an overdamped sine-Gordon equation on a sphere, with kinks represented by solitons. The theory is applied to recent experiments on dielectrophoretic stretching of DNA.

The statistical mechanics of polymer chains is highly developed, including effects such as excluded volume [64, 55, 42], finite stiffness [68], interchain interactions [65, 50], and heterogeneous intrachain interactions [161]. Recent theory [63, 140, 81], and single-molecule experiments [156], have dealt with polymers under perturbed conditions (e.g. tension [11, 131], compression [198], torsion [180], elongational flow [111], shear flow [173]).

There is increasing interest in using high-frequency electric fields to manipulate polymer molecules, especially DNA, in solution [194, 195, 182, 6, 188, 72, 48]. A field interacts with the molecular polarizability to generate forces, torques and internal stresses, a phenomenon known as dielectrophoresis (DEP) [90]. DEP-induced stresses may lead to functionally significant conformational changes in biomolecules. For instance, 16 μm -long λ -DNA, tethered by one end to an electrode, extends to its full contour length away from the electrode when an AC voltage is applied [72]. This stretching is counterintuitive because the electrode generates a field-gradient which

seeks to pull the DNA towards the electrode. In this section I develop a model for the conformation of a polymer strand in an AC field. The model explains the stretching phenomenon and suggests other experiments related to DEP manipulation of macromolecules.

The model consists of a polyelectrolyte strand of length L , subject to a spatially uniform AC field of r.m.s. amplitude E , and a tension, A , applied to the ends of the strand and parallel to the field. The tension could occur in a single-molecule pulling experiment or serve as a proxy for more complex body forces induced by fluid flow or inhomogeneities in the field.

When dielectrophoresis is performed in water, AC fields are used rather than DC fields, to avoid ionic screening, electrochemistry, and electrophoresis. Typical AC fields in DEP have frequencies of 100 KHz - 5 MHz. A recent study by Netz [141] examined short polymer strands in DC fields. We find qualitatively different behavior for long strands in AC fields.

Polarization of polyelectrolytes such as DNA is largely due to motion of counterions, some condensed on the molecule, and some surrounding it in a diffuse cloud. This polarizability is highly anisotropic, being greatest parallel to the molecular backbone. The theory of polarization of polyelectrolytes is reviewed in [136, 193].

For long molecules in high frequency fields, the local polarization depends only on the local field. This is not the case for short molecules or for low-frequency fields, where the field can induce a global reorganization of the counterions. If the frequency of the field is ν , in a half-period an ion diffuses a distance $\delta_D = \sqrt{D/\nu}$, where D is the diffusion constant. The ion also oscillates with an amplitude $\delta_\mu = \mu E/2\pi\nu$, where μ is the mobility (with the ionic charge included in its definition). For a Na^+ ion in water

($D = 1.3 \times 10^{-9} \text{ m}^2/\text{s}$, $\mu = 5 \times 10^{-8} \text{ m}^2/\text{V s}$), under typical conditions for stretching DNA ($E = 1 \text{ MV/m}$, $\nu = 1 \text{ MHz}$), we find $\delta_D = 36 \text{ nm}$ and $\delta_\mu = 8 \text{ nm}$. The induced polarization in any bit of the polymer can only depend on the field averaged over a ball whose radius is of order δ_D . DEP stretching is typically studied in DNA strands many microns long, so it is justified to assign the molecule a polarizability *per unit length*, α .

Assuming negligible transverse polarizability, the induced linear polarization density at position s is $d\mathbf{p}(s) = \alpha(\mathbf{E} \cdot \mathbf{u})d\mathbf{u}$, where $\mathbf{u}(s)$ is the unit-vector locally tangent to the polymer. The polarization interacts with the field to give a time-averaged electrostatic free energy per unit length,

$$U_n(s) = -V \cos^2 \theta(s), \quad (6.8)$$

where $V \equiv \frac{1}{2}E^2\alpha$ and $\theta(s)$ is the angle between the polymer backbone and the field. This energy seeks to align the polymer backbone with the closer of two orientations along the field axis, and is analogous to the interaction energy in the optical Kerr effect.

The time-averaged Hamiltonian for a polymer in an AC field is the same as that of a polymer dissolved in a nematic liquid crystal subject to a Maier-Saupe mean-field interaction. The latter problem has been studied in detail. De Gennes [43], and independently Khokhlov and Semenov [97], showed that kinks play a crucial role at low temperature. The statistical mechanics of polymers in a nematic field was developed by Warner, Gunn, and Baumgärtner [192] and Williams and Warner [199]. These authors used an analogy to a quantum mechanical tunnelling problem to estimate the linear density of kinks. Kamien, Le Doussal, and Nelson, developed a formal analogy between the polymeric problem and motion of Bosons in 2-dimensions [92, 93]. In

analogy to the case of polymer liquid crystals, we call U_n the *nematic energy*. Below we examine the conformation of a polymer in an AC field, first in the limit of weak field and weak tension, then in the limit of strong field and weak tension, and finally in the limit of either very strong field or very strong tension. The meanings of these limits will be explained.

6.3.1 Freely jointed chain

For weak tension and weak AC field, it is acceptable to model the polymer as a freely jointed chain (FJC) of N rigid sticks, each of length b , and each assuming an orientation independent of its neighbors. For consistency with the more realistic wormlike chain (WLC) model, the stick length should be $b = 2l_p$, where l_p is the persistence length of the WLC.

Consider the setup of Figure 6.3 in which a stick of a FJC is subjected to a

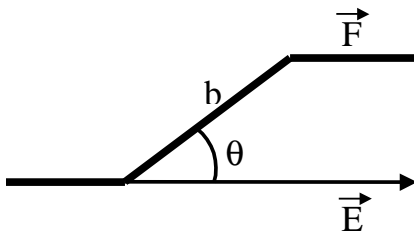


Figure 6.3: An element of a freely jointed chain in an oscillating electric field \mathbf{E} and subject to a force, \mathbf{A} , parallel to the field. The angle θ is measured between the stick and the field.

tension A and a parallel AC field E . The frequency is high enough that the polymer undergoes negligible motion over a single period. For DNA molecules in water, this assumption is valid for frequencies greater than ~ 100 KHz [81, 59]. The interaction between the field and excess charge on the polymer has zero time-average, so the

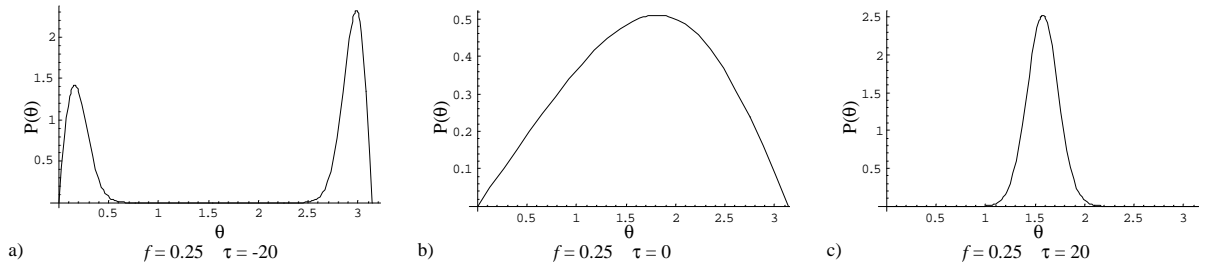


Figure 6.4: Distribution of stick orientations as a function of AC field-strength. In all cases the force ($f = 0.25$) introduces a slight bias towards the right. a) Strong alignment with the field restricts sticks to point either to the left or to the right. b) Under no AC field tension is the only influence on stick orientation. c) A field that seeks to align the sticks perpendicular to itself favors the orientation $\theta = \pi/2$. This case, called negative dielectrophoresis, requires that $\alpha < 0$, which can occur if the solvent is more polarizable than the polymer.

lowest-order interaction is between the field and the *polarizability*. The orientation-dependent energy of each stick is $U_{\text{FJC}} = -Ab \cos \theta - Vb \cos^2 \theta$. The AC field biases the sticks to point towards either pole, and tension favors one pole over the other.

The partition function of a single stick is

$$Z_{\text{FJC}} = \int_0^\pi \sin \theta \exp \left(\frac{Ab \cos \theta + Vb \cos^2 \theta}{k_{\text{B}}T} \right) d\theta. \quad (6.9)$$

The integral in Eq. 6.9 may be evaluated explicitly in terms of error functions, and from the resulting expression any thermodynamic property of the FJC determined.

For instance, the angular distribution function, $P(\theta)$, is

$$P(\theta) = 2\sqrt{\frac{\tau}{\pi}} \frac{\sin \theta \exp \left[-\frac{(f+2\tau \cos \theta)^2}{4\tau} \right]}{\text{erf} \left(\frac{f+2\tau}{2\sqrt{\tau}} \right) - \text{erf} \left(\frac{f-2\tau}{2\sqrt{\tau}} \right)}, \quad (6.10)$$

where $f \equiv -Ab/k_{\text{B}}T$ measures the dimensionless tension and $\tau \equiv -Vb/k_{\text{B}}T$ measures the dimensionless nematic energy. Figure 6.4 shows this distribution for weak force ($f = 0.25$), and for varying strengths of the AC field.

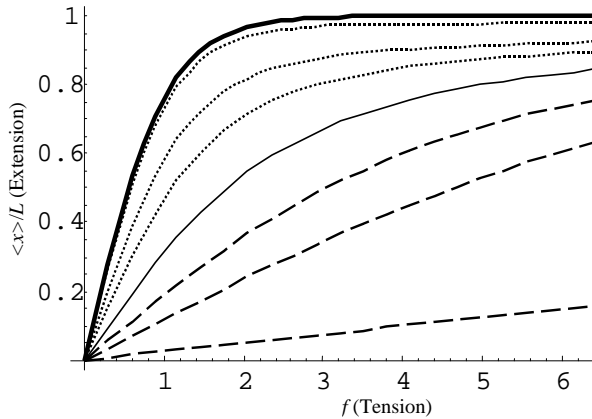


Figure 6.5: Force-extension curves for a freely-jointed chain under varying AC field strengths. (—): Langevin Function, $\langle x \rangle / L = \coth f - 1/f$, corresponding to $\tau = 0$ (no nematic field). (.....): $\tau < 0$. (—): $\langle x \rangle / L = \tanh f$ corresponding to $\tau \rightarrow -\infty$ (strong alignment with the field). (---): $\tau > 0$ (alignment perpendicular to the field).

For strong alignment ($\tau \ll 0$), the sticks act as a two-state system (analogous to a spin- $\frac{1}{2}$). For zero alignment ($\tau = 0$) the stick orientation is a continuous variable (analogous to a classical spin). For strong anti-alignment ($\tau \gg 0$) the sticks are confined to the plane perpendicular to the field (analogous to an X-Y model). Each of these cases can occur in real experiments; a single polymer may even exhibit all three behaviors, depending on the solvent, field strength, and field frequency.

Each stick has a mean end-to-end extension of $\langle x_1 \rangle = k_B T \frac{\partial}{\partial A} \ln Z_{\text{FJC}}$. Since the sticks are independent, the total extension is $\langle x \rangle = N \langle x_1 \rangle$. Figure 6.5 shows force-displacement curves for a range of AC field-strengths.

The zero-extension spring constant of the FJC is $k = \left(\frac{\partial \langle x \rangle}{\partial A} \Big|_{A=0} \right)^{-1}$. A weak AC field softens the spring constant by favoring steps with a larger displacement along

the field-axis. The zero-displacement spring constant evaluates to:

$$k = \frac{2\tau k_B T / (Nb^2)}{1 - 2\sqrt{\frac{\tau}{\pi}} \frac{\exp-\tau}{\operatorname{erf}\sqrt{\tau}}}. \quad (6.11)$$

In the limit of weak aligning field ($\tau \sim 0$), this simplifies to:

$$k \approx \frac{3k_B T}{Nb^2} + \frac{4\tau k_B T}{5Nb^2}. \quad (6.12)$$

For strong aligning fields ($\tau \ll 0$) the asymptotic spring constant is:

$$k \approx \frac{k_B T}{Nb^2}. \quad (6.13)$$

Thus a strong AC field decreases the entropic stiffness of a FJC by a factor of three along the field direction, corresponding to the transition from a 3-dimensional random walk to a 1-dimensional random walk. Khokhlov and Semenov obtained the same result for the linear susceptibility of a FJC in a nematic solvent, assuming a constant *permanent* dipole moment per unit length [97]. For strong anti-aligning fields ($\tau \gg 0$), the spring constant grows linearly with the nematic field: $k \approx 2\tau k_B T / (Nb^2)$.

The softer spring constant in a strong AC field also implies a larger radius of gyration, $R_G^2 = (kk_B T)^{-1}$, along the field-axis. We find

$$R_G^2 \approx \frac{Nb^2}{3} + \frac{4NVb^3}{45k_B T}. \quad (6.14)$$

Thus a weak AC field turns a roughly spherical random coil into a prolate spheroid aligned along the field. However, no field strength will lead to spontaneous extension of the FJC; rather in the strong-field limit the FJC undergoes a 1-dimensional random walk parallel to the field.

6.3.2 Kinks

The freely-jointed chain model utterly fails in a strong nematic field because half of the joints involve a bend through roughly 180° . These hairpins should be penalized by a large bending energy. The wormlike chain (WLC) model includes bending energy and is thus more appropriate for large nematic fields.

The Hamiltonian of a WLC under no tension in a nematic is

$$H = \int_0^L \left(\frac{1}{2} K (\theta_s)^2 - V \cos^2 \theta \right) ds. \quad (6.15)$$

We seek to find the function $\theta(s)$ that minimizes the energy H . Setting the variational derivative $\delta[H] = 0$ yields a local equation for the shape of the hairpin:

$$K \theta_{ss} - V \sin 2\theta = 0, \quad (6.16)$$

which is very similar to the equation of motion that described kinking in fibrillar aggregates (Eq. 6.4).

We are interested in the large-amplitude solution where θ swings from 0 to π (i.e. the polymer reverses direction). DeGennes first obtained an exact analytical solution to Eq. 6.16 [43] in the same way we solved for the shape of a kink in a fibrillar aggregate. The kink shape is:

$$\theta_{\text{hp}}(s) = 2 \cot^{-1} \exp(-s/s_0), \quad (6.17)$$

where $s_0 \equiv \sqrt{K/2V}$ is the characteristic size of bends in the polymer. Figure 6.6 shows the shape of a hairpin kink. The lateral displacement (see Figure 6.6) across a kink is $l = \pi s_0$. The total energy stored in a kink is given by substituting $\theta_{\text{hp}}(s)$ from Eq. 6.17 into Eq. 6.15 to yield

$$U_k = 2\sqrt{2KV} = 2k_B T \frac{l_p}{s_0}, \quad (6.18)$$

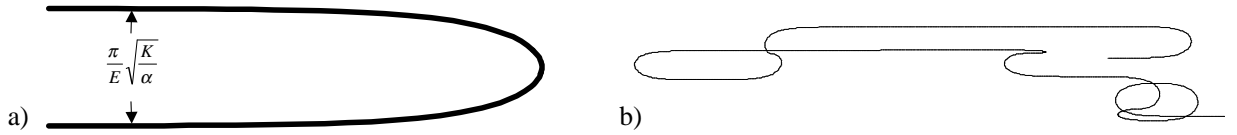


Figure 6.6: a) Shape of a hairpin kink in a polymer strand subject to a strong AC field. b) Conformation of a polymer containing ten kinks of random position and orientation. All kinks are the same size: those that appear thinner are viewed edge-on.

where $l_p \equiv K/k_B T$ is the persistence length of the polymer, the distance over which thermal fluctuations erase memory of the polymer orientation. For the kink to have a well-defined shape we require that $l_p \gg s_0$, or equivalently, that $U_k \gg 2k_B T$.

6.3.3 The kink gas

At low temperature or strong nematic field, kinks have well-defined size and energy, so we can think of them as particles and study their thermodynamics. Kinks come in two varieties: the kink of Figure 6.6, and an antikink formed by the mirror-image of Figure 6.6. Clearly kinks and antikinks must alternate along the polymer. If a kink and antikink collide they annihilate, while thermal fluctuations can create new kink-antikink pairs. The interaction between kinks decays exponentially with distance, so here we assume a low enough density to treat kinks as noninteracting particles. Following Seeger and Schiller [167] we find the number of kinks, n_{eq} , and free energy, F , for a kink-gas on a polymer of length L , with free ends. Then we consider the case where the ends of the polymer have a fixed end-to-end distance.

Free ends

We want the free energy of a gas of n kinks on a chain of length L , with free ends. Divide the chain into N sections, each of length l . Each section is short enough to contain not more than one kink ($N \gg n$), but still much larger than the size of an individual kink ($l \gg s_0$). Within these constraints, the choice of N is arbitrary—observable quantities will be independent of N . After the n kinks are distributed into the N bins, they are alternately assigned to be kinks and antikinks. The number of n -kink states available to the polymer is:

$$\Omega(n) = \frac{N^n}{n!} \quad (6.19)$$

with an entropy $S_n = k_B \ln \Omega(n)$. If the ends of the chain can point in either direction, then Eq. 6.19 should be multiplied by 2 because there is an arbitrary choice of whether the first hairpin should be a kink or an antikink. For simplicity we assume that one end of the chain has a fixed direction.

Let f_1 be the free energy of a single kink on a section of length l . The energy of a kink is just U_k , given by Eq. 6.18, but the *free* energy includes the entropy of a kink, which has contributions from the vibrational modes of the kink, its freedom to reside anywhere along the length l , and its freedom to lie in any plane parallel to the field. Here we assume that f_1 is known. In section **V** we calculate f_1 and show that its dependence on l cancels the dependence on the arbitrary choice of N , and hence l , in all observable quantities.

The total free energy is

$$F_n = nf_1 - TS_n. \quad (6.20)$$

In thermal equilibrium there is no benefit to changing the number of kinks, so

$$\frac{\partial F_n}{\partial n} = 0 = f_1 - T \frac{\partial S_n}{\partial n}. \quad (6.21)$$

Applying Stirling's approximation to Eq. 6.19 yields

$$\frac{\partial S_n}{\partial n} = k_B \ln \frac{N}{n}. \quad (6.22)$$

Inserting this result into Eq. 6.21 and solving for n gives

$$n_{eq}^0 = N \exp\left(\frac{-f_1}{k_B T}\right). \quad (6.23)$$

Substituting Eq. 6.23 into Eq. 6.20 gives the equilibrium free energy:

$$\begin{aligned} F &= -k_B T N \exp\left(\frac{-f_1}{k_B T}\right) \\ &= -k_B T n_{eq}^0. \end{aligned} \quad (6.24)$$

So each kink quasiparticle contributes a free energy of $-k_B T$.

Fixed ends

If the ends of the chain are fixed at separation x , then there is a constraint on the placement of kinks and antikinks. Let L_+ and L_- be the total chain lengths pointing to the right and left, respectively. Then

$$L_+ + L_- = L \quad (6.25a)$$

$$L_+ - L_- = x. \quad (6.25b)$$

If the entire chain is divided into a large number, N , of segments, each of length l , then the portions of the chain pointing to the right and left are divided into N_+ and

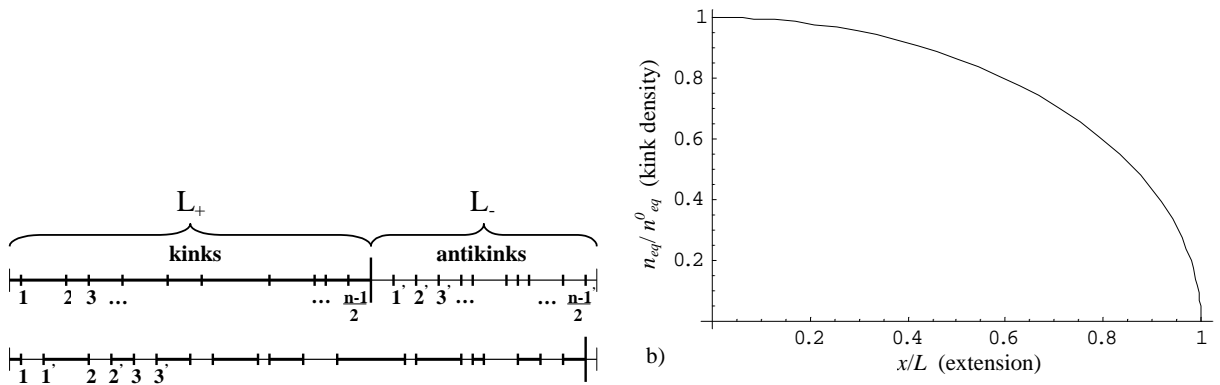


Figure 6.7: a) Partitioning of kinks along a polymer strand with fixed endpoints. Kinks are distributed with no constraints along section L_+ and antikinks are distributed along L_- . The conformation is obtained by concatenating alternate left- and right-pointing segments. b) Equilibrium density of kinks as a function of end-to-end extension.

N_- segments, respectively:

$$N_+ = \frac{1}{2}(N + x/l) \quad (6.26a)$$

$$N_- = \frac{1}{2}(N - x/l) \quad (6.26b)$$

At first the constraint on the end-to-end displacement seems to complicate matters considerably. However a simple geometrical construction makes it easy to incorporate.

Imagine sorting the polymer chain so that all the right-pointing segments are grouped together into a chain of length L_+ and all the left-pointing segments are grouped together into a chain of length L_- (Fig. 6.7). To generate an n -kink configuration with extension x , place $(n-1)/2$ kinks on the segment L_+ , *with no restriction on their placement*, and similarly place $(n-1)/2$ antikinks on the segment L_- . The position of the last kink is fixed at the junction of the L_+ and the L_- segments.² Thus

²Assuming n is odd. The same approach works for even n , placing $n/2 - 1$ kinks in each of L_+ and L_- , then placing kink number $n - 1$ anywhere on L . Kink number n is still fixed at the boundary between L_+ and L_- .

the global constraint on the segment lengths has been shifted to a local constraint on the position of the last kink.

The polymer conformation is generated by concatenating the first segment from L_+ , then the first segment from L_- , then the second segment from L_+ , etc. The arbitrary choice of the direction of the initial segment introduces a factor of 2 into the density of states, but after the initial choice there is no more freedom in assembling the chain. As before we assume that the ends of the chain have fixed direction so we can ignore the factor of 2.

The number of ways to distribute $(n-1)/2 \approx n/2$ kinks among the N_+ segments and $(n-1)/2 \approx n/2$ antikinks among the N_- segments is:

$$\Omega(n) \approx \frac{N_+^{n/2}}{\left(\frac{n}{2}\right)!} \frac{N_-^{n/2}}{\left(\frac{n}{2}\right)!}, \quad (6.27)$$

again assuming $N_+, N_- \gg n \gg 1$. The free energy is still given by Eq. 6.20, but the entropy is

$$S_n = k_B n \left(1 + \frac{1}{2} \ln \frac{4N_+ N_-}{n^2} \right), \quad (6.28)$$

so

$$\frac{\partial S_n}{\partial n} = \frac{k_B}{2} \ln \frac{4N_+ N_-}{n^2}, \quad (6.29)$$

whence from Eqs. 6.21 and 6.26 the number of kinks is

$$\begin{aligned} n_{eq} &= 2(N_+ N_-)^{1/2} \exp\left(\frac{-f_1}{k_B T}\right) \\ &= n_{eq}^0 \sqrt{1 - \frac{x^2}{L^2}}. \end{aligned} \quad (6.30)$$

Figure 6.7 shows the equilibrium density of kinks as a function of the end-to-end extension.

The free energy of the chain is given by Eq. 6.20, with S_n from Eq. 6.28 and n_{eq} from Eq. 6.30:

$$\begin{aligned} F &= -k_B T N \exp\left(\frac{-f_1}{k_B T}\right) \sqrt{1 - \frac{x^2}{L^2}} \\ &= -k_B T n_{eq}. \end{aligned} \quad (6.31)$$

The restoring force (analogous to the pressure) is $A = -\partial F/\partial x$, which yields the equation of state:

$$A = \frac{n_{eq}^0}{L} k_B T \frac{x}{\sqrt{L^2 - x^2}}. \quad (6.32)$$

The restoring force is proportional to the density of kinks in the unconstrained chain, which is exponentially suppressed by the nematic field. This result is very different from the result on the FJC. The next section is devoted to calculating the entropic contribution to f_1 .

6.3.4 Free energy of a kink

To calculate the free energy of a single kink, it is necessary to examine the internal vibrational modes of a kink. If the polymer is constrained to lie in a plane, then its Langevin equation of motion has the structure of the overdamped sine-Gordon equation, with kinks represented by solitonic solutions. Seeger and Schiller [167] first calculated the free energy of a kink obeying this equation in the context of kinked dislocation lines in crystals. They also calculated the equilibrium rates of creation and annihilation of kink-antikink pairs. Büttiker and Landauer [26, 25] went on to study the system in an external field of force, and, in collaboration with Bennett and Thomas, to develop the hydrodynamics of the kink-gas [13]. Recently there have been analytical studies on diffusion of kinks [157], the non-ideal kink-gas [79], and

creation and annihilation rates in the driven kink-gas [31, 122, 123, 36]. The last problem generated considerable controversy in the literature [23, 78, 24]. Computer simulations have also been performed on the sine-Gordon gas and the related ϕ^4 system [77, 3, 16].

The free energy is defined $F = -k_B T \ln Z$, where Z is the partition function. The change in free energy upon creating a single kink in a chain of length l is

$$f_1 = -k_B T \ln \frac{Z_k}{Z_s}, \quad (6.33)$$

where Z_k and Z_s are the partition functions of the kinked and unkinked chains, respectively. Rather than solve for the free energy, we will solve directly for the equilibrium number of kinks on a chain with free ends, given by (insert Eq. 6.33 into Eq. 6.23):

$$n_{eq} = \frac{L}{l} \frac{Z_k}{Z_s}. \quad (6.34)$$

Readers uninterested in mathematical details can skip directly to the answer, Eq. 6.60.

The partition functions Z_k and Z_s depend on the harmonic modes of a polymer with a single kink and of a straight polymer, respectively. First we restrict the polymer to lie in a plane. The derivation below closely follows Appendices B and C of [26]. In the subsequent subsection we generalize these results to the 3-dimensional case.

Planar case

If the polymer is constrained to lie in a plane, then its energy is given by Eq. 6.15. The Langevin equation describing the relaxation of a nonequilibrium conformation is:

$$\gamma \theta_t = K \theta_{ss} - V \sin 2\theta + \zeta(x, t), \quad (6.35)$$

where γ is the orientational drag coefficient of the polymer (assuming local hydrodynamics) and $\zeta(x, t)$ is a Brownian force that obeys the fluctuation-dissipation relation:

$$\langle \zeta(x, t) \zeta(x', t') \rangle = 2\gamma k_B T \delta(t - t') \delta(x - x'). \quad (6.36)$$

Eq. 6.35 is a sine-Gordon equation, except for the factor of 2 in the argument of the sine.

For the straight chain, linearizing Eq. 6.35 about $\theta = 0$ and performing separation of variables gives the eigenvalue equation:

$$\lambda_0 \theta = -K \theta_{ss} + 2V \theta, \quad (6.37)$$

where the 0 subscript indicates that λ is an eigenvalue for a straight chain. The solutions are $\theta(s) = \eta \exp(iks/s_0)$ with eigenvalue $\lambda_0 = 2V(1 + k^2)$. The partition function of the straight chain is thus:

$$\begin{aligned} Z_s^p &= \int d\eta_1 d\eta_2 \dots \exp \left(-\frac{1}{2k_B T} \sum_{k=1}^N \lambda_{0,k} (\eta_k)^2 \right) \\ &= (2\pi k_B T)^{N/2} \prod_{k=1}^N (\lambda_{0,k})^{-1/2}, \end{aligned} \quad (6.38)$$

where N represents some high-frequency cutoff, and the p superscript is a reminder that we are restricted to a planar geometry.

For the kinked chain, we linearize Eq. 6.35 about the shape of a hairpin, $\theta_{\text{hp}}(s)$, to get:

$$\lambda_1 \theta = -K \theta_{ss} + 2V (1 - 2\text{sech}^2(s/s_0)) \theta \quad (6.39)$$

where the 1 subscript indicates that λ is an eigenvalue for a kinked chain. The solutions to this equation are well known [39, 157]. There is a zero-frequency Goldstone

mode corresponding to translation of the kink:

$$\begin{aligned}\theta_{\text{GM}}(s) &= \xi_0 \text{sech}(s/s_0) \\ \lambda_{1,0} &= 0,\end{aligned}\tag{6.40}$$

and a series of harmonic modes:

$$\begin{aligned}\theta(s) &= \xi_k \frac{\exp(\imath k s/s_0)(k + \imath \tanh(s/s_0))}{\sqrt{2\pi(1+k^2)}} \\ \lambda_{1,k} &= 2V(1+k^2).\end{aligned}\tag{6.41}$$

The kinked and unkinked chains must have the same number of modes, so the existence of the zero-frequency Goldstone mode means that the kinked chain has only $N - 1$ delocalized modes.

The partition function for the kinked molecule is:

$$Z_k^p = \exp\left(\frac{-U_k}{k_B T}\right) \int d\xi_0 d\xi_1 \dots \exp\left(\frac{-1}{2k_B T} \sum_{k=0}^{N-1} \lambda_{1,k}(\xi_k)^2\right).\tag{6.42}$$

In Eq. 6.42, the Gaussian integrals over all $\xi_{i \neq 0}$ evaluate to:

$$\int d\xi_1 \dots d\xi_{N-1} \exp\left(\frac{-1}{2k_B T} \sum_{k=0}^{N-1} \lambda_{1,k}(\xi_k)^2\right) = (2\pi k_B T)^{(N-1)/2} \prod_{k=1}^{N-1} (\lambda_{1,k})^{-1/2}.\tag{6.43}$$

The integral over the Goldstone mode, $\int d\xi_0$, must be handled differently because of the exponential does not decay (recall $\lambda_{1,0} = 0$). We evaluate the integral over this mode using a technique of Langer [110]. The first step is to relate the shape of the Goldstone mode, $\delta\theta_{\text{GM}}(x)$, to the shape of the hairpin. Adding $\delta\theta_{\text{GM}}(x)$ to $\theta_{\text{hp}}(x)$ translates the kink while preserving its shape. Thus from simple geometry it follows that:

$$\delta\theta_{\text{GM}}(x) = \frac{d\theta_{\text{hp}}(x)}{dx}.\tag{6.44}$$

This result can be checked explicitly by differentiating Eq. 6.17 and comparing to Eq. 6.40.

The second step is to express the amplitude (in function-space) of the Goldstone mode in terms of its shape in real space by:

$$\begin{aligned} |d\xi_0| &= \left[\int_{-\infty}^{\infty} (\delta\theta_{\text{GM}}(x))^2 dx \right]^{1/2} ds \\ &= \left[\int_{-\infty}^{\infty} \left(\frac{d\theta_{\text{hp}}(x)}{dx} \right)^2 dx \right]^{1/2} ds. \end{aligned} \quad (6.45)$$

The integral in Eq. 6.45 is easily evaluated to yield:

$$|d\xi_0| = \left(\frac{U_k}{K} \right)^{1/2} ds, \quad (6.46)$$

whence the integral over the Goldstone mode becomes

$$\int d\xi_0 = l \left(\frac{U_k}{K} \right)^{1/2}. \quad (6.47)$$

Having now assembled all the ingredients of both partition functions we can insert Eqs. 6.38, 6.42, 6.43, and 6.47 into Eq. 6.34 to calculate the density of kinks:

$$\rho_{eq}^p = \left(\frac{U_k}{2\pi K k_B T} \right)^{1/2} \left(\frac{\prod_{k=1}^N \lambda_{0,k}}{\prod_{k=1}^{N-1} \lambda_{1,k}} \right)^{1/2} \exp \left(\frac{-U_k}{k_B T} \right). \quad (6.48)$$

The remaining challenge is to evaluate the ratio of products of the eigenvalues of Eqs. 6.37 and 6.39:

$$Q^2 = \frac{\prod_{k=1}^N \lambda_{0,k}}{\prod_{k=1}^{N-1} \lambda_{1,k}}. \quad (6.49)$$

McCumber and Halperin [128] considered the more general problem of evaluating Q^2 for the differential equations

$$\left(\frac{d^2}{dy^2} - 2\alpha(\epsilon) \right) \psi(y) = 0 \quad (6.50)$$

and

$$\left(\frac{d^2}{dy^2} - 2\alpha(\epsilon) + 2\beta \operatorname{sech}^2 y \right) \psi(y) = 0, \quad (6.51)$$

where $\alpha(\epsilon)$ is a linear function of the eigenvalue, ϵ , and β is a constant. They showed that

$$Q^2 = \lim_{\epsilon \rightarrow 0^+} \epsilon \prod_{n=1}^{\infty} \frac{[n-1 + (2\alpha)^{1/2}][n + (2\alpha)^{1/2}]}{[n-1 + (2\alpha)^{1/2}][n + (2\alpha)^{1/2}] - 2\beta}. \quad (6.52)$$

Comparison of Eqs. 6.50 and 6.51 with Eqs. 6.37 and 6.39 shows that $\alpha = \frac{1}{2} - \frac{\lambda}{4V}$ and $\beta = 1$, whence

$$Q^2 = \lim_{\lambda \rightarrow 0^+} \lambda \frac{(2\alpha)^{1/2} + 1}{(2\alpha)^{1/2} - 1}, \quad (6.53)$$

which evaluates to $Q^2 = 8V$. Inserting this result into Eq. 6.48 yields

$$n_{eq}^p = \frac{L}{l^*} \exp\left(\frac{-U_k}{k_B T}\right), \quad (6.54)$$

where the prefactor l^* is can be variously expressed as:

$$l^* = \left(\frac{\pi K k_B T}{4V U_k} \right)^{1/2} \quad (6.55a)$$

$$= s_0 \left(\frac{\pi k_B T}{2U_k} \right)^{1/2} \quad (6.55b)$$

$$= l_p \sqrt{2\pi} \left(\frac{k_B T}{U_k} \right)^{3/2}. \quad (6.55c)$$

This prefactor contains the entropic component of a kink and sets the natural scale over which kinks form in the polymer, but does not include the effect of modes transverse to the kink.

3-dimensional case

Here modes *transverse* to the kink are included in the partition functions. For the straight chain, the transverse modes clearly have the same spectrum as the in-plane

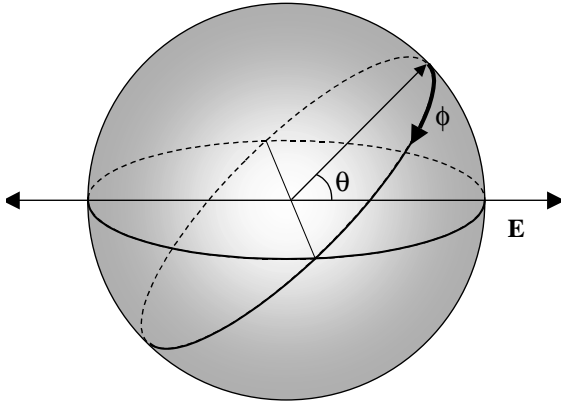


Figure 6.8: Coordinate-system used to describe fluctuations in the orientation of a polymer chain. This coordinate system is equivalent to conventional polar coordinates (with the z-axis pointing out of the page and the x-axis parallel to the field), except that the polar angle, ϕ is measured relative to the equator.

modes. Thus the full partition function of the unknicked chain is just the square of Eq. 6.38: $Z_s = (Z_s^p)^2$.

For the kinked chain we need the equation of motion for excitations perpendicular to the kink. Taking into account that the tangent vector can lie anywhere on a unit sphere, the Hamiltonian becomes:

$$U = \int_0^L \left(\frac{1}{2}K(\cos^2 \phi)\theta_s^2 + \frac{1}{2}K\phi_s^2 - V \cos^2 \theta \cos^2 \phi \right) ds, \quad (6.56)$$

where we have used the non-standard polar coordinates shown in Figure 6.8.

The equation of motion for ϕ is obtained by taking $(\delta[U]/\delta\phi)|_{\theta(s)=\theta_{hp}}$ and expanding for small $\phi(s)$. This yields:

$$\lambda_1\phi = -K\phi_{ss} + 2V(1 - 2\text{sech}^2(s/s_0))\phi, \quad (6.57)$$

which is exactly the same as the equation of motion for $\theta(s)$ (Eq. 6.39)! Thus $\phi(s)$ also has one localized Goldstone mode given by Eq. 6.40 (corresponding to rotation

of the kink about the axis of the field) and a spectrum of delocalized modes given by Eq. 6.41.

Since the transverse modes have the same spectrum as the in-plane modes, they contribute an additional factor of Eq. 6.43 to the partition function. The contribution of the transverse Goldstone mode must be evaluated separately, though, because the transverse Goldstone mode rotates the kink rather than translating it.

The translational and rotational Goldstone modes have exactly the same shape: $\delta\theta_{\text{GM}}(s) = \delta\phi_{\text{GM}}(s)$. If adding $\hat{\theta}\delta\theta_{\text{GM}}$ to θ_{hp} translates the kink by ϵ , then adding $\hat{\phi}\delta\phi_{\text{GM}}$ to θ_{hp} rotates the kink by an angle ϵ/s_0 . This result is obtained by considering the motion of the polymer at the middle of the kink, $s = 0$, and noting that $(d\theta_{\text{hp}}/ds)|_{s=0} = 1/s_0$. By analogy to Eq. 6.45, the amplitude (in function space) of the rotational Goldstone mode is:

$$|d\xi_0| = \left(\frac{U_k}{K}\right)^{1/2} s_0 d\phi, \quad (6.58)$$

whence the integral over the Goldstone mode becomes

$$\int d\xi_0 = 2\pi s_0 \left(\frac{U_k}{K}\right)^{1/2}. \quad (6.59)$$

The total partition function of the kinked chain (including in-plane and transverse modes) has two factors of Eq. 6.43 from the delocalized modes, one factor of Eq. 6.47 from the in-plane Goldstone mode, one factor of Eq. 6.59 from the transverse Goldstone mode, and a factor of $\exp(-U_k/k_{\text{B}}T)$. Combining these terms and dividing by the full partition function for the unkinked chain yields:

$$n_{eq} = 4L \frac{U_k}{k_{\text{B}}T} \left(\frac{2V}{K}\right)^{1/2} \exp\left(-\frac{U_k}{k_{\text{B}}T}\right). \quad (6.60)$$

This result agrees exactly with a calculation based on a quantum mechanical analogy [192, 75], but in our view has a simpler physical interpretation.

6.3.5 WLC under large tension

When the combination of tension and AC field reduces the density of kinks to less than one per chain length, then Eq. 6.32 is no longer applicable. In the absence of kinks, the tangent vector resides completely in one hemisphere, so small fluctuations in orientation are the only factor to prevent complete extension. To calculate the effect of these fluctuations we introduce the tension, A , explicitly into the Hamiltonian of Eq. 6.15:

$$U = \int_0^L \left(\frac{1}{2} K(\theta_s)^2 - A \cos \theta - V \cos^2 \theta \right) ds. \quad (6.61)$$

Under the assumption of almost complete extension, θ is small so we may expand Eq. 6.61 in θ , yielding

$$U \approx \frac{1}{2} \int_0^L (K(\theta_s)^2 + A_{eff} \theta^2) ds, \quad (6.62)$$

where the effective tension, $A_{eff} \equiv A + 2V$, arises because the energies due to the tension and the AC field are both quadratic in θ .

Hamiltonian (6.62) is identical to that of a WLC under tension in the absence of a field, with the replacement of A_{eff} for A . Thus we can quote the well-known force-extension relation of a WLC under large extension [125] to get

$$A_{eff} = \frac{k_B T}{4l_p} \left(1 - \frac{\langle x \rangle}{L} \right)^{-2}. \quad (6.63)$$

In a field strong enough to suppress kinks, the polymer spontaneously extends to a length given by Eq. 6.63. The effective tension, A_{eff} , is positive even if $A = 0$, because the AC field traps the polymer in an orientation centered around one pole. Tension ($A > 0$) further penalizes fluctuations in orientation and leads to additional extension. Under compression ($A < 0$), the polymer may lower its energy by an amount $2AL$

if it reverses direction. This reversal may come about through nucleation of a kink and antikink which are driven apart by the compressive force. For weak compression, the timescale for spontaneous formation of a critical kink-antikink nucleus is $\tau \propto \exp(-U_k/k_B T)$ [26].

6.3.6 Discussion

Washizu and coworkers first showed that it is possible to manipulate and stretch DNA molecules in solution by applying high frequency AC potentials to microfabricated electrodes [194, 195]. This work led to studies on fluorescence anisotropy in AC field-stretched DNA [182], studies of DNA conformation in polyacrylamide gels subject to low-frequency (0.1 - 100 Hz) AC fields, and variant trapping schemes differing in the surface attachment of the DNA and the electrode geometry [6, 48, 72].

In the above experiments, the electrode geometry creates an inhomogeneous field, and the DNA is attracted to regions of high-intensity, typically near the electrode corners. This much can be explained by simple dielectrophoresis. But as the DNA is attracted to the electrodes, it also straightens and extends to its full contour length away from the electrode (like hairs on the head of a person touching a van de Graaf machine). If the DNA experienced simple attraction to the electrodes, it would ball-up on the surface. Why does it straighten?

In the model presented here, the molecule straightens because the field is strong enough to suppress the formation of kinks. Without the inclusion of the bending energy (i.e. in the FJC model), the polymer does not spontaneously extend in any AC field strength. Experiments are under way to provide a quantitative test of this theory. Single-molecule force-extension curves measured in an AC field should provide

a quantitative test of the predictions in the various regimes, given by Eqs. 6.11, 6.32 and 6.63.

The experiments on dielectrophoretic stretching of DNA certainly contain many complex effects that were ignored in this section. One effect is the role of inhomogeneity in the field. An inhomogeneous field generates body forces on the polymer backbone, so the tension varies along the length, and at each point the tension depends on the location of all other points on the polymer. Furthermore, the position of each point depends on the tension everywhere in the molecule. Thus the problem of the molecular conformation becomes highly nonlocal.

A second effect that has been ignored is that each chain-element sees not only the applied field, but also fields due to induced dipoles on the rest of the chain and in nearby chains. This effect also introduces a nonlocal character to the problem. One approach is to introduce a Clausius-Mossotti mean-field, where the electric field is modified by the local density of chain-elements. It is justified to ignore nonlocal electrostatics in the low-density limit.

It is well known that the activity of many DNA-active enzymes depends on the conformation of the underlying strand. Through its effect on conformation, an intense AC field may provide a way to rapidly and reversibly modulate both the kinetics and thermodynamics of biochemical processes, supplementing the traditional tools of temperature and chemical environment. Furthermore, it may be possible to design nanoscale polymeric actuators in which an AC field drives a conformational change.

6.4 Kinks in confined polymers

As a final example of kinks in biological filaments, we study polymers confined to a plane. There is increasing interest in building nanofluidic devices for manipulating polymer molecules, especially DNA [121, 187]. When the confined dimension becomes less than the persistence length of the polymer (~ 50 nm for DNA), certain topological defects arise that are not stable in the unconfined polymer.

Consider a semiflexible polymer constrained to lie in a plane, with self-crossings allowed. This scenario could occur in a fluid gap of height h , provided $l_p > h \gg d$, where l_p is the persistence length and d is the molecular diameter. This scenario also pertains to the experiments of Maier and Rädler, in which DNA molecules were dissolved in a fluid lipid bilayer [121]. If the polymer is subjected to tension A , then the Hamiltonian is

$$H = \int_0^L \left(\frac{1}{2} K (\theta_s)^2 - A \cos \theta \right) ds, \quad (6.64)$$

where the angle θ is measured relative to the direction of the tension. Taking the variational derivative of Eq. 6.64 yields the Langevin equation of motion:

$$\gamma \theta_t = K \theta_{ss} - A \sin \theta + \zeta(x, t), \quad (6.65)$$

where γ and $\zeta(x, t)$ are the same as in Eq. 6.35. Eq. 6.65 is the same as Eq. 6.35 for a polymer in a nematic field, apart from the factor of 2 in the argument of the sine.

The force-extension curve for large extension is obtained by linearizing Eq. 6.65 about $\theta = 0$, as in the Marko-Siggia model. However, the Marko-Siggia model does not take into account statistically unlikely large fluctuations. In the 3-dimensional case, large fluctuations are insignificant, but in 2 dimensions there is the possibility of the polymer forming a complete loop. Such loops are unstable in 3 dimensions

(the polymer can come out of the plane, converting the loop into a twist), but are stable in two dimensions. The equation describing the shape of a loop is very similar to that of a kink in a nematic field (Eq. 6.17):

$$\theta(s) = 4 \cot^{-1} \exp(-s/s_0), \quad (6.66)$$

where $s_0 \equiv \sqrt{K/A}$ is the characteristic size of the loop. The energy of a loop is

$$U_l = 8\sqrt{AK}. \quad (6.67)$$

At finite temperature there is the possibility of nucleating loop-antiloop pairs, with a density proportional to $e^{-U_l/k_B T}$. Figure 6.9 illustrates the birth of a loop-antiloop pair. Loops may play an important role in chemical reactivity or bond breakage because of their high curvature relative to the rest of the polymer.

The loop gas is subtly different from the kink gas. There are actually *four* topologically distinct loops, provided that the polymer remains in the plane, has finite curvature everywhere along its length, and maintains fixed orientations at its endpoints. The four fundamental loops are illustrated in Figure 6.10. I have named these four loops 1, -1 , i , and $-i$, to suggest an analogy to the complex plane. The 1 and -1 may annihilate each other, as may the i and $-i$, but there is no cross-reactivity (check this with a piece of string!). Combinations of real and imaginary loops lead to more complex twists of the polymer. The topological state of a polymer is described by an ordered pair of integers (x, y) , where x is the number of real loops, and y is the number of imaginary loops. Clearly, joining segments of polymer in the states (x_1, y_1) and (x_2, y_2) leads to a state $(x_1 + x_2, y_1 + y_2)$. 2-dimensional loops on a polymer form a group isomorphic to $(\mathbb{Z}^2; +)$.

For a given two-dimensional contour of a polymer, is there a simple way to obtain

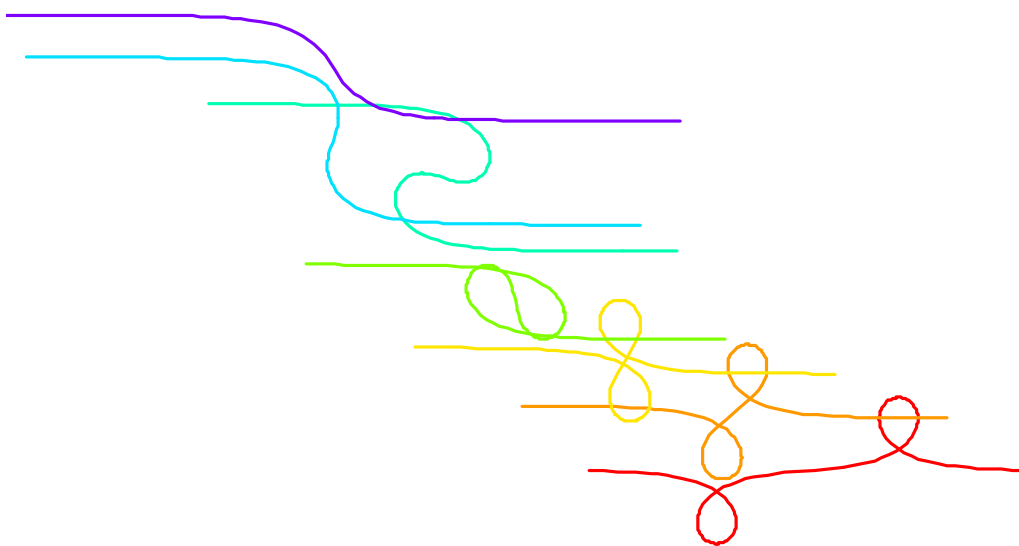


Figure 6.9: Birth of a loop-antiloop pair in a 2-dimensional polymer. The segment of polymer between the loops rotates through 360° . Once the loop and antiloop are separated, they act essentially as free particles that may diffuse along the polymer backbone.

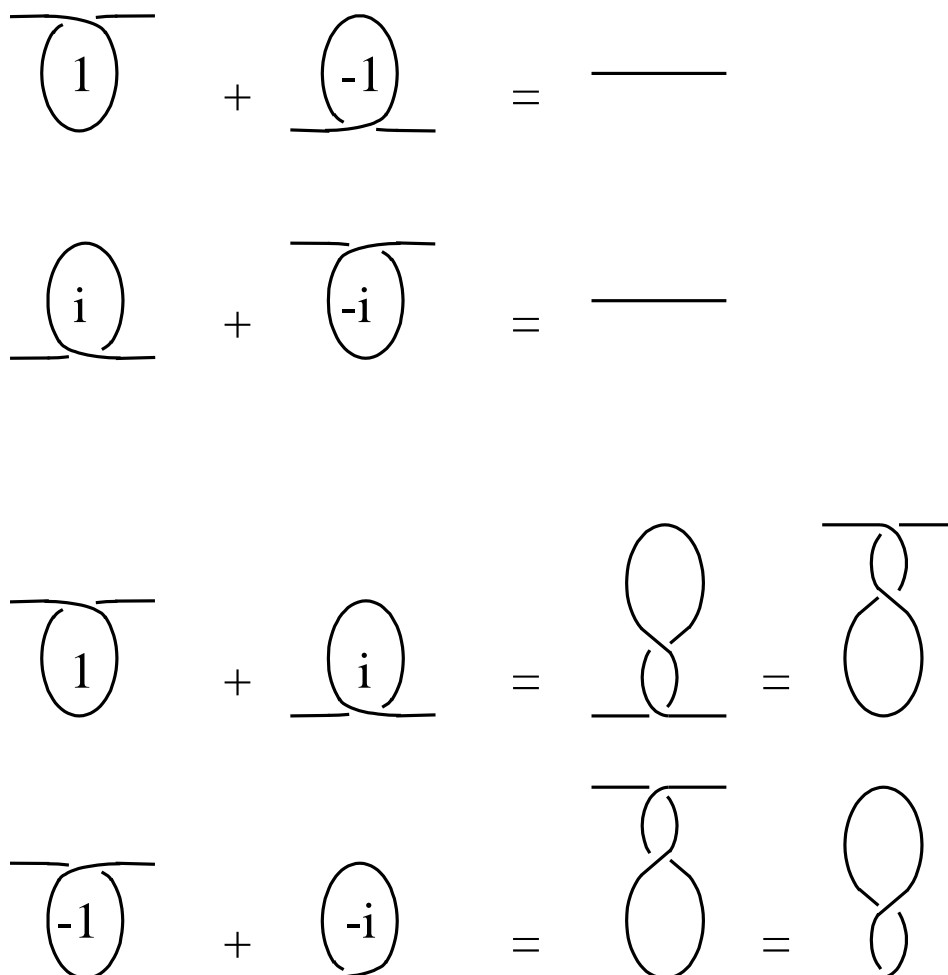


Figure 6.10: The loopy group. Loops form a group isomorphic to $(\mathbb{Z}^2; +)$, i.e. the set of all ordered pairs of integers (x, y) , with the operation of addition. The identity is a straight line, each loop has an inverse which annihilates it, and addition is implemented by concatenating segments of polymer. The four basic elements, denoted $1, -1, i, -i$ may be combined to make more complicated loops. The state of the polymer, characterized by its loop index (x, y) , is a topological invariant, provided that the polymer remains in the plane, has finite curvature, and the tangent vectors of the endpoints remain fixed. Reflection about the horizontal implements $(x, y) \rightarrow (-x, -y)$. Reflection about the vertical implements $(x, y) \rightarrow (-y, -x)$. Rotation by 180° implements $(x, y) \rightarrow (y, x)$.

its (x, y) state? Figure 6.11 illustrates such a procedure. If one starts on the left of the polymer and walks along, there are four types of intersections that may appear. The piece of polymer that one is walking along always points to the right. The intersecting strand may point up or down, and pass over or under. By walking along a contour one may classify each intersection, and at the end tally up the state of the polymer. The loop-group does not describe all possible topologies for the polymer because it misses knots that would remain if the polymer were allowed to come out of the plane, as in Figure 6.11 c. An interesting question to which I do not have the answer is, for a given 2-dimensional contour of a polymer, is there a simple way to determine whether it is in the loop group (i.e. would it be topologically straight if it were allowed to come out of the plane)? This is a problem for future pondering.

Appendix A

Symmetries of the GRFs

This appendix is on the symmetry properties of the generalized response functions. The symmetry properties of the two-time correlation functions, R^{+-} and R^{++} , have been exhaustively studied in the context of linear response theory. The principle symmetries are given by the Kramers-Kronig (K-K) relations and the fluctuation-dissipation theorem (FDT). Our goal in this section is to extend these results to the GRFs. The conditions available to us are: causality, time-translation invariance, and a density matrix in initial thermal equilibrium.

A.1 Causality and time-translation invariance

Toll showed that the conditions of causality and time-translation invariance are sufficient to establish the Kramers-Kronig (K-K) relations between the real and the imaginary parts of the susceptibility, R^{+-} [184]. In recent years there has been interest in deriving K-K relations for nonlinear response functions, $R^{+-\dots-}$. Shortly after the first observation of optical harmonic generation, Kogan sought to generalize the K-K

relations to nonlinear response, within a specific model of the matter [104]. Scandolo and Bassani recently developed model-independent K-K relations for the nonlinear response functions relying only on causality and time-translation invariance [164, 10]. We show that a variant of their result applies to GRFs.

Causality requires that the force must precede the response, so

$$R^{+\dots+ - \dots -}(t_a, \dots, t_c, t_n, \dots, t_1) = 0 \quad \text{if } \max(t_n, \dots, t_1) > \max(t_a, \dots, t_c), \quad (\text{A.1})$$

where t_a, \dots, t_c are the measurement times and t_n, \dots, t_1 are the interaction times. Eq. A.1 is easily verified from the definition of the GRFs (Eqs. 1.34 and 1.35): for $\max(t_n, \dots, t_1) > \max(t_a, \dots, t_c)$, the \mathcal{T} operator guarantees that the leftmost super-operator is a $(-)$, in which case the trace vanishes (Eq. 1.16b).

Time-translation invariance allows us to add a constant to all arguments of the GRF without affecting its value ¹:

$$R(t_a, \dots, t_c, t_n, \dots, t_1) = R(t_a + \tau, \dots, t_c + \tau, t_n + \tau, \dots, t_1 + \tau). \quad (\text{A.2})$$

This symmetry only applies to a system initially in a steady state, for which $H_{0-}\rho_0 = 0$. The most typical steady state is that of thermal equilibrium, but in open systems nonequilibrium steady states may also occur.

To express Eqs. A.1 and A.2 in the frequency domain, it is convenient to define a Green function $G(t_a, \dots, t_c, t_n, \dots, t_1) \equiv R(-t_a, \dots, -t_c, -t_n, \dots, -t_1)$. Defining the latest measurement time, $t_m \equiv \max(t_a, \dots, t_c)$, we change variables to $\tau_\epsilon \equiv t_m - t_\epsilon$. With this new notation, the n^{th} order response of a multitime correlation function is

$$\langle \mathcal{T} q_+(t_a) \dots q_+(t_c) \rangle^{(n)} = \int d\tau_n \dots \int d\tau_1 G(\tau_a, \dots, \tau_c, \tau_n, \dots, \tau_1) f(t_m - \tau_n) \dots f(t_m - \tau_1), \quad (\text{A.3})$$

¹Henceforth we omit the $+\dots+ - \dots -$ superscript on the GRFs wherever doing so will not cause confusion.

which in the frequency domain becomes

$$\begin{aligned} \langle \tilde{q}_+(\omega_a) \dots \tilde{q}_+(\omega_c) \rangle^{(n)} &= (2\pi)^n \int d\omega_n \dots \int d\omega_1 \tilde{G}(-\omega_a, \dots, -\omega_c, \omega_n, \dots, \omega_1) \\ &\quad \times \tilde{f}(\omega_n) \dots \tilde{f}(\omega_1) \delta(\omega_a + \dots + \omega_c - \omega_n - \dots - \omega_1). \end{aligned} \quad (\text{A.4})$$

To see that the δ -function constraint on the frequencies is a direct consequence of Eq. A.2, consider an arbitrary time-translation invariant function $F(t_n, \dots, t_1)$. The function obeys the identity

$$\sum_{i=1}^n \frac{\partial}{\partial t_i} F(t_n, \dots, t_1) = 0, \quad (\text{A.5})$$

whence the n -dimensional Fourier transform, $\tilde{F}(\omega_n, \dots, \omega_1)$ satisfies the constraint

$$\sum_{i=1}^n \omega_i = 0, \quad (\text{A.6})$$

which implies that the sum of the output frequencies of a GRF must equal the sum of the input frequencies. For the special case of a single output frequency (i.e. the nonlinear response), this result is well known. For the case of fluctuations of the initial state, Eq. A.6 implies that the sum of the fluctuation frequencies must equal zero. The reality of the response further requires that $\tilde{G}(\omega_a, \dots, \omega_c, \omega_n, \dots, \omega_1) = \tilde{G}(-\omega_a, \dots, -\omega_c, -\omega_n, \dots, -\omega_1)^*$.

To obtain generalized K-K relations, we apply the Titchmarsh theorem, which states:

If $\tilde{G}(\omega)$ is square integrable over the real ω -axis, then any one of the following implies the other two:

1. *The Fourier transform $G(\tau)$ is 0 for $\tau < 0$.*
2. *Replacing ω by $z = x + iy$, the function $\tilde{G}(z)$ is analytic in the complex plane z for $y > 0$ and approaches $\tilde{G}(x)$ almost everywhere as $y \rightarrow 0$.*

3. $\tilde{G}(\omega)$ and $\tilde{G}(\omega')$ are related by the Hilbert transform

$$\tilde{G}(\omega) = \frac{1}{\pi i} \mathcal{P} \int_{-\infty}^{\infty} \frac{\tilde{G}(\omega')}{\omega' - \omega} d\omega'. \quad (\text{A.7})$$

The function $G(\tau_a, \dots, \tau_c, \tau_n, \dots, \tau_1)$ satisfies requirement 1 in each of its arguments τ_n, \dots, τ_1 (causality constrains the interaction times, but not the measurement times). Therefore condition 3 applies to each of the input frequency arguments of \tilde{G} . This result is a generalization of the K-K relations to the GRFs.

A.2 Initial thermal equilibrium

Callen and Welton [28] and Kubo [106] derived a relation between the linear response function, R^{+-} , and the ground state fluctuations, R^{++} . This *fluctuation-dissipation theorem* (FDT) is a special case of the Kubo-Martin-Schwinger (KMS) condition for multitime correlation functions of systems initially in thermal equilibrium [106, 126]. Bernard and Callen tried to extend the FDT to the nonlinear response functions, but were stymied by the complexity of the expressions in Hilbert space [15]. They obtained results for the second order response, but no higher. A number of other workers have also addressed this problem, encountering similar difficulties [56, 179, 35]. Lévy and Ogielski claimed that there does not exist a generalization of the FDT to nonlinear response [154], but in 2002 Wang and Heinz proposed just such a generalization [191]. In the following we discuss the relations among the GRFs of the same order (e.g. R^{++++} , R^{+++} , R^{++--} , and, R^{+---). While we do not establish explicit formulas connecting these quantities, we suggest that they all contain the same information.

The density matrix of a system in thermal equilibrium is given by

$$\rho_0 = \frac{\exp(-\beta H_0)}{\text{Tr}\{\exp(-\beta H_0)\}}. \quad (\text{A.8})$$

The KMS condition arises because the inverse temperature in Eq. A.8 acts on the density matrix in the same way as an imaginary time. For any two Hilbert space operators, $\hat{A}(t_a)$ and $\hat{B}(t_b)$ in the Heisenberg picture, we have the following identity [60]:

$$\begin{aligned}
\left\langle \hat{A}(t_a) \hat{B}(t_b) \right\rangle_0 &= \text{Tr}\{\hat{A}(t_a) \hat{B}(t_b) \rho_0\} \\
&= \text{Tr}\{\hat{A}(t_a) e^{\frac{i}{\hbar} H_0 t_b} B e^{-\frac{i}{\hbar} H_0 t_b} e^{-\beta H_0}\} / \text{Tr}\{\exp(-\beta H_0)\} \\
&= \text{Tr}\{\hat{A}(t_a) e^{-\beta H_0} e^{\frac{i}{\hbar} H_0 (t_b - i\hbar\beta)} B e^{-\frac{i}{\hbar} H_0 (t_b - i\hbar\beta)}\} / \text{Tr}\{\exp(-\beta H_0)\} \\
&= \text{Tr}\{\hat{A}(t_a) \rho_0 \hat{B}(t_b - i\hbar\beta)\} \\
&= \left\langle \hat{B}(t_b - i\hbar\beta) \hat{A}(t_a) \right\rangle_0.
\end{aligned} \tag{A.9}$$

The translation by imaginary time $-i\hbar\beta$ can be implemented by multiplying by $e^{-i\hbar\beta\partial/\partial t_b}$, so we have the KMS condition

$$\left\langle \hat{A}(t_a) \hat{B}(t_b) \right\rangle_0 = e^{-i\hbar\beta\partial/\partial t_b} \left\langle \hat{B}(t_b) \hat{A}(t_a) \right\rangle_0 \tag{A.10}$$

Converting to the frequency domain transforms $\partial/\partial t_b \rightarrow -i\omega_b$, so Eq. A.10 becomes

$$\left\langle \tilde{A}(\omega_a) \tilde{B}(\omega_b) \right\rangle_0 = e^{-\hbar\omega_b\beta} \left\langle \tilde{B}(\omega_b) \tilde{A}(\omega_a) \right\rangle_0. \tag{A.11}$$

By Eq. A.6, $\omega_b = -\omega_a$, so

$$\left\langle \tilde{A}(\omega) \tilde{B}(-\omega) \right\rangle_0 = e^{\hbar\omega\beta} \left\langle \tilde{B}(-\omega) \tilde{A}(\omega) \right\rangle_0. \tag{A.12}$$

Eq. A.12 immediately leads to a statement of the fluctuation dissipation theorem,

$$\left\langle \{\tilde{A}(\omega), \tilde{B}(-\omega)\}_+ \right\rangle_0 = \coth\left(\frac{\hbar\omega\beta}{2}\right) \left\langle [\tilde{A}(\omega), \tilde{B}(-\omega)] \right\rangle_0. \tag{A.13}$$

Generalizing Eq. A.11 to a product of n operators, we get [80]

$$\begin{aligned}
\left\langle \tilde{B}_n(\omega_n) \dots \tilde{B}_2(\omega_2) \tilde{B}_1(\omega_1) \right\rangle_0 &= e^{-\hbar\beta\omega_1} \left\langle \tilde{B}_1(\omega_1) \tilde{B}_n(\omega_n) \dots \tilde{B}_2(\omega_2) \right\rangle_0 \\
&= e^{-\hbar\beta(\omega_1+\omega_2)} \left\langle \tilde{B}_2(\omega_2) \tilde{B}_1(\omega_1) \tilde{B}_n(\omega_n) \dots \tilde{B}_3(\omega_3) \right\rangle_0 \\
&= \dots \\
&= e^{\hbar\beta\omega_n} \left\langle \tilde{B}_{n-1}(\omega_{n-1}) \dots \tilde{B}_1(\omega_1) \tilde{B}_n(\omega_n) \right\rangle_0, \quad (\text{A.14})
\end{aligned}$$

where we used Eq. A.6 in the last line.

Now we recast the KMS condition in the language of superoperators. Consider the products of superoperators $\left\langle \hat{B}_{2+}(t_2) \hat{B}_{1-}(t_1) \right\rangle_0$ and $\left\langle \hat{B}_{2+}(t_2) \hat{B}_{1+}(t_1) \right\rangle_0$. In Hilbert space the former is $\left\langle \hat{B}_2(t_2) \hat{B}_1(t_1) \right\rangle_0 - \left\langle \hat{B}_1(t_1) \hat{B}_2(t_2) \right\rangle_0$ and the latter is $\frac{1}{2} \left(\left\langle \hat{B}_2(t_2) \hat{B}_1(t_1) \right\rangle_0 + \left\langle \hat{B}_1(t_1) \hat{B}_2(t_2) \right\rangle_0 \right)$. Comparison with Eq. A.13 shows that

$$\left\langle \tilde{B}_{2+}(\omega) \tilde{B}_{1+}(-\omega) \right\rangle = \frac{1}{2} \coth \left(\frac{\hbar\omega\beta}{2} \right) \left\langle \tilde{B}_{2+}(\omega) \tilde{B}_{1-}(-\omega) \right\rangle. \quad (\text{A.15})$$

We can replace \hat{B}_{2+} by an arbitrary sequence of \pm superoperators. Consider the sequences $\left\langle \hat{B}_{n+} \hat{B}_{(n-1)\nu_{n-1}} \dots \hat{B}_{2\nu_2} \hat{B}_{1-} \right\rangle_0$ and $\left\langle \hat{B}_{n+} \hat{B}_{(n-1)\nu_{n-1}} \dots \hat{B}_{2\nu_2} \hat{B}_{1+} \right\rangle_0$, where $\nu_\epsilon = +, -$ (the first superoperator must be a (+) or the trace vanishes; all other superoperators may be (+) or (-); the sequences differ in whether the last superoperator is a (+) or a (-)). Converting just the rightmost superoperator to Hilbert space in each expression, the former becomes $\left\langle \hat{B}_{n+} \hat{B}_{(n-1)\pm} \dots \hat{B}_{2\pm} \hat{B}_1 \right\rangle_0 - \left\langle \hat{B}_1 \hat{B}_{n+} \hat{B}_{(n-1)\pm} \dots \hat{B}_{2\pm} \right\rangle_0$ and the latter becomes $\frac{1}{2} \left(\left\langle \hat{B}_{n+} \hat{B}_{(n-1)\pm} \dots \hat{B}_{2\pm} \hat{B}_1 \right\rangle_0 + \left\langle \hat{B}_1 \hat{B}_{n+} \hat{B}_{(n-1)\pm} \dots \hat{B}_{2\pm} \right\rangle_0 \right)$. Thus we have the frequency domain relation

$$\left\langle \tilde{B}_{n+} \tilde{B}_{(n-1)\nu_{n-1}} \dots \tilde{B}_{2\nu_2} \tilde{B}_{1-} \right\rangle_0 = \frac{1}{2} \coth \left(\frac{\hbar\omega_1\beta}{2} \right) \left\langle \tilde{B}_{n+} \tilde{B}_{(n-1)\nu_{n-1}} \dots \tilde{B}_{2\nu_2} \tilde{B}_{1+} \right\rangle_0. \quad (\text{A.16})$$

Eq. A.16 cannot be used on its own to relate the various GRFs because the multitime correlation functions in Eq. A.16 are not time-ordered. However, the time-ordered

expressions can be stitched together by combining multitime correlation functions of superoperators multiplied by appropriate unit-step functions. These step-functions considerably complicate the expressions, but do not change the information content. We can say that all generalized response functions of the same order (e.g. R^{+-} , R^{++} , and R^{+++}) have the same information content.

The condition of time-reversal symmetry has recently been considered for the non-linear response functions [186], but this condition seems not to apply to some systems (e.g. magnetic materials, p-n junctions), and thus is not considered here. Certain symmetries of the Hamiltonian may place additional constraints on the GRFs [203]. For example, in a system with a center of inversion symmetry the only nonzero GRFs are those where the number of (+) terms and the number of (−) terms have the same parity.

Bibliography

- [1] *Chlorophyll spectra from oregon medical laser center* (<http://omlc.ogi.edu/spectra/photochemcad/html/index.html>); *fluorophore spectra from molecular probes* (www.probes.com)., Oct. 10 2002.
- [2] V. M. Agranovich and M. D. Galanin, *Electronic Excitation Transfer in Condensed Matter*, Academic Press, 1982.
- [3] M. Alford, H. Feldman, and M. Gleiser, *Thermal nucleation of kink-antikink pairs*, Phys. Rev. Lett. **68** (1992), 1645.
- [4] S. Amelinckx, X. B. Zhang, D. Bernaerts, X. F. Zhang, V. Ivanov, and J. B. Nagy, *A formation mechanism for catalytically grown helix-shaped graphite nanotubes*, Science **265** (1994), 635.
- [5] D. L. Andrews and A. A. Demidov, *Resonance Energy Transfer*, Wiley, 1999.
- [6] C. L. Asbury and G. van den Engh, *Trapping of DNA in nonuniform oscillating electric fields*, Biophys. J. **74** (1998), 1024.
- [7] A. Barone and G. Paternó, *Physics and Applications of the Josephson Effect*, Wiley, 1982.
- [8] D. Bartolo, A. Ajdari, J.-B. Fournier, and R. Golestanian, *Fluctuations of fluctuation-induced Casimir-like forces*, Phys. Rev. Lett. **89** (2002), 230601.

- [9] G. Barton, *The quantum radiation from mirrors moving sideways*, *Annals of Physics* **245** (1996), 361.
- [10] F. Bassani and S. Scandolo, *Dispersion-relations and sum-rules in nonlinear optics*, *Phys. Rev. B* **44** (1991), 8446.
- [11] C. G. Baumann, V. A. Bloomfield, S. B. Smith, C. Bustamante, M. D. Wang, and S. M. Block, *Stretching of single collapsed DNA molecules*, *Biophys. J.* **78** (2000), 1965.
- [12] G. S. Beddard and G. Porter, *Concentration quenching in chlorophyll*, *Nature* **260** (1976), 366.
- [13] C. H. Bennett, M. Büttiker, R. Landauer, and H. Thomas, *Kinematics of the forced and overdamped sine-Gordon soliton gas*, *J. Stat. Phys.* **24** (1981), 419.
- [14] D. Bernaerts, X. B. Zhang, X. F. Zhang, S. Amelinckx, G. Vantendeloo, J. Vanlanduyt, V. Ivanov, and J. B. Nagy, *Electron-microscopy study of coiled carbon tubules*, *Phil. Mag. A* **71** (1995), 605.
- [15] W. Bernard and H. B. Callen, *Irreversible thermodynamics of nonlinear processes and noise in driven systems*, *Rev. Mod. Phys.* **31** (1959), 1017.
- [16] A. I. Bochkarev and Ph. de Forcrand, *Study of kink-antikink pair production at finite temperature by means of the Langevin equation*, *Phys. Rev. Lett.* **63** (1989), 2337.
- [17] P. Borowicz, J. Hotta, K. Sasaki, and H. Masuhara, *Laser-controlled association of poly(*n*-vinylcarbazole) in organic solvents: Radiation pressure effect of a focused near-infrared laser beam*, *J. Phys. Chem. B* **101** (1997), 5900.
- [18] T. H. Boyer, *Recalculations of long-range van der Waals potentials*, *Phys. Rev.* **180** (1969), 19.

- [19] O. M. Braun and Y. S. Kivshar, *Concentration dependence of the conductivity and diffusivity in one-dimensional anharmonic lattices*, Phys. Rev. B **50** (1994), 13388.
- [20] O. Bschorr, *The force between two parallel rigid plates due to the radiation pressure of phonons*, J. Acoust. Soc. Am. **106** (1999), 3730.
- [21] M. M. Burns, J.-M. Fournier, and J. A. Golovchenko, *Optical binding*, Phys. Rev. Lett. **63** (1989), 1233.
- [22] ———, *Optical matter: Crystallization and binding in intense optical fields*, Science **249** (1990), 749.
- [23] M. Büttiker and T. Christen, *Nucleation of weakly driven kinks*, Phys. Rev. Lett. **75** (1995), 1895.
- [24] ———, *Büttiker and Christen reply*, Phys. Rev. Lett. **77** (1996), 788.
- [25] M. Büttiker and R. Landauer, *Nucleation theory of overdamped soliton motion*, Phys. Rev. Lett. **43** (1979), 1453.
- [26] ———, *Nucleation theory of overdamped soliton motion*, Phys. Rev. A **23** (1981), 1397.
- [27] N. Calander and M. Willander, *Optical trapping of single fluorescent molecules at the detection spots of nanoprobe*s, Phys. Rev. Lett. **89** (2002), 143603.
- [28] H. B. Callen and T. A. Welton, *Irreversibility and generalized noise*, Phys. Rev. **83** (1951), 34.
- [29] H. B. G. Casimir, *Sur les forces van der Waals-London*, J. Chim. Phys. **46** (1949), 407.

- [30] H. B. G. Casimir and D. Polder, *The influence of retardation on the London-van der Waals forces*, Phys. Rev. **73** (1948), 360.
- [31] C. Cattuto, M. Borromeo, and F. Marchesoni, *Thermal decay of a metastable elastic string*, Chemical Physics **235** (1998), 51.
- [32] H. B. Chan, V. A. Aksyuk, R. N. Kleiman, D. J. Bishop, and F. Capasso, *Quantum mechanical actuation of microelectromechanical systems by the Casimir force*, Science **291** (2001), 1941.
- [33] Y. M. Chan and A. Dalgarno, *The third-order interaction energy between atoms*, Mol. Phys. **14** (1968), 101.
- [34] P. C. Chaumet and M. Nieto-Vesperinas, *Optical binding of particles with or without the presence of a flat dielectric surface*, Phys. Rev. B **64** (2001), 035422.
- [35] K. Chou, Z. Su, B. Hao, and L. Yu, *Equilibrium and nonequilibrium formalisms made unified*, Physics Reports **118** (1985), 2.
- [36] T. Christen and M. Büttiker, *Diffusion controlled initial recombination*, Phys. Rev. E **58** (1998), 1533.
- [37] S. Chu, J. E. Bjorkholm, A. Ashkin, and A. Cable, *Experimental observation of optically trapped atoms*, Phys. Rev. Lett. **57** (1986), 314.
- [38] A. E. Cohen and S. Mukamel, *A mechanical force accompanies fluorescence resonance energy transfer (FRET)*, J. Phys. Chem. A **107** (2003), 3633.
- [39] J. F. Currie, J. A. Krumhansl, A. R. Bishop, and S. E. Trullinger, *Statistical mechanics of one-dimensional solitary-wave-bearing scalar fields: Exact results and ideal-gas phenomenology*, Phys. Rev. B **22** (1980), 477.
- [40] V. Czikkely, H. D. Försterling, and H. Kuhn, *Light absorption and structure of aggregates of dye molecules*, Chem. Phys. Lett. **6** (1970), 11.

- [41] A. S. Davydov, *Theory of Molecular Excitons*, McGraw Hill, 1962.
- [42] P. G. de Gennes, *Phys. Lett. A* **38** (1972), 229.
- [43] ———, *Mechanical properties of nematic polymers*, *Polymer Liquid Crystals* (A. Ciferri, W. R. Krigbaum, and R. B. Meyer, eds.), Academic Press, 1982.
- [44] J. P. Delville, C. Lalaude, S. Buil, and A. Ducasse, *Late stage kinetics of a phase separation induced by a CW laser wave in binary liquid mixtures*, *Phys. Rev. E* **59** (1999), 5804.
- [45] J. P. Delville, C. Lalaude, and A. Ducasse, *Kinetics of laser-driven phase separation induced by a tightly focused wave in binary liquid mixtures*, *Physica A* **262** (1999), 40.
- [46] D. DeRosier, L. Tilner, and P. Flicker, *A change in the twist of the actin-containing filaments occurs during the extension of the acrosomal process in limulus sperm*, *J. Mol. Biol.* **137** (1980), 375.
- [47] D. J. DeRosier and L. G. Tilney, *How to build a bend into an actin bundle*, *J. Mol. Biol.* **175** (1984), 57.
- [48] F. Dewarrat, M. Calame, and C. Schönenberger, *Orientation and positioning of DNA molecules with an electric field technique*, *Single Molecules* **3** (2002), 189.
- [49] J. F. Dobson, K. McLennan, A. Rubio, J. Want, T. Gould, H. M. Le, and B. P. Dinte, *Prediction of dispersion forces: Is there a problem?*, *Aust. J. Chem.* **54** (2001), 513.
- [50] M. Doi, *Introduction to Polymer Physics*, Oxford Science Publications, 1995.
- [51] V. P. Dravid, X. Lin, Y. Wang, X. K. Wang, A. Yee, J. B. Ketterson, and R. P. H. Chang, *Buckytubes and derivatives: Their growth and implications for buckyball formation*, *Science* **259** (1993), 1601.

- [52] B. I. Dunlap, *Constraints on small graphitic helices*, Phys. Rev. B **50** (1994), 8134.
- [53] ———, *Relating carbon tubules*, Phys. Rev. B **49** (1994), 5643.
- [54] I. E. Dzyaloshinskii, E. M. Lifshitz, and L. P. Pitaevskii, *The general theory of van der Waals forces*, Advanc. Phys. **10** (1961), 165.
- [55] S. F. Edwards, Proc. Phys. Soc. **85** (1965), 613.
- [56] G. F. Efremov, *A fluctuation dissipation theorem for nonlinear media*, JETP **28** (1969), 1232.
- [57] A. Ehrlicher, T. Betz, B. Stuhrmann, D. Koch, V. Milner, M. G. Raizen, and J. Kas, *Guiding neuronal growth with light*, Proc. Nat. Acad. Sci. USA **99** (2002), 16024.
- [58] R. Eisenschitz and F. London, Z. Physik **60** (1930), 491.
- [59] J. G. Elias and D. Eden, *Transient electric birefringence study of the persistence length and electrical polarizability of restriction fragments of DNA*, Macromolecules **14** (1981), 410.
- [60] G. Emch and C. Liu, *The Logic of Thermostatistical Physics*, Springer, 2002b.
- [61] S. W. Englander, N. R. Kallenbach, A. J. Heeger, J. A. Krumhansl, and S. Litwin, *Nature of the open state in long polynucleotide double helices: Possibility of soliton excitations*, Proc. Natl. Acad. Sci. USA **77** (1980), 7222.
- [62] U. Enz, *Discrete mass, elementary kength, and a topological invariant as a consequence of a relativistic invariant variational principle*, Phys. Rev. **131** (1963), 1392.

- [63] M. Fixman and J. Kovac, *Polymer conformational statistics. III. Modified Gaussian models of stiff chains*, J. Chem. Phys. **58** (1973), 1564.
- [64] P. J. Flory, J. Chem. Phys. **17** (1949), 303.
- [65] ———, *Principles of Polymer Chemistry*, Cornell University Press, 1953.
- [66] F. C. Frank and J. H. van der Merwe, *One-dimensional dislocations. I. Static theory*, Proc. R. Soc. (A) **198** (1949), 205.
- [67] K. Freed, *Renormalization Group Theory of Macromolecules*, Wiley, 1987.
- [68] K. F. Freed, *Wiener integrals and models of stiff polymer chains*, J. Chem. Phys. **54** (1971), 1453.
- [69] J. Frenkel and T. Kontorova, Phys. Z. Sowjet **13** (1938), 1.
- [70] R. Gao, Z. L. Wang, and S. Fan, *Kinetically controlled growth of helical and zigzag shapes of carbon nanotubes*, J. Phys. Chem. B **104** (2000), 1227.
- [71] B. A. Garetz, J. Matic, and A. S. Myerson, *Polarization switching of crystal structure in the nonphotochemical light-induced nucleation of supersaturated aqueous glycine solutions*, Phys. Rev. Lett. **89** (2002), 175501.
- [72] W. A. Germishuizen, C. Wälti, R. Wirtz, P. Tosch, M. Pepper, A. G. Davies, and A. P. J. Middelberg, *Dielectrophoretic manipulation of surface-bound DNA*, Proceedings of 11th Conference on Electrostatics (IOP) (2003).
- [73] G. H. Goedecke and R. C. Wood, *Casimir-polder interaction at finite temperature*, Phys. Rev. A **60** (1999), 2577.
- [74] R. Golestanian and M. Kardar, *Mechanical response of vacuum*, Phys. Rev. Lett. **78** (1999), 3421.

- [75] J. M. F. Gunn and M. Warner, *Giant dielectric response and hairpins in polymeric nematics*, Phys. Rev. Lett. **58** (1987), 393.
- [76] E. Haas, M. Wilchek, E. Katchalski-Katzir, and I. Z. Steinberg, *Distribution of end-to-end distances of oligopeptides in solution as estimated by energy transfer*, Proc. Nat. Acad. Sci. USA **72** (1975), 1807.
- [77] S. Habib and G. Lythe, *Dynamics of kinks: Nucleation, diffusion, and annihilation*, Phys. Rev. Lett. **84** (2000), 1070.
- [78] P. Hänggi and F. Marchesoni, *Comment on 'breathers and kink-antikink nucleation'*, Phys. Rev. Lett. **77** (1996), 787.
- [79] P. Hänggi, F. Marchesoni, and P. Sodano, *Nucleation of thermal sine-Gordon solitons: Effect of many-body interactions*, Phys. Rev. Lett. **60** (1988), 2563.
- [80] B. Hao, *Closed time path Green's functions and nonlinear response theory*, Physica A **109** (1981), 221.
- [81] J. W. Hatfield and S. R. Quake, *Dynamic properties of an extended polymer in solution*, Phys. Rev. Lett. **82** (1999), 3548.
- [82] K. Hernadi, L. Thiên-Nga, and L. Forró, *Growth and microstructure of catalytically produced coiled carbon nanotubes*, J. Phys. Chem. B **105** (2001), 12464.
- [83] J. Hofkens, J. Hotta, K. Sasaki, H. Masuhara, and K. Iwai, *Molecular assembling by the radiation pressure of a focused laser beam: Poly(*N*-isopropylacrylamide) in aqueous solution*, Langmuir **13** (1997), 414.
- [84] J. Hofkens, J. Hotta, K. Sasaki, H. Masuhara, T. Taniguchi, and T. Miyashita, *Molecular association by the radiation pressure of a focused laser beam: Fluorescence characterization of pyrene-labeled PNIPAM*, J. Am. Chem. Soc. **119** (1997), 2741.

- [85] J.-I. Hotta, K. Sasaki, H. Masuhara, and Y. Morishima, *Laser-controlled assembling of repulsive unimolecular micelles in aqueous solution*, J. Phys. Chem. B **102** (1998), 7687.
- [86] K. L. C. Hunt, *Nonlocal polarizability densities and van der Waals interactions*, J. Chem. Phys. **78** (1983), 6149.
- [87] S. Ihara, S. Itoh, and J. I. Kitakami, *Helically coiled cage forms of graphitic carbon*, Phys. Rev. B **48** (1993), 5643.
- [88] J. N. Israelachvili, *Intermolecular and Surface Forces*, Academic Press, 1991.
- [89] M.-T. Jaekel and S. Reynaud, *Movement and fluctuations of the vacuum*, Rep. Prog. Phys. **60** (1997), 863.
- [90] T. B. Jones, *Electromechanics of Particles*, Cambridge University Press, 1995.
- [91] S. Juodkazis, N. Mukai, R. Wakaki, A. Yamaguchi, S. Matsuo, and H. Misawa, *Reversible phase transitions in polymer gels induced by radiation forces*, Nature **408** (2000), 178.
- [92] R. D. Kamien, P. Le Doussal, and D. R. Nelson, *Theory of directed polymers*, Phys. Rev. A **45** (1992), 8727.
- [93] ———, *Rotational invariance and the theory of directed nematic polymers*, Phys. Rev. E **48** (1993), 4116.
- [94] M. Kardar and R. Golestanian, *The “friction” of vacuum, and other fluctation-induced forces*, Rev. Mod. Phys. **71** (1999), 1233.
- [95] L. V. Keldysh, JETP **20** (1965), 1018.
- [96] B. T. Kelly, *The Physics of Graphite*, Applied Science Publishers, 1981.

- [97] A. R. Khokhlov and A. N. Semenov, *Susceptibility of liquid-crystalline solutions of semiflexible macromolecules in an external orientational field*, J. Phys. A: Math. Gen. **15** (1982), 1361.
- [98] G. W. King and J. H. Van Vleck, *Dipole-dipole resonance forces*, Phys. Rev. **55** (1939), 1165.
- [99] A. Kis, S. Kasas, B. Babi, A. J. Kulik, W. Benoît, G. A. D. Briggs, C. Schönenberger, S. Catsicas, and L. Forró, *Nanomechanics of microtubules*, Phys. Rev. Lett. **89** (2002), 248101.
- [100] J. Knoester and S. Mukamel, *Intermolecular forces, spontaneous emission, and superradiance in a dielectric medium: Polariton-mediated interactions*, Phys. Rev. A **40** (1989), 7065.
- [101] ———, *Nonlinear optical response in condensed phases: A microscopic theory using the multipolar Hamiltonian*, Phys. Rev. A **41** (1990), 3812.
- [102] R. S. Knox, *Spectral effects of exciton splitting in “statistical pairs”*, J. Phys. Chem. **98** (1994), 7270.
- [103] T. Kobayashi (ed.), *J-Aggregates*, World Scientific, 1996.
- [104] M. Kogan, *On the electrodynamics of weakly nonlinear media*, JETP **16** (1963), 217.
- [105] J. Krug and H. Spohn, *Anomalous fluctuations in the driven and damped sine-Gordon chain*, Europhys. Lett. **8** (1989), 219.
- [106] R. Kubo, *Statistical-mechanical theory of irreversible processes. i.*, J. Phys. Soc. Japan **12** (1957), 570.
- [107] ———, *Fluctuation Relaxation and Resonance in Magnetic Systems* (D. Ter Haar, ed.), Oliver and Boyd, 1962.

- [108] G. L. Lamb, *Analytical descriptions of ultrashort pulse propagation in a resonant medium*, Rev. Mod. Phys. **43** (1971), 99.
- [109] D. Langbein, *Theory of Van der Waals Attraction*, Springer Tracts in Modern Physics, 1974.
- [110] J. S. Langer, *Theory of the condensation point*, Ann. Phys. (NY) **41** (1967), 108.
- [111] R. G. Larson, T. T. Perkins, D. E. Smith, and S. Chu, *Hydrodynamics of a DNA molecule in a flow field*, Phys. Rev. E **55** (1997), 1794.
- [112] D. M. Leitner, *Vibrational energy transfer in helices*, Phys. Rev. Lett. **87** (2001), 188102.
- [113] H. Li and M. Kardar, *Fluctuation-induced forces between manifolds immersed in correlated fluids*, Phys. Rev. A **46** (1992), 6490.
- [114] K. Liand, M. S. Farahat, J. Perlstein, K.-Y. Law, and D. G. Whitten, *Exciton interactions in nonconjugated squaraine dimers. Mechanisms for coupling and consequences for photophysics and photochemistry.*, J. Am. Chem. Soc. **119** (1997), 830.
- [115] E. M. Lifshitz, *The theory of molecular attractive forces between solids*, JETP **2** (1956), 73.
- [116] W. Wang Z. Lin, Z. Su, and B. Hao, *The closed time path Green's functions and the theory of nonlinear response (I)*, Acta Phys. Sin. **31** (1982), 1483.
- [117] ———, *The closed time path Green's functions and the theory of nonlinear response (II)*, Acta Phys. Sin. **31** (1982), 1493.
- [118] F. London, Z. Physik **63** (1930), 245.

- [119] L. Lu, R. J. Lachicotte, T. L. Penner, J. Perlstein, and D. G. Whitten, *Exciton and charge-transfer interactions in nonconjugated merocyanine dye dimers: Novel solvatochromic behavior for tethered bichromophores and excimers*, J. Am. Chem. Soc. **121** (1999), 8146.
- [120] J. Mahanty and B. W. Ninham, *Dispersion Forces*, Academic Press, 1976.
- [121] B. Maier and J. O. Rädler, *Conformation and self-diffusion of single DNA molecules confined to two dimensions*, Phys. Rev. Lett. **82** (1999), 1911.
- [122] F. Marchesoni, *Nucleation of kinks in 1 + 1 dimensions*, Phys. Rev. Lett. **73** (1994), 2394.
- [123] F. Marchesoni, C. Cattuto, and G. Costantini, *Elastic strings in solids: Thermal nucleation*, Phys. Rev. B **57** (1998), 7930.
- [124] H. Margenau and N. R. Kestner, *Theory of Intermolecular Forces*, Pergamon Press, 1969.
- [125] J. F. Marko and E. D. Siggia, *Stretching DNA*, Macromolecules **28** (1995), 8759.
- [126] P. C. Martin and J. Schwinger, *Theory of many-particle systems. i*, Phys. Rev. **115** (1959), 1342.
- [127] N. Mataga, *Properties of molecular complexes in the electronic excited states*, Molecular Interactions, vol. 2 (H. Ratajczak and W. J. Orville-Thomas, eds.), John Wiley and Sons, 1981.
- [128] D. E. McCumber and B. I. Halperin, *Time scale of intrinsic resistive fluctuations in thin superconducting wires*, Phys. Rev. B **1** (1970), 1054.
- [129] A. D. McLachlan, *Retarded dispersion forces between molecules*, Proc. Roy. Soc. Lond. Ser. A **271** (1963), 387.

- [130] ———, *Retarded dispersion forces in dielectrics at finite temperatures*, Proc. Roy. Soc. Lond. Ser. A **274** (1963), 80.
- [131] J.-C. Meiners and S. R. Quake, *Femtonewton force spectroscopy of single extended DNA molecules*, Phys. Rev. Lett. **84** (2000), 5014.
- [132] P. W. Milonni, *The Quantum Vacuum: An Introduction to Quantum Electrodynamics*, Academic Press, 1994.
- [133] P. W. Milonni and M. L. Shih, *Source theory of the Casimir force*, Phys. Rev. A **45** (1992), 4241.
- [134] P. W. Milonni and A. Smith, *van der Waals dispersion forces in electromagnetic fields*, Phys. Rev. A **53** (1996), 3484.
- [135] D. J. Mitchell, B. W. Ninham, and P. Richmond, *On black body radiation and the attractive force between two metal plates*, Am. J. Phys. **40** (1972), 674.
- [136] U. Mohanty and Y. Zhao, *Polarization of counterions in polyelectrolytes*, Biopolymers **38** (1996), 377.
- [137] S. Mukamel, *Principles of Nonlinear Optical Spectroscopy*, Oxford University Press, 1995.
- [138] ———, *Superoperator representation of nonlinear response: Unifying quantum field and mode coupling theories*, Phys. Rev. E **submitted** (2003).
- [139] P. A. Maia Neto and S. Reynaud, *Dissipative force on a sphere moving in vacuum*, Phys. Rev. A **47** (1993), 1639.
- [140] R. R. Netz, *Strongly stretched semiflexible extensible polyelectrolytes and DNA*, Macromolecules **34** (2001), 7522.

- [141] ———, *Nonequilibrium unfolding of polyelectrolyte condensates in electric fields*, Phys. Rev. Lett. **90** (2003), 128104.
- [142] K. Niemax, *Transition from second- to first-order dipole-dipole interaction in the excited EuSr molecule*, Phys. Rev. Lett. **55** (1985), 56.
- [143] L. Novotny and B. Hecht, *Nano-Optics (Lecture notes on nano-optics)*, University of Rochester, 2002.
- [144] R. Pantell and H. Puthoff, *Fundamentals of Quantum Electronics*, Wiley, 1969.
- [145] R. H. Picard and C. R. Willis, *Time-dependent projection-operator approach to master equations for coupled systems. ii. systems with correlations*, Phys. Rev. A **16** (1977), 1625.
- [146] E. A. Power, *Introductory Quantum Electrodynamics*, Longmans, 1964.
- [147] E. A. Power and T. Thirunamachandran, *Casimir-Polder potential as an interaction between induced dipoles*, Phys. Rev. A **48** (1993), 4761.
- [148] ———, *A new insight into the mechanism of intermolecular forces*, Chem. Phys. **171** (1993), 1.
- [149] ———, *Dispersion forces between molecules with one or both molecules excited*, Phys. Rev. A **51** (1995), 3660.
- [150] ———, *Two- and three-body dispersion forces with one excited molecule*, Chem. Phys. **198** (1995), 5.
- [151] E. Brückner, P. Sonntag, and H. Rehage, *Light-induced shape transitions of unilamellar vesicles*, Langmuir **17** (2001), 2308.
- [152] H. Bücher and H. Kuhn, *Scheibe aggregate formation of cyanine dyes in monolayers*, Chem. Phys. Lett. **6** (1970), 183.

- [153] Th. Förster, *Intermolecular energy migration and fluorescence*, *Annalen der Physik* **2** (1948), 55.
- [154] L. P. Lévy and A. T. Ogielski, *Dissipation in nonlinear response*, *J. Math. Phys.* **30** (1989), 683.
- [155] H. Wennerström, J. Daicic, and B. W. Ninham, *Temperature dependence of atom-atom interactions*, *Phys. Rev. A* **60** (1999), 2581.
- [156] S. R. Quake, H. Babcock, and S. Chu, *The dynamics of partially extended single molecules of DNA*, *Nature* **388** (1997), 151.
- [157] N. R. Quintero, A. Sánchez, and F. G. Mertens, *Thermal diffusion of sine-Gordon solitons*, *Eur. Phys. J. B* **16** (2000), 361.
- [158] W. J. Rugh, *Nonlinear System Theory: the Volterra/Wiener Approach*, Johns Hopkins University Press, 1981.
- [159] S. A. Safran, *Curvature elasticity of thin films*, *Advances in Physics* **48** (1999), 395.
- [160] M. Salerno, *Discrete model for DNA-promoter dynamics*, *Phys. Rev. A* **44** (1991), 5292.
- [161] A. Sali, E. I. Shakhnovich, and M. Karplus, *How does a protein fold*, *Nature* **369** (1994), 248.
- [162] A. Sánchez, C. Cai, N. Grønbech-Jensen, A. R. Bishop, and Z. J. Wang, *Roughening transitions of driven surface growth*, *Phys. Rev. B* **51** (1995), 14664.
- [163] E. Sassaroli, Y. N. Srivastava, and A. Widom, *Photon production by the dynamical Casimir effect*, *Phys. Rev. A* **50** (1994), 1027.

- [164] S. Scandolo, *Kramers-Kronig relations and sum rules for nonlinear susceptibilities*, Ph.D. thesis, Scuola Normale Superiore Pisa, 1992.
- [165] U. S. Schwarz, S. Komura, and S. A. Safran, *Deformation and tribology of multi-walled hollow nanoparticles*, Europhys. Lett. **50** (2000), 762.
- [166] J. Schwinger, J. Math. Phys. **2** (1967), 407.
- [167] A. Seeger and P. Schiller, *Kinks in dislocation lines and their effects on the internal friction in crystals*, Physical Acoustics (W. P. Mason, ed.), vol. 3A, Academic Press, 1966.
- [168] P. R. Selvin, *The renaissance of fluorescence resonance energy transfer*, Nature Structural Biol. **7** (2000), 730.
- [169] M. B. Sherman, J. Jakana, S. J. Sun, P. Matsudaira, W. Chiu, and M. F. Schmid, *The three-dimensional structure of the limulus acrosomal process: a dynamic actin bundle*, J. Mol. Biol. **294** (1999), 139.
- [170] R. Sigel, G. Fytas, N. Vainos, S. Pispas, and N. Hadjichristidis, *Pattern formation in homogeneous polymer solutions induced by a continuous-wave visible laser*, Science **297** (2002), 67.
- [171] T. H. R. Skyrme, *A non-linear theory of strong interactions*, Proc. Roy. Soc. London A **247** (1958), 260.
- [172] ———, *Particle states of a quantized meson field*, Proc. Roy. Soc. London A **262** (1961), 237.
- [173] D. E. Smith, H. P. Babcock, and S. Chu, *Single-polymer dynamics in a steady shear flow*, Science **283** (1999), 1724.
- [174] D. J. Srolovitz, S. A. Safran, M. Homyonfer, and R. Tenne, *Morphology of nested fullerenes*, Phys. Rev. Lett. **74** (1995), 1779.

- [175] D. J. Srolovitz, S. A. Safran, and R. Tenne, *Elastic equilibrium of curved thin films*, Phys. Rev. E **49** (1994), 5260.
- [176] H. Stapelfeldt and T. Seideman, *Aligning molecules with strong laser pulses*, Rev. Mod. Phys. **75** (2003), 543.
- [177] M. J. Stephen, *First-order dispersion forces*, J. Chem. Phys. **40** (1964), 669.
- [178] A. J. Stone, *The Theory of Intermolecular Forces*, Oxford University Press, 1996.
- [179] R. L. Stratonovich, *Contribution to the quantum nonlinear theory of thermal fluctuations*, JETP **31** (1970), 864.
- [180] T. Strick, J.-F. Allemand, V. Croquette, and D. Bensimon, *Twisting and stretching single DNA molecules*, Prog. Biophys. Mol. Biol. **74** (2000), 115.
- [181] L. Stryer, *Fluorescence energy transfer as a spectroscopic ruler*, Ann. Rev. Biochem. **47** (1978), 819.
- [182] S. Suzuki, T. Yamanashi, S. Tazawa, O. Kurosawa, and M. Washizu, *Quantitative analysis of DNA orientation in stationary ac electric fields using fluorescence anisotropy*, IEEE Transactions on Industry Applications **34** (1998), 75.
- [183] L. G. Tilney, *Actin filaments in the acrosomal reaction of Limulus sperm*, J. Cell. Biol. **64** (1975), 289.
- [184] J. S. Toll, *Causality and the dispersion relation: Logical foundations*, Phys. Rev. **104** (1956), 1760.
- [185] S. Tretiak, C. Middleton, V. Chernyak, and S. Mukamel, *Exciton-Hamiltonian and delocalized electronic excitations in the LH2 antenna complex of purple bacteria*, J. Phys. Chem. B **104** (2000), 4519.

- [186] M. Trzeciacki and W. Hübner, *Time-reversal symmetry in nonlinear optics*, Phys. Rev. B **62** (2000), 13888.
- [187] S. W. P. Turner, M. Cabodi, and H. G. Craighead, *Confinement-induced entropic recoil of single DNA molecules in a nanofluidic structure*, Phys. Rev. Lett. **88** (2002), 128103.
- [188] M. Ueda, K. Yoshikawa, and M. Doi, *Molecular motion of long deoxyribonucleic acid chains in a concentrated polymer solution depending on the frequency of alternating electric field*, Polymer Journal **31** (1999), 637.
- [189] H. van Amerongen, L. Valkunas, and R. van Grondelle, *Photosynthetic Excitons*, World Scientific, 2000.
- [190] A. I. Volokitin and B. N. J. Persson, *Theory of friction: the contribution from a fluctuating electromagnetic field*, J. Phys.: Condens. Matter **11** (1999), 345.
- [191] E. Wang and U. Heinz, *Generalized fluctuation-dissipation theorem for nonlinear response functions*, Phys. Rev. D **66** (2002), 025008.
- [192] M. Warner, J. M. F. Gunn, and A. B. Baumgärtner, *Rod to coil transitions in nematic polymers*, J. Phys. A: Math. Gen **18** (1985), 3007.
- [193] H. Washizu and K. Kikuchi, *Electrical polarizability of polyelectrolytes in salt-free aqueous solution*, J. Phys. Chem. B **106** (2002), 11329.
- [194] M. Washizu and O. Kurosawa, *Electrostatic manipulation of DNA in micro-fabricated structures*, IEEE Transactions on Industry Applications **26** (1990), 1165.
- [195] M. Washizu, O. Kurosawa, I. Arai, S. Suzuki, and N. Shimamoto, *Applications of electrostatic stretch-and-positioning of DNA*, IEEE Transactions on Industry Applications **31** (1995), 445.

- [196] J. D. Weeks and G. H. Gilmer, *Adv. Chem. Phys.* **40** (1979), 157.
- [197] S. Weiss, *Fluorescence spectroscopy of single biomolecules*, *Science* **283** (1999), 1676.
- [198] F. W. Wiegel, *Introduction to Path-Integral Methods in Physics and Polymer Science*, World Scientific, 1986, Ch. 3.4.
- [199] D. R. M. Williams and M. Warner, *Statics and dynamics of hairpins in worm-like main chain nematic polymer liquid crystals*, *J. Phys. France* **51** (1990), 317.
- [200] C. R. Willis and R. H. Picard, *Time-dependent projection-operator approach to master equations for coupled systems*, *Phys. Rev. A* **9** (1977), 1343.
- [201] S. Woutersen and H. J. Bakker, *Resonant intermolecular transfer of vibrational energy in liquid water*, *Nature* **402** (1999), 507.
- [202] H. Xu and M. Käll, *Surface-plasmon-enhanced optical forces in silver nanoaggregates*, *Phys. Rev. Lett.* **89** (2002), 246802.
- [203] A. Yariv, *Quantum Electronics*, John Wiley and Sons, 1989.
- [204] S. Zeena and K. G. Thomas, *Conformational switching and exciton interactions in hemicyanine-based bichromophores*, *J. Am. Chem. Soc.* **123** (2001), 7859.
- [205] M. Zhang, Y. Nakayama, and L. Pan, *Synthesis of carbon tubule nanocoils in high yield using iron-coated indium tin oxide as catalyst*, *Jpn. J. Appl. Phys.* **39** (2000), L1242.
- [206] X. B. Zhang, X. F. Zhang, D. Bernaerts, G. T. Vantendeloo, S. Amelinckx, J. Vanlanduyt, V. Ivanov, J. B. Nagy, P. Lambin, and A. A. Lucas, *The texture of catalytically grown coil-shaped carbon nanotubules*, *Europhys. Lett.* **27** (1994), 141.